

Structuring Silicones and Silica at Interfaces

STRUCTURING SILICONES AND SILICA AT INTERFACES

By

VINODH RAJENDRA, Honours B.Sc.

A Thesis

Submitted to the School of Graduate Studies

in Partial Fulfillment of the Requirements

for the Degree

Doctor of Philosophy

McMaster University

© Copyright by Vinodh Rajendra, January 2014

DOCTOR IN PHILOSOPHY (2014)

Chemistry

McMaster University, Hamilton, ON

Title: Structuring silicones and silica at interfaces

Author: Vinodh Rajendra, Honours B.Sc. (McMaster University)

Supervisor: Dr. Michael A. Brook

Number of Pages: xx, 151

Abstract

Structuring silicones and silica at interfaces with a variety of compounds has led to the formation of several well-defined materials that have found applications in a variety of fields. This thesis explores various parameters and factors that enable the structuring of elastomers, colloids/suspensions, films and foams with the use of unconventional or new organosilicon chemistries.

Silicone elastomers are typically cured with metal-based catalysts (tin or platinum): the elastomers can be interfaced with a variety of hydrophilic polymers to form continuous hydrophobic and hydrophilic domains. The use of a non-metallic, basic amine catalyst was utilized to form silicone elastomers that were interfaced with a hydrophilic polymer. The parameters that are important for structuring the internal hydrophilic domains into a variety morphologies (globules, interconnected channels, etc.) were investigated. In addition, the parameters that control elastomer cure and surface morphology were varied to form several differently structured elastomers. Understanding these factors will help tune the properties of the structured silicone elastomers for applications such as drug delivery.

The formation of these structured elastomers simultaneously led to the formation of well-defined silica particles within a hydrophobic environment. This was highly unusual, as silica particles are typically formed in water or, in model systems, within an alcoholic-aqueous environment with the use of a basic catalyst. Thus, the mechanism of particle formation, including the colloidal stability of intermediate structures, within a hydrophobic environment with non-traditional catalysts was investigated. Their morphology could also be varied between solid, porous and hollow particles by utilizing different amine-based catalytic surfactants. The interfacial interactions between these catalysts with the hydrophobic silicone and the hydrophilic polymers determined which particle morphology would form. The silica particles could be formed in either crosslinkable or non-crosslinkable silicone oils. The ability to encapsulate drug surrogates within these silica particles is briefly discussed.

The next chapter discusses the use of a relatively new organosilicon chemistry to produce siloxane-based films. This chemistry is known as the Piers-Rubinsztajn reaction, which uses a boron catalyst to couple hydrosilanes and alkoxy silanes together. To produce these films, stable siloxane-in-water emulsions were first formed by combining a tetrafunctional hydrosilane, alkoxy silane and boron catalyst together in water. Water acts as an inhibitory solvent by coordinating to the boron catalyst to prevent the coupling reaction. However, this reaction could still occur slowly within the siloxane droplets over time to form a crosslinked material. Thus, the chemical composition and the emulsion stability was investigated over time. Siloxane films were then formed from these S/W emulsion by drop casting them on glass slides. Foamed, monolithic and particulate film morphologies could be produced from these S/W emulsions by varying other factors such as temperature and reaction time. The formation of particulate-based films was of great interest due to its potential applications in gas chromatography columns.

The final chapter of the thesis utilizes the Piers-Rubinsztajn reaction to inkjet print hydrophobic barriers for paper-based microfluidics and biosensors. Current paper-based biosensors print hydrophobic wax or alkyl ketene dimer (AKD) barriers to contain the contents of the sensor and the analyte, which allows for both qualitative and quantitative measurements. However, surfactant solutions cannot be contained by either of these materials. Therefore, the potential to print more robust hydrophobic silicone barriers was investigated. Using an inexpensive inkjet printer, siloxanes were printed onto paper with alcohols to temporarily inhibit the boron catalyst. The robustness of the hydrophobic wax, AKD and silicone barriers was compared by testing them against different surfactant solutions and solvents. The silicone barriers were then implemented in an assay with an established biosensor to demonstrate their usefulness in surfactant-based assays.

Acknowledgements

Throughout the years during my Ph.D., there have been many people that have aided and supported me to make this thesis possible. Whether scientific input or emotional support was given, I am grateful to everyone involved. First, I would like to thank my supervisor Professor Michael A. Brook for giving me this opportunity. His guidance, knowledge, encouragement and down-to-earth personality created a challenging environment that allowed me to be creative and explorative in my research. I would also like to thank my other supervisory committee members, Professors Alex Adronov and Todd Hoare for their support and helpful discussions. The members of the Brook group including the undergraduates, graduates, postdoctoral fellows and our research associate, Dr. Dan Chen, have my gratitude for all the troubleshooting suggestions and for making the lab such a friendly and inviting place.

The many projects that I worked on required me to use a variety of instruments and to collaborate with several people with different backgrounds, which include Dr. Clémence Sicard, Dr. Nick Burke, Professor Harald D. Stöver, Professor Robert Pelton and Professor John D. Brennan. Without their help and expertise, several of these projects would not have gone to completion. There are many more people to thank at McMaster University and I would like to thank those that helped me along the way in whatever capacity it came in.

Finally I give a heartfelt thanks to my parents, Mekala and Ravi Rajendra, who have nurtured me, encouraged me, pushed me and always believed in me, even when I didn't believe in myself. They never missed a week to come and visit me at my home away from home whenever I couldn't see them and they also made sure I never went hungry throughout my Ph.D. Their genuine curiosity in my research showed that they wanted to learn with me and that my journey through this degree was also theirs. For all these reasons and many more, I dedicate this thesis to my parents for shaping me into the person I am today. I am, and will be forever grateful to them.

Table of Contents

Abstract	iii
Acknowledgements	v
List of Figures	xi
List of Tables	xvii
Abbreviations	xix
Chapter 1 – Introduction	1
1.1 General.....	1
1.2 Formation of Silica based Materials	3
1.2.1 Silica Particles and Films	4
1.3 Silicone Elastomers.....	9
1.3.1 Interfacial Structuring of Hydrophilic Materials in Silicone Elastomers.....	11
1.4 Siloxane Materials via the Piers-Rubinsztajn Reaction	13
1.5 Scope of the Thesis	16
1.6 References.....	17
Chapter 2 – Structured Hydrophilic Domains on Silicone Elastomers	22
2.1 Abstract.....	22
2.2 Introduction.....	22
2.3 Experimental section.....	23
Materials	23
Characterization	24
Elastomer preparation	24
Preparation of ninhydrin solution and testing for the location of amines in the elastomer....	25
Soxhlet extraction	25
Surface analysis and imaging.....	26
Surface roughness – profilometry	27

Preparation of fluorescein-containing elastomers and use of the optical microscope	28
2.4 Results.....	28
Controlling cure asymmetry.....	29
Effect of varying crosslinker concentration	32
Effect of varying catalyst concentration	32
Effects of Humidity.....	32
Relative rates: cure vs. reagent diffusion in the silicone.....	33
Structuring silicone interfaces.....	33
Surface chemistry.....	33
Surface roughness	35
Internal structural organization	35
Effect of crosslinker concentration	36
Addition of surfactant	37
2.5 Discussion	38
Internal structural organization	41
2.6 Conclusion	43
2.7 Acknowledgements.....	43
2.8 Supplementary Information	43
Experimental for Optical Microscopy Amplitude Measurements of Wave Structures.....	44
2.9 References.....	47
Chapter 3 – Nearly Monodisperse Silica Microparticles From Silicone (Pre)elastomer Mixtures	49
3.1 Abstract.....	49
3.2 Introduction.....	50
3.3 Experimental Section	52
Materials	52

Particle Formation in Silicone Elastomers.....	53
Extraction of Samples.....	53
Imaging of Samples.....	54
Hardness Tests.....	54
X-ray photoelectron Spectroscopy (XPS).....	54
3.4 Results and Discussion.....	55
Effect of TEOS and AT-PDMS Catalyst Concentrations.....	57
Effect of Atmospheric Water and PEG.....	61
Origin of the Nearly Monodisperse Silica Particles.....	63
3.5 Conclusion.....	66
3.6 Acknowledgments.....	67
3.7 Supporting Information.....	67
3.8 References.....	70
Chapter 4 – Controlled Formation of Macroporous or Hollow Silica Particles in Non-aqueous Silicone Dispersions.....	72
4.1 Abstract.....	72
4.2 Introduction.....	72
4.3 Experimental Section.....	74
4.3.1 Materials.....	74
4.3.2 Preparation of Silica Particles.....	75
4.3.3 Soxhlet Extraction of cured Samples.....	77
4.3.4 Isolation of Silica Particles from Silicone Oil.....	77
4.3.5 Imaging of Samples.....	77
4.3.6 Porosity Measurements.....	78
4.3.7 Fluorescence Measurements of Fluorescein and HSA-Loaded Silica Particles.....	78
4.4 Results and Discussion.....	79

Particle Size and Morphology.....	80
Fluorescein and HSA Release from Silica Particles	92
4.5 Conclusion	94
4.6 Acknowledgments.....	95
4.7 Supporting Information.....	95
4.8 References.....	100
Chapter 5 – Silicone Resin Films from Reactive Siloxane-in Water Emulsions	102
5.1 Abstract	102
5.2 Introduction.....	103
5.3 Experimental	104
Materials	104
Characterization	104
Catalyst Stock Solutions	105
Aqueous Emulsions	105
Film Formation	106
Coating of Capillary Tubes and GC columns	106
5.4 Results.....	107
Colloidal Stability	107
Film Formation	113
High Surface Area Coatings	119
5.5 Conclusion	120
5.6 Acknowledgments.....	121
5.7 References.....	121
Chapter 6 – Inkjet Printed Siloxane-Based Hydrophobic Barriers on Paper for Microfluidic Assays	123
6.1 Abstract	123

6.2	Introduction.....	123
6.3	Experimental	125
	Materials	125
	Siloxane formulations	125
	Printing hydrophobic siloxane barriers	126
	Surface tension measurements	128
	Testing the robustness of the hydrophobic barriers	128
	Paper sensor: Detecting β -galactosidase from lysed <i>E. coli</i> cells within the hydrophobic barriers	128
	Imaging of hydrophobic barriers.....	129
6.4	Results.....	129
	Testing barrier robustness to surfactant solutions.....	132
	Applications of printed silicone barriers for diagnostics	141
6.5	Conclusions.....	142
6.6	Acknowledgments.....	143
6.7	References.....	143
	Chapter 7 – Summary	145
	7.1 References.....	148
	Appendix	149
	Papers Published in Peer-Reviewed Journals	149
	Filed Patents.....	149
	Conference Presentations.....	149

List of Figures

Figure 1.1: Structure of A: growing silica structure and B: PDMS.....	1
Figure 1.2: Nomenclature for different Si-O units.....	2
Figure 1.3: General route to silicone formation.....	2
Figure 1.4: Scanning electron microscope (SEM) images of A: Navicula and B: Stephanodiscus diatoms. ^{8,9}	3
Figure 1.5: Sol-gel methodology for forming silica ¹⁵	4
Figure 1.6: Synthesis of mesoporous MCM-41 silica particles ³⁶	7
Figure 1.7: Formation of hollow silica particles with a colloidal template. ⁴⁶	8
Figure 1.8: General reaction of tin catalyzed silicone elastomers.	10
Figure 1.9: Acid and base catalyzed crosslinking of silicones.	11
Figure 1.10: Generic depiction of a two phase IPN. ⁵⁶	12
Figure 1.11: Piers-Rubinsztajn and metathesis reactions between hydrosilane and alkoxy silane.	14
Figure 1.12: Silyl ether formation (A), silanol coupling with a hydrosilane (B) and silanol coupling with two silanol groups (C).....	15
Figure 2.1: Structure of DC 3225C.....	24
Figure 2.2: Preparation of elastomers for fluorescence microscopy.....	25
Figure 2.3: General chemical equation for RTV silicone crosslinking.....	29
Figure 2.4: A: Nitrogen (catalyst) concentration (XPS) at surface with varying TEOS concentrations at different take-off angles (the 15% sample was examined at 2 different angles than the other samples. B: Ninhydrin staining showing presence of catalyst preferentially at the air interface.	34
Figure 2.5: A: Roughness of surfaces with increasing crosslinker by profilometry (Table 2.2, entries 6 - 10). B: Roughness of surfaces with increasing crosslinker at 90% RH by profilometry (Table 2.2, entries 14 - 23). C: Wavelength of elastomers cured at 90% RH (Table 2.2, entries 16, 17, 19-23).....	36

Figure 2.6: Profilometry images of elastomers prepared with 15% TEOS and A: 10% catalyst (Table 2.2, entry 11), B: 4% catalyst (Table 2.2, entry 13). Scale bars = 50µm. C: SEM image of elastomer prepared with 25% TEOS, 10% catalyst and 90% RH (Table 2.2, entry 23). Scale bar = 1 mm.....37

Figure 2.7: Fluorescence images of elastomers with varying amounts of crosslinker. A: 5%, B: 15%, C: 25% (Table 2.2, entries 6, 8 and 10). Scale bar = 500 µm.37

Figure 2.8: Fluorescence images of elastomers prepared with 15% TEOS and A: 1% surfactant (S), 10% catalyst (C), B: 5%(S) and 10% (C), C: 5%(S) and 7% (C), D: 5%(S) and 4%(C) (Table 2.2, entries 24-27). Scale bar = 500 µm.....38

Figure 2.9: Asymmetry caused by increasing crosslinker. With increasing TEOS concentration, A: dispersed PEG droplets, B: then assembled into ribbons and finally, C: into three-dimensional networks.....39

Figure 2.10: Model interfaces between silica/silicone controlled by surface-active materials.....42

Figure 3.1: A: SEM of 25% TEOS with PEG elastomer cured with AT-PDMS at ambient conditions showing exposed, narrowly dispersed silica particles directly below the elastomer surface. B: Expansion of A. C: Expansion of B. D: SEM cross-section of dibutyltin dilaurate-catalyzed elastomer at 25% TEOS loading.....52

Figure 3.2: Cartoon showing different 3D structural features of elastomer cross-sections prepared using different catalysts. A: AT-PDMS cured elastomers for all formulations that form particles (Table 3.4) except for the formulation in the next pictorial. B: AT-PDMS, humidity 90%, 25% TEOS and with PEG; surface covered with a thin silicone layer interrupted by ‘silica particle pock marks,’ Figure 3.1A. C: Dibutyltin dilaurate, homogeneous elastomer. D: Ninhydrin-stained elastomer showing presence of amine at the air interface.....58

Figure 3.3: SEM cross-sections (air interface is at the top of all images) of AT-PDMS-catalyzed elastomers containing PEG with varying TEOS concentrations (%T) at 20-30% RH (A, B, C); varying catalyst concentration (%C) 4%, 7% and 10% with 15%T at 20-30% RH (D, E, F), and varying TEOS concentrations at 90% RH (G, H, I).....60

Figure 3.4: Model for steric stabilization of silica by AT-PDMS. A, hydrolysis; B, condensation; C, precipitation of silica oligomers; D, growth of sterically stabilized silica (by particle capture and growth through hydrolysis/condensation); E, aggregation once particle size exceeds available surfactant, liberation of surfactant that can lead to additional particle layers (if TEOS is present).....61

Figure 4.1: Amine-catalyzed reactions lead to both elastomers and silica. Silica particles are entrapped in silicone rubber formed from HO-PDMS, but can be isolated when VT-PDMS is used. PEG is required to form the structured silica structures described below.76

Figure 4.2: SEM Cross-sections of **BA**- and **DDA**-derived particles are shown at different TEOS concentrations and magnifications. Images J and K show **BA**-catalyzed particles at 20%T and 15%T. Image L shows monolithic silica formation at the air-surface interface with **DDA** in the absence of PEG. Images M–O are expanded images of the **BA**-catalyzed porous silica at 25%, 20% and 15%T, respectively. Selected additional photos with identical scaling may be found in the SI.83

Figure 4.3: Model of silica structuring occurring in A: **BA**-catalyzed elastomers, B: **DDA**-catalyzed elastomers with low %TEOS, C: **DDA** with high %TEOS, D: **DDA** with high %TEOS and no PEG.85

Figure 4.4: SEM images of isolated and crushed silica particles using PEG600 and catalyzed with **BA**-containing 25%T (A), 20%T (B), 15%T (C) and **DDA**-catalyzed particles with 25%T (D), 20%T (E) and 15%T (F).86

Figure 4.5: Nitrogen adsorption-desorption isotherms of A: **BA** catalyzed B: **DDA** catalyzed particles and BJH pore size distribution data during nitrogen adsorption for C: **BA** catalyzed and D: **DDA** catalyzed particles.88

Figure 4.6: General schematic of BA (A) and DDA (B) phase separation from continuous silicone oil phase into PEG droplets for the formation of particles.90

Figure 4.7: Fluorescence profiles of **BA**- and **DDA**-catalyzed particles loaded with fluorescein (F) or HSA over time.94

Figure 5.1: General reaction scheme of A:Piers-Rubinsztajn, B: hydrosilane with water and C: silanol coupling with a hydrosilane.104

Figure 5.2: General procedure for forming S/W emulsions.....	106
Figure 5.3: Model for the formation of stable siloxane-in water emulsions that can be aged and dried to give 3 distinct film structures.	109
Figure 5.4: Zeta potential measurements over 1 week of QM ^H ₄ and TEOS with varying concentrations of catalyst.....	110
Figure 5.5: Model showing changes in particles over time as a function of catalyst concentration.....	111
Figure 5.6: ATR-IR data of W2 A: over 1 week in solution, B: drying on the instrument after 60-100 mins in ambient conditions.	112
Figure 5.7: Dried films from both ageing the S/W emulsions and then by drying them at RT or ~100°C using optical and scanning electron microscopy (SEM). Scale bars for optical images = 5 mm.....	114
Figure 5.8: SEM images of W3 samples (highest catalyst concentration) as a function of dispersion age and drying temperature.	116
Figure 5.9: Solid state ²⁹ Si NMR spectra of dried S/W emulsions at A: 0d (W2T & W2), B: 3d (W2A3T & W2A3) and C: 7d (W2A7T & W2A7).	118
Figure 5.10: SEM images of W2A7 (A,B) and W3A10 (C,D) emulsions dried within standard capillary tubes coated with hydrophobic silica particles. E, F, G: Fused silica GC column coated with W2A7 was allowed to dry.....	120
Figure 6.1: Structure of two AKD compounds, A: Precis and B: Aquapel. ¹⁴	124
Figure 6.2: General schemes of: A) the PR reaction to form new siloxanes; B) silyl ether synthesis of alcohols with hydrosilanes, with B(C ₆ F ₅) ₃ as the catalyst in all of the reactions; and C) the PR reaction with tetrafunctional precursors.	130
Figure 6.3: Wax based hollow circles stained with CPR surfactant solutions from the printed side (A). 4 wax layers were breached by the same solutions (B). P3 printed hollowed circles on Whatman #1 paper with CPR surfactant solutions on the printed side (C) and back side (D). Scale bars = 5 mm.	134
Figure 6.4: Cross-sectional representation of Whatman 1 paper with a surfactant solution/solvent contained by a silicone barrier that is rectangular (A) or rhombus (B)	

shaped. The dotted line in B represents the triangular slice that appears as a light corona from the printed side.	134
Figure 6.5: P4A and P4B silicone barriers using the 2 printer method in the form of A: 90 hollowed circles, B: rectangular blocks with unmodified paper channels loaded with a 10% B-PER solution (darker region). Images of one printed side (C) and the other printed side (D) of the hollowed circles with the added surfactant solutions. Scale bars = 2 cm (A), 1 cm (B) and 5 mm (C, D).....	135
Figure 6.6: Fluorescent images of a 10% B-PER (A – D) and 1% SDS solution (E,F) with a CPR dye added to the wax (A,B), P3- (C,D) and P4A/P4B-s (E,F), respectively. Image C shows the printed side and D shows the backside of the Whatman #1 paper, while E and F show both printed sides of the paper. Arrows indicate the observed corona that corresponds to the thick interlayer on the backside of the paper. Scale bars = 500 μm (A, C – F) and 200 μm (B).....	138
Figure 6.7: SEM images of Whatman #1 paper that is unmodified (A, B), wax modified (C, D) and siloxane-modified with P3 (E, F).....	139
Figure 6.8: Potential chemical modification of cellulose fibers (A) and the cross-sectional diagram of siloxane modified cellulose fibers (B).....	140
Figure 6.9: Inkjet printed P-Arg and CPR/ β -galactopyranoside solutions (yellow) within wax barriers (A) and P4A/P4B-barrier (B, C) with the addition of lysed E. Coli cells in a 10% B-PER solution (purple) for total coliform detection. Image C shows the back side of the printed sensor. Scale bars = 1 cm.	142
Figure S 2.1: Formation of 'domains with increasing TEOS. Scale bars = 50 μm	44
Figure S 2.2: Selected surface images showing wave structures using A: 5% T. B: 10% T and C: 15% T at 90% RH (Table 2.2, entries 19 - 21). Scale bars = 200 μm	45
Figure S 2.3: Fluorescence images of elastomers with varied amounts of crosslinker.	46
Figure S 2.4: Internal structuring with varying catalyst.....	46

Figure S 4.1: SEM images of various BA and DDA catalyzed elastomers at different magnifications. Arrow in B points out few solid particles that appear non-reproducibly in BA catalyzed systems without PEG.99

List of Tables

Table 2.1: Composition of elastomers (all values in 2.5g total mass) ^a	27
Table 2.2: General observations and homogeneity of all elastomers	30
Table 3.1: Atomic % of nitrogen from AT-PDMS catalyst on cured elastomers at 20-30% RH as measured by XPS at a takeoff angle of 30°	55
Table 3.2: Typical formulations of AT-PDMS catalyzed silicone elastomers with varying TEOS loadings (5 - 25% in 5% increments) (2.5 g total in each formulation).....	56
Table 3.3: Typical formulations of silicone elastomers cured with varying amounts of AT-PDMS (4, 7 and 10%) at 15% TEOS (2.5 g)	56
Table 3.4: Particle diameters (µm) with standard deviations in elastomers prepared with varying amounts of TEOS	57
Table 3.5: Summary of parameter effects on particle formation	59
Table 4.1: Composition of BA and DDA -catalyzed elastomers and silica particles	78
Table 4.2: Average diameter, standard deviation (µm) and polydispersity index (PDI) of BA and DDA-derived particles in HO-PDMS with varying amounts of TEOS ^a	84
Table 4.3: Average diameter, standard deviation (µm) and PDI of BA and DDA -catalyzed particles isolated from VT-PDMS with varying amounts of TEOS	86
Table 4.4: Surface Area and total pore volume of BA and DDA catalyzed particles	88
Table 5.1: S/W emulsion formulations	107
Table 5.2: Particle size measurements (nm) of S/W emulsions after 1 week using DLS.	110
Table 6.1: Key siloxane formulations to form silicone barriers on paper. Siloxanes and catalyst amounts are reported in mmol and alcohols are reported in mL.	126
Table 6.2: Solvents tested against wax and siloxane based barriers (P3 and P4A/P4B) to determine if they are contained (Y), not contained (N) or partially contained (P) ^a . Surface tension values are reported at 25°C. ³⁷	136
Table S 2.1: Phase separated liquid on 5% TEOS elastomer (Table 2.2, entry 6).....	43

Table S 2.2: Atomic % of nitrogen at 30 for elastomers with PEG (Table 2.2, entries 7-10)	44
Table S 2.3: Amplitudes of wave structures on elastomer surfaces	45
Table S 3.1: Control formulations utilizing dibutyltin catalyzed silicone elastomer formulations with varying TEOS loadings (5-25% in 5% increments) (2.5 g total in each formulation)	67
Table S 3.2: AT-PDMS catalyzed formulations (2.5g) with varying TEOS loadings and the thickness of the silica particle layers formed	68
Table S 3.3: Silicone elastomers cured with varying amounts of AT-PDMS at 15% TEOS (2.5g).....	69
Table S 4.1: BA-catalyzed formulations (2.5g) with varying TEOS loadings and their average particle sizes (μm) ^a	95
Table S 4.2: DDA-catalyzed formulations (2.5g) with varying TEOS loadings and their average particle sizes (μm) ^a	97

Abbreviations

μPAD	Microfluidic, paper-based analytical devices
AKD	Alkyl ketene dimer
AT-PDMS	Aminopropyl-terminated poly(dimethylsiloxane)
ATR-IR	Attenuated total reflectance infrared spectroscopy
BA	Benzylamine
CPR	Chlorophenol Red
CTAB	Cetyl trimethylammonium bromide
DDA	Dodecylamine
DGS	Diglyceroxysilane
DLS	Dynamic light scattering
DMTMDMS	1,3-Dimethyltetramethoxydisiloxane
GC	Gas chromatography
HO-PDMS	Hydroxy-terminated poly(dimethylsiloxane)
HSA	Human serum albumin
IPN	Interpenetrating network
IPTG	Isopropyl-β-D-thiogalactopyranoside
LF	Lateral flow
P-Arg	Poly-L-arginine hydrochloride
PDADMAC	Poly(diallyldimethylammonium chloride)
PDMS	Poly(dimethylsiloxane)
PEG	Poly(ethylene glycol)
PEO	Poly(ethylene oxide)
PMMA	Poly(methylmethacrylate)
PR	Piers-Rubinsztajn
PVAm	Poly(vinylamine)
QM ^H ₄	Tetrakis(dimethylsiloxy)silane
RH	Relative Humidity

R _q	Root mean square roughness
RTV	Room temperature vulcanization
SDS	Sodium dodecyl sulfate
SEM	Scanning electron microscopy
SiO ₂	Silica
TEOS	Tetraethyl orthosilicate
TMB	Trimethoxybenzene
TMOS	Tetramethyl orthosilicate
TPOS	Tetrapropyl orthosilicate
TSB	Tryptic soy broth
VT-PDMS	Vinyl-terminated poly(dimethylsiloxane)
XPS	X-ray photoelectron spectroscopy

Chapter 1 – Introduction

1.1 General

The development of both silica and silicones has led to enormous improvements in available products over the last 50 years: the compounds have now found practical applications in fields ranging from electronics to biomaterials. Both of these materials have several desirable intrinsic properties. The compounds can be combined as a blend, in a composite or at an interface with other compounds to tune the chemical and physical properties to those desired. On their own, silica and silicones also have many applications. Structuring either of them at interfaces enables new materials to be formed under a variety of conditions.

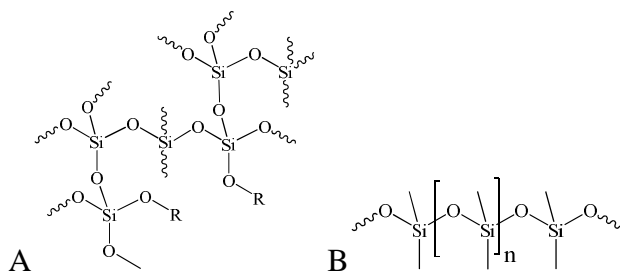


Figure 1.1: Structure of A: growing silica structure and B: PDMS.

Silica or silicon dioxide (SiO_2), the natural form of silicon on the earth, is the main constituent in several common materials like glass. Silica has several desirable properties that make it an ideal material for various applications, which include low chemical reactivity, biocompatibility, high temperature and electrical resistance, etc. Silica contains silicon and oxygen constituents and has a branched alternating Si-O network (Figure 1.1B) that gives rise to crystalline or amorphous network structures. Silica only contains Q units (silicon atom containing 4 oxygen atoms), however, the network structure can be modified by M, D, or T units (Figure 1.2) to give elastomers or resins.¹ Silica itself is hydrophilic (water-loving) in nature, however, a combination of different organically-modified Si-O units (M, D or T) typically leads to a hydrophobic (water-hating) siloxane due to the hydrocarbon residues off the silicon atoms. This

effectively lowers the surface energy of a siloxane material, as fewer surface silanol groups are present, thus leading to a loss of surface hydration from water.

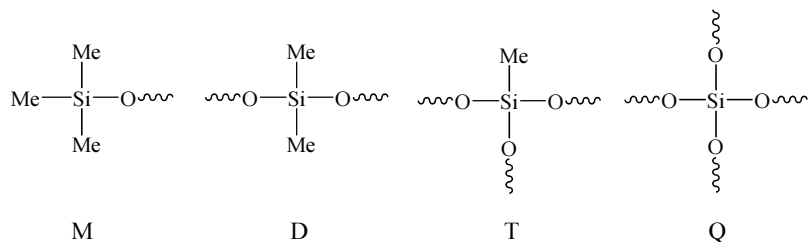


Figure 1.2: Nomenclature for different Si-O units.

Silicones are silicon-based polymers composed of a silicon and oxygen backbone, and a variety of R- groups bound to the silicon atoms. Figure 1.1A depicts poly(dimethylsiloxane) (PDMS), which is one of the most common silicones. Unlike carbon-based polymers, silicones are capable of remaining in a fluid state even at very high molecular weights, which can be attributed to their low intermolecular forces and rotational energy.^{2,3} Additionally, silicones such as PDMS are highly hydrophobic due to the methyl groups being ‘visible’ – they are exposed at interfaces. Silicones possess several desirable properties that include low chemical/physical reactivity, low toxicity, flexibility, high gas permeability, thermal stability, electrical resistance and many others.²⁻⁵ Contact lenses, electrical sheaths, car wax, and defoamers are some specific materials that are enabled by the presence of silicones.

The common method to produce silicones is the Rochow Direct Process that introduces carbon to silicone atoms.⁶ This energy intensive process, the Direct Process, produces several different chlorosilane by-products in addition to the key product $(\text{CH}_3)_2\text{SiCl}_2$. The reaction is followed by chlorosilane hydrolysis, which (re)introduces two oxygens to the silicon atoms.⁷ The key products, in addition to HCl, are small cyclic siloxanes ($n = 3-6$) or low molecular weight oligomers ($n = 30-50$).

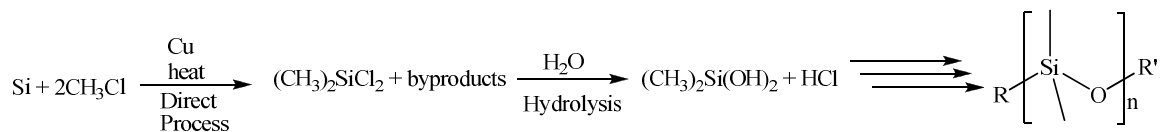


Figure 1.3: General route to silicone formation.

1.2 Formation of Silica based Materials

The most common process to form amorphous silica is biosilification by diatoms, which are a group of algae that produce cell walls composed of silica. Some of the structures and shapes of the diatoms' cell walls can be highly complex: they come in various shapes and sizes and can contain highly ordered pores as shown in Figure 1.4 (with permission to reprint)^{8,9}. Kröger et al. were the first to demonstrate that the majority of diatoms utilize proteins known as silaffins as templates to condense silicates to form ornate silica based cells walls, while a few other diatoms were later discovered to use long chained polyamines.^{10,11} A combination of both silaffins and polyamines for biosilification may also occur in various diatoms. The complex molecular interactions between the intracellular silicate, silaffins and/or polyamines are the cause of these highly ordered silica structures although the processes involved are currently not well understood.¹² The chemistry utilized to form silica within these diatoms is similar to the sol-gel process, which will be discussed further on.

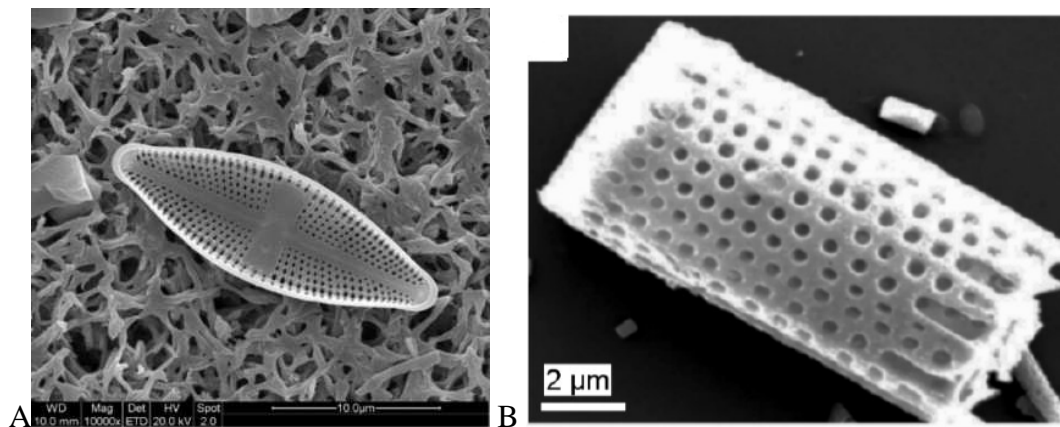


Figure 1.4: Scanning electron microscope (SEM) images of A: *Navicula* and B: *Stephanodiscus* diatoms.^{8,9}

Two common synthetic processes to form amorphous silica include the pyrogenic and hydrolysis/precipitation methodologies.² By burning chlorosilanes with the addition of water, fumed silica particles (5-50 nm) can be formed, which is an important filler/additive for several other materials.^{13,14} An alternative process to silica-based materials involves the hydrolysis of alkoxy silanes in either acidic or basic media to

silanols (Si-OH) that then condense to form silica.¹⁵ This is known as the sol-gel process and has been utilized primarily in an academic setting to form a variety of silica colloids,¹⁶⁻¹⁸ films,^{19,20} gels,^{21,22} etc. Figure 1.5 demonstrates tetraethyl orthosilicate (TEOS) – an alkoxy silane – undergoing hydrolysis and subsequent condensation reactions between two silanols, or a silanol and alkoxy group to form a silica network.¹⁵ Depending on the reagents and reaction conditions, the process can be utilized to form various silica based colloids and films for various applications. Precipitated silica is formed by reacting an alkaline sodium silicate solution with an acid such as sulfuric acid to cause condensation of the silanol groups.² After condensing, the silica precipitates out of the aqueous solution and is collected.

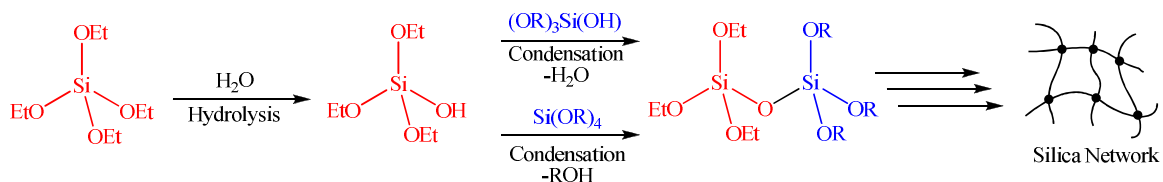


Figure 1.5: Sol-gel methodology for forming silica¹⁵

1.2.1 Silica Particles and Films

Particles with diameters ranging from 1 – 1000 nm, which are dispersed within another continuous phase are known as colloids.²³ Particle suspensions with larger diameters are typically known as suspended solids. The particle motion of colloids and suspended solids differ within a solution, as colloids are susceptible to Brownian motion whereas suspended solids are not. Brownian motion is the random movement of particulates within a liquid or gas. This can be attributed to the moving gas/liquid molecules interacting with the particulate.²³ Suspended solids are too large to be affected by these molecules in the continuous phase, however, they are still susceptible to gravity and convection forces.

For particle stability, the interfacial interaction between the particulate and the continuous phase is paramount. Repulsive electrostatic forces and/or sterics help stabilize various colloids and suspended solids in a liquid. The DLVO (Derjaguin, Landau, Verwey, Overbeek) theory explains interparticle interactions by accounting for the

attractive van der Waals forces and repulsive electrostatic forces.²⁴⁻²⁶ According to the theory, the charged surface of the particles are covered with counterions from solution and the two layers of charged molecules are known as the electrical double layer (EDL). For colloids and/or suspended solids to remain stable, the repulsive force of the EDL must overcome the attractive van der Waals forces. By varying certain parameters such as the choice of solvent, salt concentration, temperature, etc., the particle stability can be controlled.

Stöber et al. were one of the first groups that described the ability to form narrowly dispersed silica particles using the sol-gel methodology.¹⁶ Using TEOS as the silica precursor, ammonium hydroxide as the basic catalyst within an aqueous alcoholic mixture, monodisperse silica particles $\sim 1 \mu\text{m}$ in diameter were produced. The polydispersity and size of the particles could also be varied by changing the alcoholic solvents used for particle formation. Aggregation is avoided due to the deprotonated silanol groups that lead to a negatively charged silica particle surface. As explained by DLVO theory, the surrounding silica particles electrostatically repel one another preventing aggregation. The concentration of the basic catalyst was shown to affect particle stability in this study, as lower concentrations of ammonium hydroxide led to more aggregated silica particles. The higher the concentration of ammonium hydroxide, the more negatively charged the silica particle surfaces became, which resulted in a larger and more defined EDL and more effective particle repulsion.

Silica film formation undergoes a different set of conditions compared to particle formation. As shown with Stöber et al., particle formation typically occurs under basic conditions, as dense silica structures can be formed due to the high rate of condensation and slow rate of hydrolysis. Under acidic conditions, the rate of hydrolysis is high and condensation occurs much more slowly, thus leading to larger, more linear networks with higher concentrations of unreacted silanol groups. These acidic sols eventually lead to gels, as the sprawling silica networks with unreacted silanol groups contain water when formed. These larger networks are ideal for forming silica-based films. In addition, the morphology of the films can be tuned similarly to silica particles from basic sols. Meso-

and macrostructured silica films can be produced with the aid of surfactants^{27,28} and particle templates.^{29,30}

1.2.1.1 Controlling Particle and Film Morphologies

The ability to control the morphology of silica based particles and films allows for properties such as their surface area and porosity to be tuned for a wide variety of applications. The number of different structures and methods developed for their formation are highly diverse. Due to the fact that similar processes exist for structuring silica particles and films, only examples of structuring particles will be discussed. Porous silica particles are one morphological class that is of great interest, as their applications include drug delivery,^{31,32} chromatography³³ and catalysis.³⁴ In terms of pore size, porous silica particles fall under three different categories, which include micro- (< 2 nm), meso- (2 – 50 nm) and macroporous (> 50 nm). In this introduction, a brief description of mesoporous and macroporous silica particles will be provided, as they are relevant to this thesis. Mesoporous silica particles are highly sought after due to their high surface area (> 1800 m²g⁻¹)³⁵ and facile synthesis. For many years though, forming highly ordered mesoporous structures was problematic until the Mobil Corporation developed mesoporous MCM-41 particles. Silica-based MCM-41 particles have highly ordered cylindrical pores organized in a hexagonal packing due to the templating process utilized to form them. Cetyl trimethylammonium bromide (CTAB), is used as the templating agent by forming rod-like micelles, as shown in Figure 1.6 (with permission to reprint),³⁶ whereby a silica precursor such as TEOS associates with the surfactant, hydrolyzes and then undergoes templated condensation. CTAB removal is achieved either through calcination or through an aqueous washing. There are several other templating methodologies that exist to form mesoporous silica particles which include the use of various liquid crystals³⁷ and polymers.^{38,39}

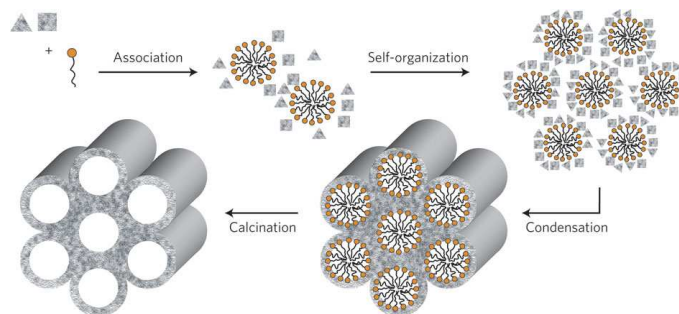


Figure 1.6: Synthesis of mesoporous MCM-41 silica particles³⁶

Another method for forming mesoporous silica particles was demonstrated by Voss et al. when utilizing sugar-modified silanes and poly(ethylene glycol) (PEG) as a steric stabilizer.⁴⁰ After synthesizing diglyceroxysilane (DGS), DGS was dissolved within an aqueous medium in the presence of PEG to form mesoporous silica particles. The cause for the porosity can be attributed to the entrainment of PEG within the silica particle and a phenomenon known as spinodal decomposition, which is the phase separation of a mixture that can still be highly interconnected.⁴¹ As the silica particles were forming, the silica- and PEG-rich components phase separated in a highly interconnected fashion. After the particles were calcined (heated at 450 °C) to burn off the PEG, a mesoporous structure was formed.

There are fewer literature reports on the synthesis of macroporous silica particles due to the limited number of methodologies. The most common methodology involves the use of other colloids as templates, which form the macropores of the final silica particle. Yi et al. described the use of polystyrene latex particles as a template from which the silica particle can grow, similar to the process shown in Figure 1.6.⁴² They demonstrated that various particle shapes (ellipsoid, concaved disk, etc.) with a high surface area ($> 180 \text{ m}^2\text{g}^{-1}$) could be achieved. On a slightly different note, Cademartiri et al. demonstrated that macroporous silica structures could be formed from silica particles. Similarly to the study done by Voss et al., DGS was used as the silica precursor and PEG was utilized for particle stabilization. However the use of high molecular weight PEG ($> 2000 \text{ g/mol}$) resulted in the formation of “sticky” silica particles that aggregated with one another to form a macroporous silica structure.

The hollow core-shell silica particle is another morphology that is widely used and studied as it has practical applications in drug delivery,⁴³ coatings⁴⁴ and as protective barriers.⁴⁵ The most common method to synthesize hollow silica particles involves the use of templates, similarly to the porous silica particles discussed above. Caruso et al. described the use of polystyrene colloids as templates for the formation of hollow silica particles.⁴⁶ As shown in Figure 1.7 (with permission to reprint)⁴⁶, the polystyrene colloid was first coated with a cationic polymer poly(diallyldimethylammonium chloride) (PDADMAC), which caused pre-formed silica particles to adhere to the polymer. Additional polymer and particle layers can be included in a layer-by-layer process to form a thicker particle shell. Finally, the template can be removed with an appropriate solvent or be calcined at high temperatures to form a pure hollow silica particle. Other methods for forming hollow silica particles include the use of emulsions,⁴⁷ microemulsions,⁴⁸ template-free mixtures,⁴⁹ etc.

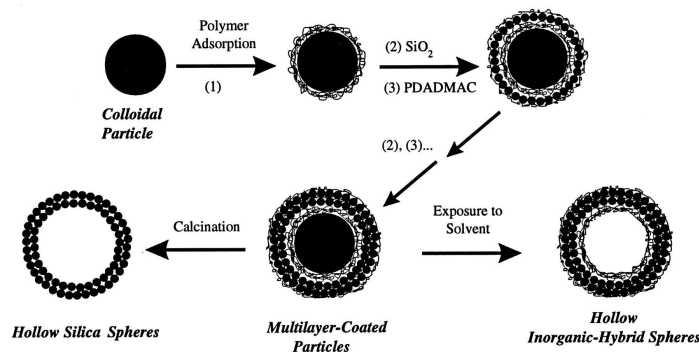


Figure 1.7: Formation of hollow silica particles with a colloidal template.⁴⁶

1.2.1.2 New Methodology for Forming Silica Particles

Although there are several efficient methods to form silica particles and films with a variety of morphologies, all of the sol-gel processes require an aqueous medium. This thesis explores the possibility of forming well defined silica particles within a hydrophobic medium. To be able to form and control silica particle morphology within an aqueous free medium was highly interesting, as water is required for hydrolysis and condensation to form particles. This gives rise to anionic and cationic interactions between the particle surface and the aqueous solution for particle stabilization. Due to

these issues, we have been unable to find any prior literature reporting well-defined silica particles within an organic medium without post-modifying existing silica particles. The different factors that affect particle growth, stability and morphology in a hydrophobic medium were investigated in detail. The motivation for this work was the development of new drug delivery vehicles. Traditionally, silica particles are first synthesized using the sol-gel method, isolated and then soaked within a saturated drug solution, which all could take several days. We considered that a one-pot methodology for forming drug loaded silica particles from a hydrophobic medium could be accomplished to give an alternative method.

1.3 Silicone Elastomers

Crosslinking silicone oils results in elastomeric materials that can vary dramatically in their physical properties. Several different cure chemistries, which differ in their mechanisms, can be used to produce silicone elastomers. Room temperature-catalyzed reactions will be the focus of the discussion below.

One of the most common methods for silicone elastomer curing involves the use of tin-based catalysts, which are commonly utilized for silicone sealants (caulking). Using a hydroxy-terminated silicone, alkoxy silane crosslinker and water as a co-catalyst, for example, a crosslinked silicone network is formed quite efficiently as seen in Figure 1.8.^{2,50} There are several different organotin compounds that can be utilized to catalyze silicone elastomer formation, which include dibutyltin dilaurate, dibutyltin diacetate, dimethyltin dibutyrate, etc.⁵¹ Hydrolysis of the tin catalyst by water is the first step of the catalytic sequence, followed by a nucleophilic attack of the alkoxy silane crosslinker. Once bound to tin, silicone silanol groups act as nucleophiles and attack the silicon atom bound to the tin alkoxide to form a Si-O-Si bond. This process then repeats and continues until a silicone network is formed.¹ Platinum-cured silicone elastomers are another industry standard: the cure process involves an addition reaction of Si-H compounds to C=C pi bonds. Two common Pt catalysts are Speier's H_2PtCl_6 and Karstedt's

¹ Note that regulators have expressed concern about the biological safety of tin compounds, and these catalysts have been identified for replacement.

$\text{Pt}_2(\text{H}_2\text{CHCSiMe}_2\text{OSiMe}_2\text{CHCH}_2)_n$ catalysts. Several products including implantable medical devices, prosthetics, etc., utilize this silicone elastomeric curing process.

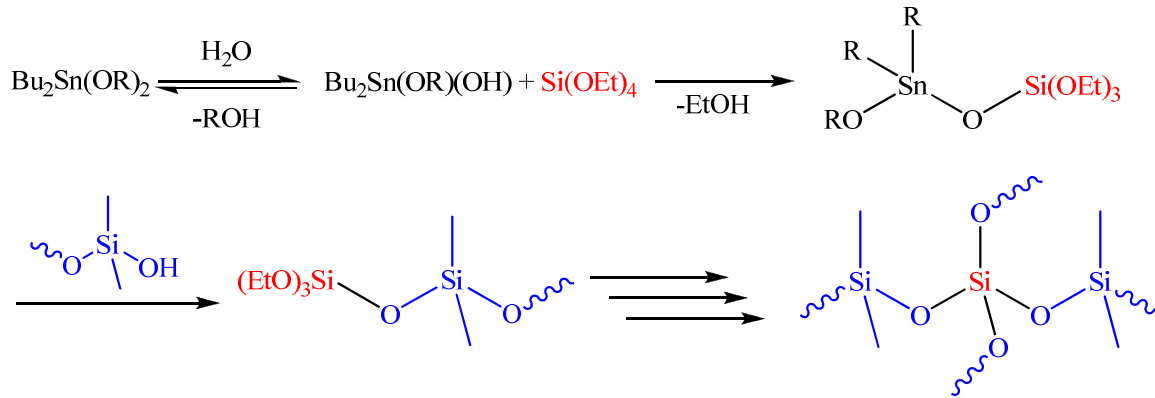


Figure 1.8: General reaction of tin catalyzed silicone elastomers.

These metal catalysts can also be utilized to promote other hydrosilane reactions. As an example, tin-based catalysts can promote the reduction of carbonyl and hydroxyl groups with hydrosilanes to form new silyl ethers. Platinum-based catalysts can reduce hydroxyl and carbonyl functional groups in commercial environments to produce various products, including silicone foams. For example, multifunctional hydrosilanes and vinylsilanes in the presence of water and Speier's catalyst (H_2PtCl_6) can crosslink to produce a silicone network with a few free silanol groups. The catalyst, with the addition of the hydrosilane, also reduces water to form an alkoxy silane and hydrogen gas, which acts as a "blowing agent" and gets trapped within the silicone network, thus forming a foam.² Other formulations stop at the elastomer stage.

The curing mechanisms of the tin and platinum catalysts are highly efficient, however, they can be biologically toxic, particularly tin (dibutyltin dilaurate \rightarrow $\text{LD}_{50} = 175\text{mg/kg}$). Removal of these catalysts at low concentrations is also difficult, thus medical or food-based silicone materials do not generally utilize tin-based catalysts. Acidic and basic catalysts, which are less toxic, are one alternative form for curing silicones. Catalysts such as acetic acid and triethylamine are examples of acidic and basic catalysts, respectively, that have been examined previously.⁵² This methodology for crosslinking is mechanistically identical to the sol-gel methodology mentioned earlier for silica formation, except that hydroxy-terminated silicone polymers are utilized for

elastomer formation, as shown in Figure 1.9. In acidic media, the alkoxy silane becomes protonated and the silanol functional group off the silicone acts as a nucleophile and attacks the alkoxy silane Si atom, thus forming alcohol as the byproduct. With base, the silicone silanol group becomes deprotonated to a silanolate group, which nucleophilically attacks the crosslinking alkoxy silane to form an elastomer. In the presence of water, a condensation side reaction between two silanol groups can occur, forming crosslinks. The stronger the acidic/basic catalyst is, the higher the rate of cure. However, the majority of acidic/basic catalysts are quite inefficient in comparison to their tin and platinum catalyst counterparts.

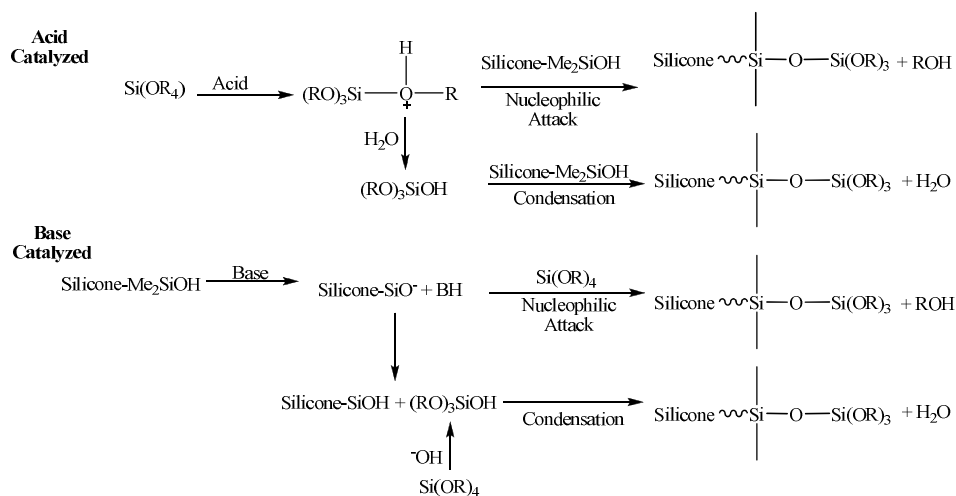


Figure 1.9: Acid and base catalyzed crosslinking of silicones.

1.3.1 Interfacial Structuring of Hydrophilic Materials in Silicone Elastomers

Silicone elastomers typically contain reinforcing agents such as fumed silica, since silicones are not mechanically robust on their own.^{13,53} Silica can be added to hydroxy-terminated silicone elastomers as silanol groups from both the silicone and silica undergo the condensation reaction to form new crosslinks (Figure 1.8 and Figure 1.9). Unmodified silica with surface silanol groups acts to provide rigid crosslinking sites, thus increasing the crosslink density of the elastomer.

Silicone interpenetrating networks (IPNs) are a class of elastomers that combine two or more polymers together, where at least one polymer forms a crosslinked network.^{54,55} The formation of two or more continuous phases is an important

morphological feature of IPNs (Figure 1.10⁵⁶) (with permission to reprint) and these materials are commonly utilized in the medical, automotive, industrial and construction based fields.⁵⁴ Silicone IPNs have been utilized as drug delivery depots⁵⁷⁻⁵⁹ or contact lens materials⁶⁰⁻⁶³ for medical based applications, due to their desirable properties. When forming silicone IPNs, the different continuous phases are typically hydrophobic (silicone) and hydrophilic. Abbasi et al. demonstrated that hydrophilic poly(hydroxyethyl methacrylate) (pHEMA) could be crosslinked within a swollen silicone rubber via radical polymerization to form a silicone hydrogel IPN.⁶⁴ A hydrogel is a solid/gelatinous material that is swollen with water due to the hydrophilic polymers in the material. The silicone-pHEMA IPN they formed was capable of swelling in the presence of water and was more mechanically robust (tensile strength, shear modulus, etc.) than a pure silicone rubber. Silicone IPNs are typically used in contact lenses to increase oxygen permeability, which is important to maintain healthy eyes.⁶⁵ As mentioned earlier, silicones have one of the highest oxygen permeability values of synthetic polymers,^{66,67} thus oxygen can travel through the silicone channels of the IPN towards the eye to prevent several complications.⁶⁸ Typical hydrophilic phases used in contact lenses include various methacrylates, methacrylic acid, *N*-vinylpyrrolidinone, etc.^{63,69} For applications in drug delivery, Brook et al. demonstrated that silicone IPNs could be utilized as drug release depots by using aminopropyl-terminated PDMS (AT-PDMS) as the basic catalyst, poly(ethylene oxide) (PEO) as the hydrophilic component and nicotine as the drug surrogate.⁵⁸ As water penetrated through the nicotine loaded PEO network, it carried the nicotine out of the continuous PEO phase and into solution.

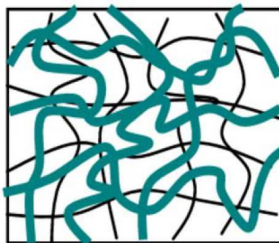


Figure 1.10: Generic depiction of a two phase IPN.⁵⁶

1.3.1.1 Determining the Factors that Affect the Structuring of Silicone-PEG Elastomers

One major issue with developing materials for drug delivery applications is the ability to control their structure. By understanding and controlling the factors that affect a material's morphology and internal structuring, drug delivery can be fine tuned. The structured silicone-PEO elastomer described by Brook et al.⁵⁸ demonstrated that a drug surrogate could be delivered, however the factors controlling the internal structuring of the elastomer and the surface morphology were not well understood. The atypical basic catalyst AT-PDMS is far less efficient at crosslinking silicone elastomers compared to the traditional metal catalysts and could potentially behave differently in the silicone-PEO pre-elastomer mixtures. Thus, the various factors that affect formation of these RTV cured silicone elastomers were investigated and varied to determine how to control their internal structuring of PEO and the surface morphology of these elastomers for potential drug delivery applications.

1.4 Siloxane Materials via the Piers-Rubinsztajn Reaction

Recently, the Piers-Rubinsztajn (PR) reaction has received a great deal of attention as it provides new synthetic routes to form organosilicon complexes in a rapid and facile manner. This reaction involves the coupling of hydrosilanes with alkoxy silanes with the use of the Lewis acidic $B(C_6F_5)_3$ catalyst (Figure 1.11).⁷⁰ This synthetic route can be utilized to form small siloxane molecules,⁷¹ large 3D structures⁷² and even elastomers/foams.⁷³ Many of the synthetic molecules and 3D networks produced with this reaction are either unavailable or difficult to form when using conventional organosilicon chemistry. For example, forming complex 3D siloxane architectures was shown to be rapid and facile by Thompson et al.⁷² Additionally, the use of expensive metals catalysts such as platinum can be avoided altogether.

Although this reaction is rapid and facile, metathesis of the different reagents can occur leading to the formation of different hydrosilane reaction partners (Figure 1.11). This becomes an issue, as a variety of products are now possible due to a loss of synthetic control. However, one effective method to reduce the magnitude of metathesis utilizes

different organic moieties. Silicon atoms bearing phenyl groups, for example, greatly reduce the possibility for metathesis to occur.⁷⁰

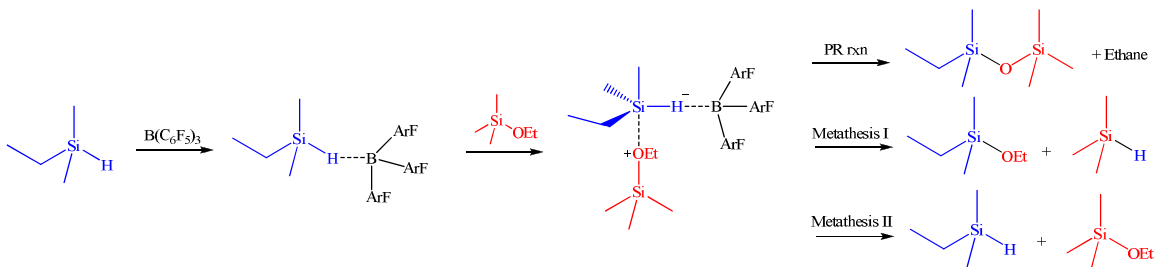


Figure 1.11: Piers-Rubinsztajn and metathesis reactions between hydrosilane and alkoxy silane.

Thompson et al. demonstrated that both sterics and temperature affect the efficiency of the PR reaction.⁷² The coupling of 1,1,1,3,5,5,5-heptamethyltrisiloxane and tetramethyl orthosilicate (TMOS) occurred at room temperature (RT), however, no reaction was observed with TEOS under the same conditions. By elevating the temperature to 60 °C, enough energy was present in the system for the PR reaction to occur and overcome steric hindrance. Thus, this reaction is highly sensitive to sterics due to the already bulky catalyst. Before this steric threshold is reached, the coupling of reagents such as tetramethyldisiloxane and tetrapropyl orthosilicate (TPOS) achieved higher yields compared to the less bulky TEOS and TMOS. Slower, milder conditions appear to favor higher product yields of the PR reaction.

Beyond the PR reaction, the boron catalyst can be utilized to form new silyl ethers between alcohols and hydrosilanes (Figure 1.12A). Blackwell et al. demonstrated that several silyl ethers (alkoxysilanes) can be formed by coupling hydrosilanes with a variety of alcohols.⁷⁴ Silyl ether formation is not as rapid as the PR reaction: in the former case typical reaction times run from tens of minutes to days. However, high yields of silyl ethers can be obtained depending on the reagents used and the reaction conditions. Additionally, the more sterically hindered the alcohol is, the faster the reaction proceeds. Alcohols are much better Lewis bases than alkoxy silanes, which results in them coordinating to the boron catalyst more strongly. Thus the larger the alcohol, the more difficult it is for it to co-ordinate to the bulky catalyst and inhibit silyl ether formation.

Silyl ether reactions that occur over days can be attributed to small alcohols coordinating quite strongly to the catalyst and leaving only small amounts of free catalyst available at any one time.

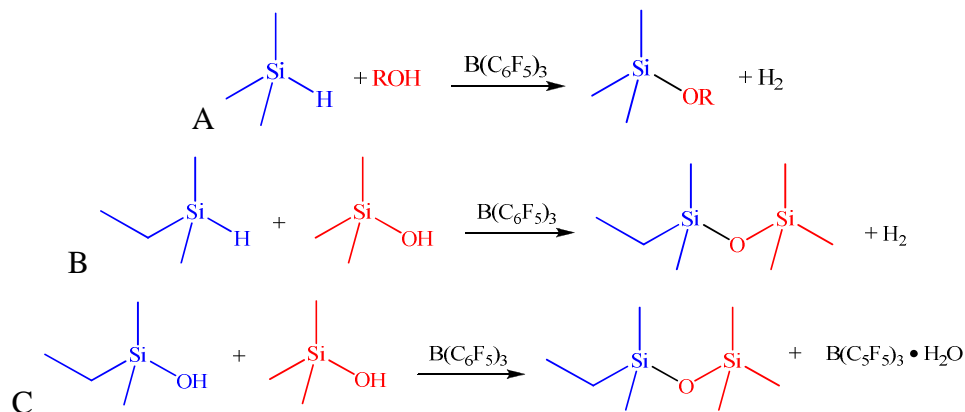


Figure 1.12: Silyl ether formation (A), silanol coupling with a hydrosilane (B) and silanol coupling with two silanol groups (C).

In general, the boron catalyst is quite robust in the presence of atmospheric water, as water is a good Lewis base that can bind to the boron catalyst and inhibit the PR reaction. Most of the reported articles on the PR reaction occur under bench top conditions and do not usually require moisture free conditions. In fact, Longuet et al. utilized the catalyst within an aqueous emulsion to form linear siloxane polymers via the PR reaction.⁷⁵ When the catalyst is added directly to water, several different boron-water complexes arise. One to three water molecules can be complexed to the boron catalyst which then act as weak acids.⁷⁶ The monohydrate complex $[\text{H}_2\text{O} \cdot \text{B}(\text{C}_6\text{F}_5)_3]$ has a pKa comparable to toluenesulfonic acid: surprisingly silicone redistribution is not normally observed.⁷⁰ Another reaction that is observed in the presence of the boron catalyst is silanol coupling (Figure 1.12B). Both hydrosilanes and alkoxy silanes can easily be hydrolyzed by water in the presence of the boron catalyst to produce hydrogen gas and water.⁷⁰ Similarly to alcohols, hydrosilanes can then couple with silanol groups to form new Si-O-Si linkages, which has frequently been observed in aqueous conditions. Two silanol groups also have the ability to couple together to form new siloxane linkages

(Figure 1.12C). These side reactions could be problematic as it results in a loss in synthetic control.

These mechanistic notes are important for the formation of silicone resins, which are insoluble crosslinked networks that contain a variety of different silicon units (M, D, T and Q). These materials are typically produced with a variety of chlorosilanes or epoxy modified silicones,^{4,77} in processes that can be difficult to control synthetically. More recently, Chojnowski et al. demonstrated that the PR reaction can be utilized to rapidly form various silicone resins.^{78,79} By varying the temperature and by carefully controlling the reaction conditions, hydrophobic DQ and TQ resins were formed without hydrolysis of the alkoxy silanes, which eliminated silanol formation. Developing Siloxane-based Films, Particles and Printable Inks

As mentioned earlier, the PR reaction provides a facile and rapid method to create siloxane based compounds and materials. There is still much to be understood with this reaction and its potential to form new and interesting materials is still in its infancy. Adapting from the various siloxane based resins that Chojnowski et al. developed, this thesis explores whether siloxane-based films and particles can be formed utilizing this chemistry. This methodology to form films and particles is an interesting alternative to the sol-gel method. Due to the completely different mechanisms of the PR reaction and water-based sol-gel chemistry, the different morphologies of films and particles are also discussed in this thesis. Furthermore, the ability to interface these boron-catalyzed siloxane resins with other materials was investigated. Porous substrates like paper (cellulose) were interfaced with the siloxane resins and were discovered to be rapid and effective methods to hydrophobize paper. This was important, as several paper-based technologies – including microfluidics – require effective hydrophobic barriers on paper. Thus, the ability for these boron catalyzed siloxane resins to effectively hydrophobize paper for potential paper-based applications is discussed.

1.5 Scope of the Thesis

This thesis explores unconventional methods for structuring silicones and silica at various interfaces to produce a variety of materials including silicone elastomers, silica

particles, siloxane-based films/particles and siloxane-modified paper. There are several studies already available that discuss forming these different materials. However, as shown in this introduction conventional chemistry, such as transition metal catalyzed hydrosilylation to form silicone elastomers and water-based sol-gel chemistry to form silica colloids and films, has some disadvantages. This thesis discusses the use of atypical amine-based catalysts to structure silicone elastomers with hydrophilic domains (Chapter 2). The function and effect of each parameter on internal hydrophilic structuring and surface morphology is investigated. From these same silicone elastomer systems, nearly monodisperse silica particles were formed in the absence of liquid water and discussed in Chapter 3. The ability to create such large silica particles in a hydrophobic environment is highly unusual, as most studies have followed the Stöber silica method, which occurs within an aqueous environment to form small (< 1 micron) silica particles. Further investigations in Chapter 4 demonstrate that silica particle morphology can also be controlled in either crosslinkable and non-crosslinkable silicone oils to form hollow and porous silica particles, respectively.

Expanding on unconventional methods to form siloxane-based materials, this thesis explores the use of the PR reaction to form silicone films and particles in Chapter 5. These materials are formed from siloxane-in-water (S/W) emulsions, which were investigated for their stability and chemical composition over time. The various film morphologies that could be produced with this system were investigated. Chapter 6 discusses the modification of paper utilizing siloxane-based inks. Instead of using the S/W emulsions, homogeneous mixtures of siloxanes with alcohols are delivered to the paper via an ink-jet printing methodology to form hydrophobic barriers. Their efficacy and potential application in paper-based microfluidics and diagnostics are discussed.

1.6 References

(1) Andriot, M.; Chao, S.; Colas, A.; Cray, S.; deBuyl, F.; DeGroot, J.; Dupont, A.; Easton, T.; Garaud, J.; Gerlach, E. *Silicones in Industrial Applications*; Nova Science Publishers, New York, 2009.

(2) Brook, M. A. *Silicon in Organic, Organometallic, and Polymer Chemistry*; Wiley-VCH Verlag, 2000.

- (3) Owen, M. J. *Chimie Nouvelle*, **2004**, 27.
- (4) Owen, M. J. *Siloxane Polymers*; Prentice Hall: Englewood Cliffs, 1993.
- (5) Colas, A.; Curtis, J. *Silicone biomaterials: history and chemistry*, 2004.
- (6) Ward, W. J.; Ritzer, A.; Carroll, K. M.; Flock, J. W. *J. Catal.*, **1986**, 100, 240.
- (7) de Buyl, F. *Int. J. Adhes.*, **2001**, 21, 411.
- (8) Hu, S.; Liu, C.; Wen, J.; Dai, W.; Wang, S.; Su, H.; Zhao, J. *Forensic Sci. Int.*, **2013**, 226, 48.
- (9) Losic, D.; Yu, Y.; Aw, M. S.; Simovic, S.; Thierry, B.; Addai-Mensah, J. *Chem. Commun.*, **2010**, 46, 6323.
- (10) Kröger, N.; Deutzmann, R.; Sumper, M. *Science*, **1999**, 286, 1129.
- (11) Sumper, M. *Science*, **2002**, 295, 2430.
- (12) Otzen, D. *Scientifica*, **2012**, 2012, 22.
- (13) Boonstra, B. B.; Cochrane, H.; Dännenberg, E. M. *Rubber. Chem. Technol.*, **1975**, 48, 558.
- (14) Edwards, D. C. *J. Mater. Sci.*, **1990**, 25, 4175.
- (15) Brinker, C. J.; Scherer, G. W. *Sol-gel science: The physics and chemistry of sol-gel processing*; Access Online via Elsevier, 1990.
- (16) Stöber, W.; Fink, A.; Bohn, E. *J. Colloid Interface Sci.*, **1968**, 26, 62.
- (17) Bridger, K.; Fairhurst, D.; Vincent, B. *J. Colloid Interface Sci.*, **1979**, 68, 190.
- (18) Van Blaaderen, A.; Van Geest, J.; Vrij, A. *J. Colloid Interface Sci.*, **1992**, 154, 481.
- (19) Strawbridge, I.; James, P. F. *J. Non-Cryst. Solids*, **1986**, 82, 366.
- (20) Morikawa, A.; Iyoku, Y.; Kakimoto, M.-a.; Imai, Y. *Polym. J.*, **1992**, 24, 107.
- (21) Glaser, R. H.; Wilkes, G. L.; Bronnimann, C. E. *J. Non-Cryst. Solids*, **1989**, 113, 73.
- (22) Sharp, K. G. *J. Mater. Chem.*, **2005**, 15, 3812.
- (23) Everett, D. H. *Basic Principles of Colloid Science*; RSC Paperbacks, 1988.
- (24) Verwey, E.; Overbeek, J. T. G. *Theory of the stability of lyophobic colloids*; Amsterdam: Elsevier, 1948.
- (25) Schenkel, J. H.; Kitchener, J. A. *Trans. Faraday Soc.*, **1960**, 56, 161.
- (26) Hogg, R.; Healy, T. W.; Fuerstenau, D. W. *Trans. Faraday Soc.*, **1966**, 62, 1638.
- (27) Lu, Y.; Ganguli, R.; Drewien, C. A.; Anderson, M. T.; Brinker, C. J.; Gong, W.; Guo, Y.; Soyez, H.; Dunn, B.; Huang, M. H.; Zink, J. I. *Nature*, **1997**, 389, 364.
- (28) Grosso, D.; Babonneau, F.; Albouy, P.-A.; Amenitsch, H.; Balkenende, A. R.; Brunet-Bruneau, A.; Rivory, J. *Chem. Mater.*, **2002**, 14, 931.
- (29) Khramov, A. N.; Collinson, M. M. *Chem. Commun.*, **2001**, 767.

- (30) Kanungo, M.; Collinson, M. M. *Chem. Commun.*, **2004**, 548.
- (31) Slowing, I. I.; Vivero-Escoto, J. L.; Wu, C.-W.; Lin, V. S. Y. *Adv. Drug Deliv. Rev.*, **2008**, *60*, 1278.
- (32) Manzano, M.; Aina, V.; Areán, C. O.; Balas, F.; Cauda, V.; Colilla, M.; Delgado, M. R.; Vallet-Regí, M. *Chem. Eng. J.*, **2008**, *137*, 30.
- (33) Gallis, K. W.; Araujo, J. T.; Duff, K. J.; Moore, J. G.; Landry, C. C. *Adv. Mater.*, **1999**, *11*, 1452.
- (34) Takahashi, H.; Li, B.; Sasaki, T.; Miyazaki, C.; Kajino, T.; Inagaki, S. *Chem. Mater.*, **2000**, *12*, 3301.
- (35) Thanabodeekij, N.; Sathayanon, S.; Gulari, E.; Wongkasemjit, S. *Mater. Chem. Phys.*, **2006**, *98*, 131.
- (36) Tolbert, S. H. *Nat. Mater.*, **2012**, *11*, 749.
- (37) Beck, J. S.; Vartuli, J. C.; Roth, W. J.; Leonowicz, M. E.; Kresge, C. T.; Schmitt, K. D.; Chu, C. T. W.; Olson, D. H.; Sheppard, E. W. *J. Am. Chem. Soc.*, **1992**, *114*, 10834.
- (38) Fan, H.; Van Swol, F.; Lu, Y.; Brinker, C. J. *J. Non-Cryst. Solids*, **2001**, *285*, 71.
- (39) Ciriminna, R.; Fidalgo, A.; Pandarus, V.; Béland, F.; Ilharco, L. M.; Pagliaro, M. *Chem. Rev.*, **2013**, *113*, 6592.
- (40) Voss, R.; Brook, M. A.; Thompson, J.; Chen, Y.; Pelton, R. H.; Brennan, J. D. *J. Mater. Chem.*, **2007**, *17*, 4854.
- (41) Favvas, E.; Mitropoulos, A. C. *J. Eng. Sci. Tech. Rev.*, **2008**, *1*, 25.
- (42) Yi, G.-R.; Moon, J. H.; Yang, S.-M. *Chem. Mater.*, **2001**, *13*, 2613.
- (43) Yang, J.; Lee, J.; Kang, J.; Lee, K.; Suh, J.-S.; Yoon, H.-G.; Huh, Y.-M.; Haam, S. *Langmuir*, **2008**, *24*, 3417.
- (44) Chen, J.-F.; Ding, H.-M.; Wang, J.-X.; Shao, L. *Biomaterials*, **2004**, *25*, 723.
- (45) Lu, A.-H.; Salabas, E. L.; Schüth, F. *Angew. Chem. Int. Ed.*, **2007**, *46*, 1222.
- (46) Caruso, F.; Caruso, R. A.; Möhwald, H. *Science*, **1998**, *282*, 1111.
- (47) Park, J.-H.; Oh, C.; Shin, S.-I.; Moon, S.-K.; Oh, S.-G. *J. Colloid Interface Sci.*, **2003**, *266*, 107.
- (48) Jafelicci Jr, M.; Rosaly Davolos, M.; José dos Santos, F.; José de Andrade, S. *J. Non-Cryst. Solids*, **1999**, *247*, 98.
- (49) Hah, H. J.; Kim, J. S.; Jeon, B. J.; Koo, S. M.; Lee, Y. E. *Chem. Commun.*, **2003**, 1712.
- (50) Vanderweij, F. W. *Makromol. Chem.*, **1980**, *181*, 2541.
- (51) Beers, M. D.; Thompson, J. E., *US 4673750*, **1987**, *Loctite Corporation*.
- (52) Chu, H.-K.; Cross, R. P.; Crossan, D. I. *J. Organomet. Chem.*, **1992**, *425*, 9.
- (53) Galanti, A. V.; Sperling, L. H. *Polym. Eng. Sci.*, **1970**, *10*, 177.
- (54) Sperling, L. H.; Mishra, V. *Polym. Adv. Tech.*, **1996**, *7*, 197.

- (55) Sperling, L. H. In *Encyclopedia of Polymer Science and Technology*; John Wiley & Sons, Inc.: 2002.
- (56) Suo, Z.; Zhu, J. *Appl. Phys. Lett.*, **2009**, *95*, 232909.
- (57) Liu, L.; Sheardown, H. *Biomaterials*, **2005**, *26*, 233.
- (58) Brook, M. A.; Holloway, A. C.; Ng, K. K.; Hrynyk, M.; Moore, C.; Lall, R. *Int. J. Pharm.*, **2008**, *358*, 121.
- (59) Ratner, B. D.; Kwok, C.; Walline, K.; Johnston, E.; Miller, R. J., WO2004000382, **2003**, Genzyme Corporation.
- (60) Jones, D. *Elastomerics*, **1988**, *120*, 12.
- (61) Jones, L.; Senchyna, M.; Glasier, M. A.; Schickler, J.; Forbes, I.; Louie, D.; May, C. *Eye Contact Lens*, **2003**, *29*, S75.
- (62) Lai, Y.-C.; Baccei, L. J. US 6312706 B1, **2001**, Bausch & Lomb Incorporated
- (63) Nicolson, P. C.; Vogt, J. *Biomaterials*, **2001**, *22*, 3273.
- (64) Abbasi, F.; Mirzadeh, H.; Katbab, A. A. *J. Appl. Polym. Sci.*, **2002**, *85*, 1825.
- (65) Holden, B. A.; Mertz, G. W. *Invest. Ophthalmol. Vis. Sci.*, **1984**, *25*, 1161.
- (66) Robb, W. L. *Ann. N. Y. Acad. Sci.*, **1968**, *146*, 119.
- (67) Zhang, H.; Cloud, A. Global advances in materials and process engineering; Dallas, TX, 2006.
- (68) Baron, R. C.; Chabreck, P.; Domschke, A.; Griesser, H. J.; Ho, A.; Hopken, J.; Laycock, B. G.; Liu, Q.; Lohmann, D.; Meijs, G. F., US 5965631, **1999**, Ciba Vision Corporation
- (69) Bohnert, J. L.; Horbett, T. A.; Ratner, B. D.; Royce, F. H. *Invest. Ophthalmol. Vis. Sci.*, **1988**, *29*, 362.
- (70) Brook, M.; Grande, J.; Ganachaud, F.; Muzafarov, A. M., Ed.; Springer Berlin: 2011; Vol. 235, p 161.
- (71) Grande, J. B.; Thompson, D. B.; Gonzaga, F.; Brook, M. A. *Chem. Commun.*, **2010**, *46*, 4988.
- (72) Thompson, D. B.; Brook, M. A. *J. Am. Chem. Soc.*, **2007**, *130*, 32.
- (73) Grande, J. B.; Fawcett, A. S.; McLaughlin, A. J.; Gonzaga, F.; Bender, T. P.; Brook, M. A. *Polymer*, **2012**, *53*, 3135.
- (74) Blackwell, J. M.; Foster, K. L.; Beck, V. H.; Piers, W. E. *J. Org. Chem.*, **1999**, *64*, 4887.
- (75) Longuet, C.; Joly-Duhamel, C.; Ganachaud, F. *Macromol. Chem. Phys.*, **2007**, *208*, 1883.
- (76) A. Danopoulos, A.; R. Galsworthy, J.; L. H. Green, M.; H. Doerrer, L.; Cafferkey, S.; B. Hursthouse, M. *Chem. Commun.*, **1998**, 2529.
- (77) Ariga, K.; Gomyo, S. US 4141926 A, **1979**, Shin-Etsu Chemical Co., Ltd.

(78) Chojnowski, J.; Rubinsztajn, S.; Fortuniak, W.; Kurjata, J. *Macromolecules*, **2008**, *41*, 7352.

(79) Kurjata, J.; Fortuniak, W.; Rubinsztajn, S.; Chojnowski, J. *Eur. Polym. J.*, **2009**, *45*, 3372.

Chapter 2 – Structured Hydrophilic Domains on Silicone Elastomers[†]

2.1 Abstract

The controlled generation of hydrophilic structures within hydrophobic polymers can be challenging. Very few examples of such structures have been described for silicones. We now report that such structures can be encoded in the air-contacting layer of a silicone elastomer by the formation of silica domains from tetraethoxysilane, optionally in the presence of poly(ethylene glycol) (PEG), using a surface active aminopropylsilicone catalyst and moisture cure. The control of the relative modulus at the upper versus lower layers and the degree and type of hydrophilic structuring requires control over the efficiency of delivery of water to the core of the pre-elastomer, which is facilitated by the surface active catalyst and may additionally be manipulated by the addition of PEG.

2.2 Introduction

Silicone elastomers are widely used as biomaterials, amongst other reasons, because of their facile fabrication in a variety of complex shapes, their high oxygen permeability, which is required in ophthalmic applications such as contact lenses,¹ and the very low degree to which the human body responds to these synthetic materials.² However, silicones are exceptionally hydrophobic, with surface energies at or below 23 nN m⁻¹.^{3,4} While this can be beneficial in treatments to reduce the intensity of scar tissue,⁵ more frequently, consequent lipid uptake⁶ and protein adsorption⁷ at biomaterials interfaces can compromise otherwise useful silicone-based devices. Silicone elastomers

[†] The following chapter was reproduced by permission of the Royal Society of Chemistry. The paper was published in *Polymer Chemistry* with the citation: Vinodh Rajendra, Yang Chen, Michael A. Brook, *Polym. Chem.*, **2010**, *1*, 312.

I was responsible for all synthesis and analysis. Both Dr. Chen and Dr. Brook gave some useful advice and troubleshooting ideas. I wrote the 1st draft of the manuscript and Dr. Brook helped with editing the document for final submission to the above journal.

have also been broadly used as components in drug delivery systems. With rare exception,⁸⁻¹⁰ only hydrophobic drugs that readily diffuse through silicones have been delivered, either internally or topically.¹¹ The delivery of hydrophilic drugs from silicones, by contrast, requires internal structuring of the silicone such that water can penetrate, and the hydrophilic drug can then escape the body of the silicone elastomer. Such structuring has previously been achieved by the use of proteins,⁸ or the use of surfactants generated by the drug itself.⁹ The objective of the current study was to develop synthetic strategies that would permit the structuring of silicones in two different ways. First, it should be possible to control the hydrophilicity and roughness of the interface that would ultimately contact a biological environment and, second, the silicone elastomer proximal to the external interface should be internally structured so that the modulus can be controlled and that hydrophilic domains can be incorporated, which would ultimately mediate the release profile of hydrophilic drugs. Both elements should affect in a positive way the biocompatibility of silicone elastomers. The strategy adopted makes use of previous observations⁹ that poly(ethylene glycol) (PEG), a polymer widely recognized for its biocompatibility,¹² can be incorporated in silicones to facilitate water ingress and subsequent rates of bioactive release. Although there have been several studies in which internal structuring of two different domains was accomplished using covalent linkages,^{13,14} we chose to use PEG that was not chemically tethered to the silicone. Instead, structuring was provided by the presence of silica synthesized in situ during polymerization. We describe below the preparation of silicone elastomers with structurally controlled surface chemistry, morphology and, additionally, internal structuring of the silicone in the vicinity of the air interface, by use of a combination of cure kinetics and surface active agents.

2.3 Experimental section

Materials

Fluorescein (Aldrich), ninhydrin (Pierce), tetraethoxysilane (TEOS, 99.999%, Aldrich), hydroxy-terminated PDMS (1800–2200 cSt, ~36 000 g mol⁻¹, Aldrich)

aminopropyl-terminated PDMS (10–15 cSt, $\sim 875 \text{ g mol}^{-1}$, Gelest), poly(ethylene glycol)(PEG, 1000 g mol^{-1} , Aldrich), and the rake surfactant seen in 1 (silicone backbone, ethylene oxide/propylene oxide side chains, DC 3225C (Figure 2.1), (Dow Corning) were used as received.

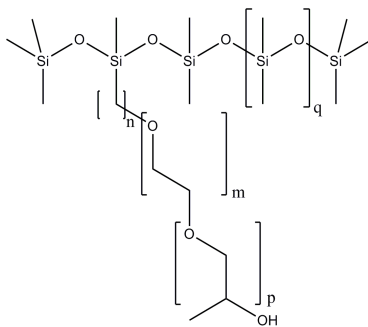


Figure 2.1: Structure of DC 3225C.

Characterization

Detection and characterization of PDMS, aminopropyl-terminated PDMS and PEG content of elastomers were established using ^1H NMR performed on a Bruker AV-200 spectrometer operating at 200.13 MHz. In the case of extracts from the elastomer disks, trimethoxybenzene (TMB) was used as an internal standard and was prepared by first making a stock solution containing approximately 0.03g of TMB in 1 mL of CDCl_3 .

Elastomer preparation

Silicone elastomers were prepared by mixing various quantities of hydroxy-terminated PDMS, PEG, aminopropyl-terminated PDMS, and TEOS (Table 2.1). Efficient mixing required a precise order of adding ingredients. PDMS was measured using a 5 ml plastic syringe and poured into a 20 ml glass vial. PEG was pre-weighed and then placed into the glass vial where it was weighed once again, TEOS was added using an Eppendorf 1000 ml pipette and then the mixture was gently heated to a temperature of $\sim 60^\circ\text{C}$ for approximately 1–2 min. This step was continued until the PEG liquefied. After cooling for 30 s, the aminosilicone catalyst was added to the mixture and then manually mixed for approximately 5 min, leading to a cloudy liquid. Some of the formulations additionally made use of the surfactant DC3225c, in which case it was added using a

1000 μ l Eppendorf pipette immediately after the mixture had cooled to room temperature. The mixture was then poured into a plastic Petri dish (35 mm diameter) lined with a Teflon film and allowed to cure at room temperature for 3–4 days. Some of the elastomers were cured under constant humidity using an ESL-2CA constant humidity chamber (ESPEC) at room temperature at 90% relative humidity, over the course of 3–4 days. In some experiments, disposable polystyrene cuvettes (1 x 1 x 4.5 cm, Aldrich) were used instead of Petri dishes. Once cured, the elastomers were cut out as circular disks using a 0.6 cm diameter coring tool for further use.

Preparation of ninhydrin solution and testing for the location of amines in the elastomer

Circular elastomer disks were prepared as shown in Figure 2.2, and placed within 20 ml glass vials to which approximately 5 ml of a 1wt% ninhydrin solution in reagent grade methanol were added. Samples were left for 30 min in the solution and thereafter the samples were checked by eye for a positive response (purple color change).¹⁵

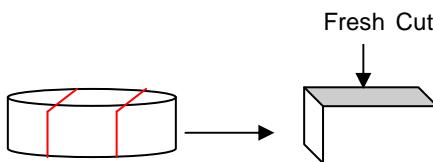


Figure 2.2: Preparation of elastomers for fluorescence microscopy.

Soxhlet extraction

Elastomer disks were placed in cellulose extraction thimbles and then Soxhlet extracted with reagent grade hexanes overnight. Elastomers were then dried in a vacuum oven at room temperature overnight. The differences in weight were noted and ^1H NMR spectra were taken of the extracted solution after evaporation of the hexanes. Characterization of elastomer extracts except the elastomers made with 5% TEOS exhibited a phase-separated liquid on the surface. The characterization of the surface liquid involved coring a circular disk 0.6 cm in diameter and then washing it with 1 mL of CDCl_3 , with which the ^1H NMR was taken (see Supplementary Information).

Surface analysis and imaging

Circular disks were cut out as described below and characterized by X-ray photoelectron spectrophotometry (XPS, University of Toronto) using a Thermo Scientific Theta Probe XPS spectrometer (ThermoFisher, E. Grinstead, UK) in standard mode. The angles were taken relative to the surface normal. A monochromatic Al K α X-ray source was used, with a spot area of 400 μm . Charge compensation was provided utilizing the combined e $^-$ /Ar $^+$ flood gun. The position of the energy scale was adjusted to place the main C 1s feature (C–C) in the high resolution spectrum at 284.4 eV, the literature value for PDMS.¹⁶ Data processing was performed using the software (Avantage) provided with the instrument. Figure 2.4 shows an approximately linear decrease in the atomic% of nitrogen measured on elastomer surfaces at take-off angles of 30°, 50° and 70° as a function of TEOS concentration. For one sample, XPS was performed using the K α probe at 20°, 30° and 90°.

Scanning electron microscope (SEM) images of elastomers were obtained using a JEOL 7000F SEM at an accelerating voltage of 5 kV. Energy dispersive X-ray (EDX) analysis was performed on the JEOL 7000F SEM at 10 kV. When obtaining cross sections, elastomers were initially frozen in liquid nitrogen and then fractured before mounting.

Table 2.1: Composition of elastomers (all values in 2.5g total mass)^a

Entry	PDMS	TEOS	Aminopropyl-terminated PDMS	PEG	DC 3225c
Controls (entries 1-5)	2.125-1.625 (85-65%)	0.125-0.625 (5-25%)	0.250 (10%)	0	0
Varying TEOS (entries 6-10)	2.000-1.500 (80-60%)	0.125-0.625 (5-25%)	0.250 (10%)	0.125 (5%)	0
Varying Catalyst (entries 11-13)	1.900-1.750 (76-70%)	0.375 (15%)	0.100-0.250 (4-10%)	0.125 (5%)	0
Controls at 90% Humidity (entries 14-18)	2.125-1.625 (85-65%)	0.125-0.625 (5-25%)	0.250 (10%)	0	0
Varying TEOS at 90% Humidity (entries 19-23)	2.000-1.500 (80-60%)	0.125-0.625 (5-25%)	0.250 (10%)	0.125 (5%)	0
1% 3225C (entry 24)	1.725 (69%)	0.375 (15%)	0.250 (10%)	0.125 (5%)	0.025 (1%)
5% 3225C (entries 25-27)	1.775-1.700 (71-68%)	0.375 (15%)	0.100-0.175 (4-7%)	0.125 (5%)	0.125 (5%)

^a Refers to specific formulations described more detail in SI.

Surface roughness – profilometry

Circular elastomer disks, with a diameter of 0.6 cm, were gold coated with an Edwards Sputter Coater S150B (using a rate of $\sim 15 \text{ nm min}^{-1}$) for 30 s to give a 7.5 nm thick coating. Surface roughness was measured with a WYKO NT1100 optical profiler equipped with the Vision32 software that imaged the surface texture of the silicone elastomers. Imaging was performed at 5x and 20x magnification with the low magnification PSI setting turned on at the profilometer, but run in VSI mode in the software, as greater image quality was achieved.

Preparation of fluorescein-containing elastomers and use of the optical microscope

Optical microscopy was used to image the surface of the elastomers and to determine the type of internal structuring of the silicone. Surfaces and hydrophilic PEG/silica domains were visualized using a 1.2 mM solution of fluorescein (0.008 g, 0.024 mmol) in distilled water (20 mL). The circular elastomer disks of interest were cut as shown in Fig. 2 and then were placed within 20 ml glass vials. Approximately 5ml of fluorescein solution were added to the vials using a glass pipette, which were stored in the dark for approximately 3–4 days and then analyzed using fluorescence spectroscopy. For imaging, the samples were first quickly rinsed with distilled water and then placed onto glass slides underneath an Olympus BX51 microscope fitted with a Q-imaging, Retiga EXi camera. Fluorescence and light microscopy images were taken of the elastomers and recorded on the Image Pro-Plus software by Media Cybernetics. Wavelengths of the elastomer surfaces were performed using the Image Pro-Plus software.

2.4 Results

Silicone elastomers were prepared using a room temperature vulcanization (RTV) system that involved TEOS ($\text{Si}(\text{OEt})_4$) as the crosslinker and hydroxy-terminated dimethylsilicone ($\text{HO}(\text{Me}_2\text{SiO})_n\text{H}$) 36 000 M_w as the bridging linear polymer (Figure 2.3). No filler was added. However, excess TEOS was added to the recipe, which led to the generation of silica in situ, a process described by Mark and others.¹⁷ Low molecular weight aminopropyl- terminated PDMS (referred to as ‘catalyst’ below) was utilized as the hydrolysis/condensation catalyst. Note that amine catalysts are far inferior, with respect to rate of cure, to the more commonly used tin- and titanium-based catalysts.¹⁸ This can be attributed to the amine’s slow deprotonation water or silanol groups to catalyze crosslinking ($\text{pK}_a_{\text{NH}_4^+} = 9.3$ vs. $\text{pK}_a_{\text{H}_2\text{O}} = 15.6$ and $\text{pK}_a_{\text{Si-OH}} = 13.6$). However, we wished to avoid the use of metals in these elastomers that may be targeted for biomaterials’ applications. The final requirement for cure is water, which is important both for cure, and for the generation of silica. Hydrophilic domains were to be introduced into the elastomer using two strategies: silica formed from TEOS hydrolysis, as noted above, and the use poly(ethylene glycol), which was optionally added into the pre-

elastomer formulation. It was recognized that efficient distribution of the PEG into the silicone, particularly as channels rather than droplets, might require the presence of surface-active agents because of the near immiscibility of the two materials. Therefore, a silicone surfactant based on PEG and silicones (DC 3225C) was optionally added to the pre-elastomer mixture. Thus, mixing the precursors (Table 2.1, Table 2.2), placing them in an open vessel lined with a Teflon® film and allowing them to cure at ambient temperature for up to 4 days led to translucent or opaque silicone elastomers.

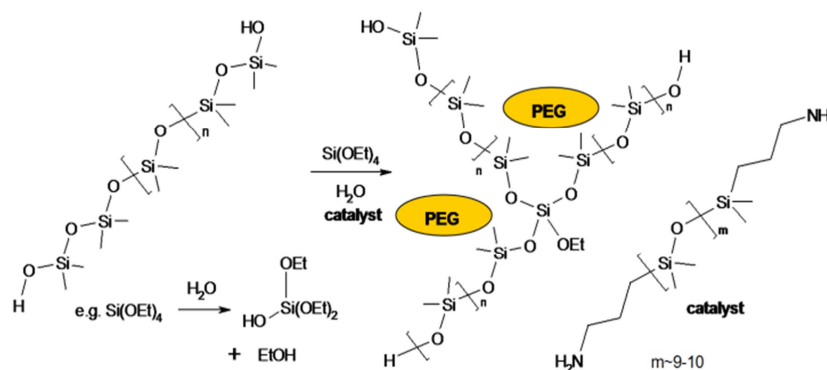


Figure 2.3: General chemical equation for RTV silicone crosslinking

Controlling cure asymmetry

RTV silicones are usually formulated with all required reagents, except water, which is provided by humidity in the environment. As a consequence, cure in such silicones initially takes place at the outer, air-contacting surface, and then proceeds further into the uncured body as moisture migrates through the silicone. Formulation is normally optimized so that a homogeneous elastomer is produced. Our objective was to create surface-modified silicones with hydrophilic domains, which could be accomplished by controlling the relative rates of crosslinking, silica formation, and the rates of diffusion of reagents through the uncured mixture. The silicones formulated here cured slowly and, only exceptionally, led to homogenous materials. In general, the elastomer cured asymmetrically, generating an elastomer with a higher modulus proximal to the air-contacting surface, and softer elastomers beneath. The natures of the silicones produced were examined as a function of aminopropylsilicone catalyst, water, and TEOS concentrations.

Table 2.2: General observations and homogeneity of all elastomers

Entry	Elastomer ^a	Translucent or Opaque	Phase Separation	Homogeneous (Y/N)	Surface Hardness ^b	Bottom Hardness ^b
Effect of TEOS		Humidity = 20-30%				
Samples	Without PEG					
1	5% TEOS	T	Liquid on surface	Y	3	3
2	10% TEOS	T	None	N	5	3
3	15% TEOS	T	None	N	7	4
4	20% TEOS	T	None	N	8	2
5	25% TEOS	T	None	N	10	1
Samples	Containing PEG					
6	5% TEOS	O	Liquid on surface	Y	4	4
7	10% TEOS	O	None	N	5	4
8	15% TEOS	O	None	N	7	4
9	20% TEOS	O	None	N	8	4
10	25% TEOS	O	None	N	10	5
Effect of Catalyst		Humidity = 20-30%				
11	10% Cat.	O	None	N	7	4
12	7% Cat.	O	None	N	6	4
13	4% Cat.	O	None	Y	5	5
Effect of Humidity		Humidity = 90%				
Samples	Without PEG					
14	5% TEOS	T	Liquid on surface	Y	4	4
15	10% TEOS	T	None	Y	5	5

16	15%TEOS	T	None	Y	5	5
17	20%TEOS	T	None	N	6	5
18	25%TEOS	T	None	N	8	4
Samples	Containing PEG					
19	5%TEOS	O	Liquid on surface	Y	4	4
20	10%TEOS	O	None	Y	5	5
21	15%TEOS	O	None	Y	5	5
22	20%TEOS	O	None	N	6	5
23	25%TEOS	O	None	N	6	5
Effect of Surfactant		Humidity = 20-30%				
24	1% S, 10% Cat.	O	None	N	7	5
25	5%S, 10% Cat.	O	None	N	7	5
26	5%S, 7% Cat.	O	None	N	6	5
27	5%S, 4% Cat.	O	None	Y	5	5

^a For more detailed formulations see Table 2.2. ^b Arbitrary hardness scale where 1 = viscous liquid, 5 = shore A hardness of 40, 10 = hard/brittle rubber.

Effect of varying crosslinker concentration

A series of elastomers were prepared with and without PEG in which the crosslinker wt% was varied (Table 2.2). At low crosslinker concentrations (5 wt%), a viscous liquid was extruded onto the surface of the elastomer after cure. The nature of this separated liquid will be discussed below. Otherwise, the greater the concentration of TEOS, the greater was the difference in modulus between the outer surface (from 10 μm to 2 mm) and the remainder of the elastomer. At the extremes of the materials prepared, the outer surface was a brittle, friable layer, and the underlying silicone an almost uncured gel-like material. When PEG was also included in a given formulation, the elastomers cured more homogeneously, with lower differences in moduli between exposed and underlying elastomers (Table 2.2).

Effect of varying catalyst concentration

Elastomers were prepared using high catalyst concentrations between 4 and 10%, with the crosslinker fixed at 15%. The asymmetry of cure increased with increasing catalyst concentration: only elastomers prepared with 4% catalyst were homogeneous (Table 2.2).

Effects of Humidity

Atmospheric water is a co-catalyst for silicone crosslinking and a reagent for TEOS hydrolysis. The cure rate, not surprisingly, was directly affected by moisture in the environment. More significant was the interplay between humidity, TEOS concentration and asymmetry with which the elastomers cured. At high humidity (e.g., 90% relative humidity, RH) and TEOS concentrations below 15%, the resulting elastomers were homogenous: less water or more TEOS led to asymmetric elastomers that were more highly cured at the air interface. Lower surface/volume ratios of the curing vessel will reduce the efficiency with which water can penetrate the curing pre-elastomer. For example, a recipe that led to homogenous elastomers prepared in a high surface area/volume Petri dish (e.g., 15% TEOS, 90% RH), was asymmetric when cured in a 1 x 1 x 4.5 cm cuvette; the top 0.5 cm was much harder than the remaining 4 cm depth.

Relative rates: cure vs. reagent diffusion in the silicone

The ingress of atmospheric water controls the asymmetry of cure. Under conditions of high water concentration (e.g., 90% RH), diffusion of water through the curing silicone occurred more rapidly than crosslinking and diffusion of TEOS to the air interface, such that the entire body underwent nearly simultaneous cure. PEG, when added into the pre-elastomer mixture, acts to wick or transmit water into the silicone, leading to a lower degree of cure asymmetry than when PEG is omitted from formulae. Any factor that reduces the rate of water ingress, when compared to diffusion or crosslinking processes through the silicone, will lead to an asymmetric cure. At higher catalyst or TEOS loadings, for instance, the rates of cure/silica formation at the interface overwhelm the ability of water to penetrate the silicone, leading to asymmetry and, at the extremes, brittle resins on the surface, and lightly cured gels beneath. Asymmetric RTV systems are avoided in commerce by controlling the viscosity of the uncured silicone, for example by the use of fillers.

Structuring silicone interfaces

The development of more biocompatible surfaces requires control of a variety of different structural features including surface geometry, hydrophilicity, and internal structuring. Control of the hydrophilic silica/PEG domains within the elastomer is important for the delivery of bioactives.⁹ In the remainder of the manuscript, we examine in detail the structural features of the more highly cured, upper elastomer interface.

Surface chemistry

Asymmetric cure is a consequence of higher reaction rates at the air interface. The distribution of amine groups, from the RTV catalyst, aminopropylsilicone, within the silicone matrix was investigated colorimetrically, and by XPS. After submersing elastomer disks into a ninhydrin solution, asymmetric elastomers exhibited the characteristic purple color, arising from reaction of ninhydrin with amines,¹⁵ preferentially at the air interface (Figure 2.4): a gradient in color existed from air interface inwards and, therefore, catalyst concentration decreased from the air surface to the

silicone interior. Note that sides of the elastomer disks cut from a larger sample, and bottom surfaces that contacted the Teflon® sheet exhibited no color.

Angular-dependent XPS measurements also showed that the amine preferentially resided at the air interface. As noted above, asymmetry of the elastomer increased with TEOS concentration. Asymmetry correlated inversely with the amine concentration at the air interface (Figure 2.4, see also SI): more highly asymmetric materials exhibited lower surface levels of amine. In the case of the elastomer prepared with only 5 wt% TEOS (Table 2.2, entry 6), a viscous liquid phase separated from the elastomer. ^1H NMR spectra showed that the phase-separated liquid contained ~40 mg of catalyst (of 250 mg, 16%), ~12.5 mg of PEG (of 125 mg, 10%) and less than ~21.3 mg of PDMS (of 2.0 g, Table 2.1, Table 2.2, about 1%). The preferential presence of the amine at the interface, a consequence of efficient migration to the interface which has previously been seen with aminopropyltrialkoxysilanes in epoxy polymers,¹⁹ manifests itself in various ways. The aminopropylsilicone, while less effective than the traditional and more efficient tin- or titanium-based RTV catalysts, still facilitates both curing of the silicone and formation of silica. Appropriate formulation thus permits simultaneous control of surface morphology, roughness and hydrophilicity: at pH values near neutrality, amine groups will be protonated leading to surface charge and, as discussed below in more detail, surface active species that may assist in geometric control of the silica formed.

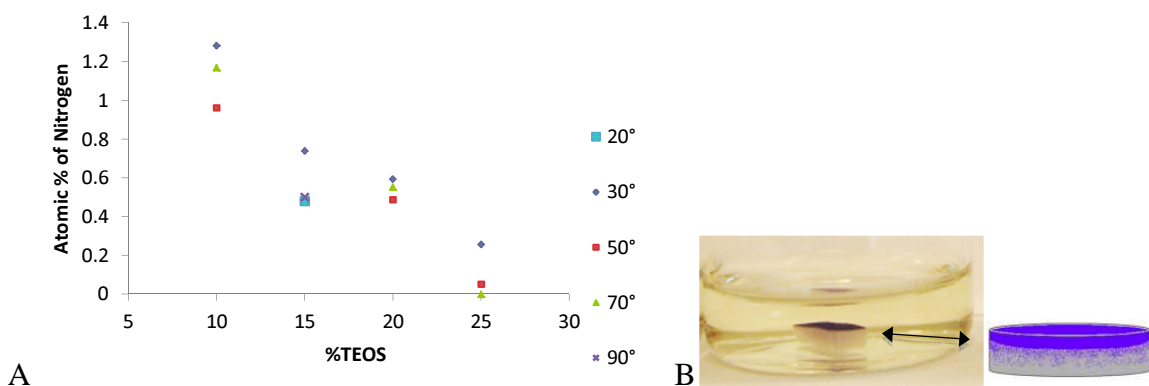


Figure 2.4: A: Nitrogen (catalyst) concentration (XPS) at surface with varying TEOS concentrations at different take-off angles (the 15% sample was examined at 2 different angles than the other samples). B: Ninhydrin staining showing presence of catalyst preferentially at the air interface.

Surface roughness

At low humidity levels there was a clear trend between increasing TEOS concentration and increasing surface roughness[‡] up to 20% TEOS, at which point the roughness then decreases (Figure 2.5A): the presence of PEG led to slightly smoother surfaces (see SI).

There was an inverse trend between catalyst concentration and roughness. With the crosslinker TEOS concentration fixed at 15 wt%, elastomers were prepared using catalyst concentrations between 4 and 10%. The highly inhomogeneous elastomers prepared at 10% and 7% catalyst, respectively, exhibited roughnesses of 2.86 μm and 2.16 μm (Figure 2.6A, SI). By contrast, the homogenous elastomer prepared with 4% catalyst had an R_q value of 364 nm, making it significantly smoother than those prepared with higher catalyst levels (Figure 2.6B).

Atmospheric moisture also had a significant impact on the surface roughness of the elastomers. When the same formulations as those just described were cured at high humidity (90% RH) random structures on the surface did not form and instead highly corrugated, macroscopic wave structures formed on elastomers (Figure 2.5B, C). These waves could be readily seen by eye, with wavelengths of up to 880 μm (Figure 2.6C, SI). In the absence of PEG, only pre-elastomers containing 15% or 20% crosslinker developed these structures. In the presence of PEG, however, all elastomer formulations developed waves but with shorter wavelengths and greater amplitudes than when PEG was absent (Figure 2.5B, C).

Internal structural organization

Internal hydrophilic structures could arise from the presence of PEG, when present, and silica formed by the hydrolysis and condensation of TEOS.²⁰ In asymmetric elastomers, the harder layer near the air interface exhibited a different distribution of

[‡] Surface profilometry provides roughness as R_q , $R_q = \sqrt{\frac{1}{MN} \sum_{j=1}^M \sum_{i=1}^N Z^2(x_i, y_i)}$, the root mean square roughness (Wyko surface Profilors Technical Reference Manual, Veeco Metrology Group, 1990, 16) where x and y = spatial axes, M and N = number of data points in the x and y direction, respectively, and Z = surface height relative to the reference mean plane.

hydrophilic structures than the softer underlayer. The greater organization in the more highly crosslinked upper layer could be readily seen, after staining with fluorescein, using fluorescence microscopy (Figure 2.7).

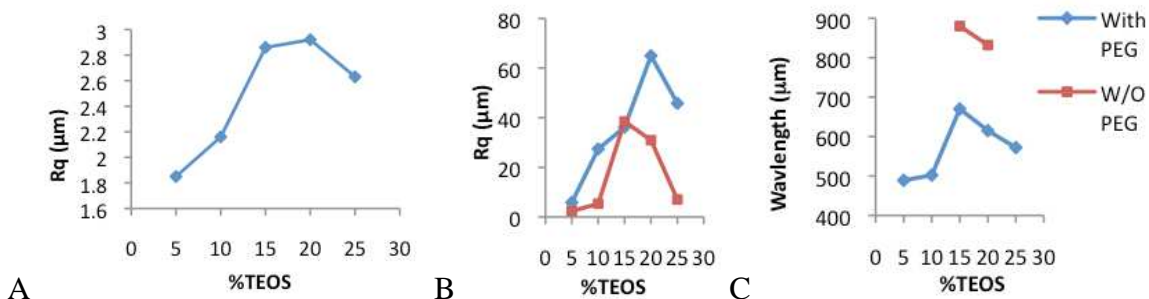


Figure 2.5: A: Roughness of surfaces with increasing crosslinker by profilometry (Table 2.2, entries 6 - 10). B: Roughness of surfaces with increasing crosslinker at 90% RH by profilometry (Table 2.2, entries 14 - 23). C: Wavelength of elastomers cured at 90% RH (Table 2.2, entries 16, 17, 19-23).

Effect of crosslinker concentration

The structure of hydrophilic domains in PEG-containing samples changed significantly with TEOS concentration (Table 2.2, entries 6–10). At 5 wt% TEOS, the dispersed PEG/silica globules were approximately 10 μm in diameter and relatively monodisperse. With the higher concentration of 15% TEOS, the hydrophilic structures appear as thick ribbons on the order of 100–500 μm at their widest point, more than 10 times larger than the globules seen at 5%. At 25% TEOS, a highly reticulated 3D structure had evolved with structures of 50–100 μm in width. Other factors that increase asymmetry in the elastomer, such as increased catalyst concentration, similarly lead to more internal organization (see SI).

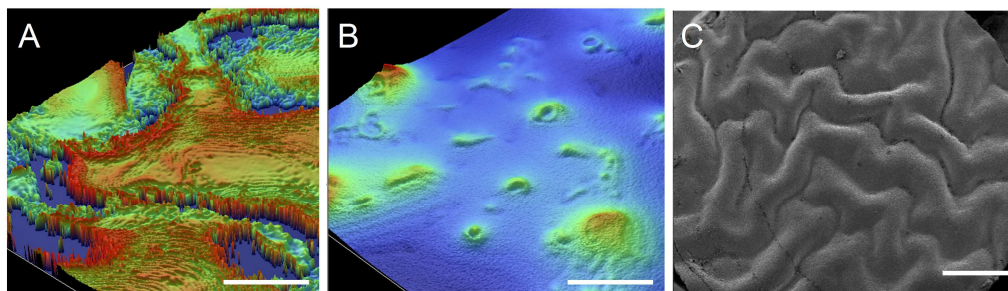


Figure 2.6: Profilometry images of elastomers prepared with 15% TEOS and A: 10% catalyst (Table 2.2, entry 11), B: 4% catalyst (Table 2.2, entry 13). Scale bars = 50 μ m. C: SEM image of elastomer prepared with 25% TEOS, 10% catalyst and 90% RH (Table 2.2, entry 23). Scale bar = 1 mm.

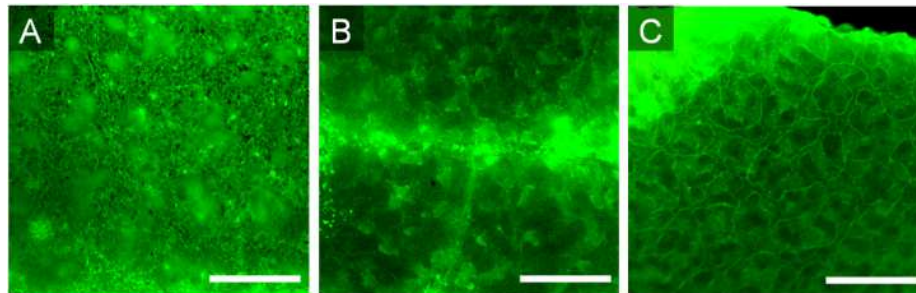


Figure 2.7: Fluorescence images of elastomers with varying amounts of crosslinker. A: 5%, B: 15%, C: 25% (Table 2.2, entries 6, 8 and 10). Scale bar = 500 μ m.

Addition of surfactant

It will be proposed below that internal structuring is facilitated by surface-active materials, including the aminopropylsilicone catalyst. This hypothesis was tested by adding a PEG/silicone rake surfactant, DC 3225C, to the pre-elastomer. Using a 15% TEOS formula, the surfactant was added at levels of 1% and 5%, respectively; three different catalyst loadings were used (Table 2.2, entries 24–27, Figure 2.8). It can be seen that increased concentrations of surfactant and of catalyst both contribute to the formation of greater interconnectivity of hydrophilic channels. The sample containing 5% surfactant and 10% catalyst has hydrophilic domains of sizes below the resolution of light microscopy.

2.5 Discussion

Asymmetric cure and surface modification RTV silicone elastomers are normally designed to be homogeneous throughout the polymer body. Commercial samples are pre-filled, normally with silica, but also with less expensive, non-reinforcing fillers such as calcium carbonate.²¹ In such cases, the only reaction designed to occur during cure of a one-part RTV is hydrolysis/condensation between silicones terminated with silanols and TEOS; silica formation is not anticipated. The crosslinking reaction occurs first at the air interface, which is normally the only source of water (water is a co-catalyst in the case of tin- or titanium-based catalysts²⁰). The air-presenting surface thus cures and becomes tack-free much more rapidly than the layer beneath. The high viscosity of a filled silicone pre-elastomer normally leads to homogeneous materials, consistent with diffusion of water through the matrix being faster than diffusion of other materials within the formulation, and because cure (silanols + crosslinker) occurs more rapidly than TEOS hydrolysis/condensation with the activated catalysts.

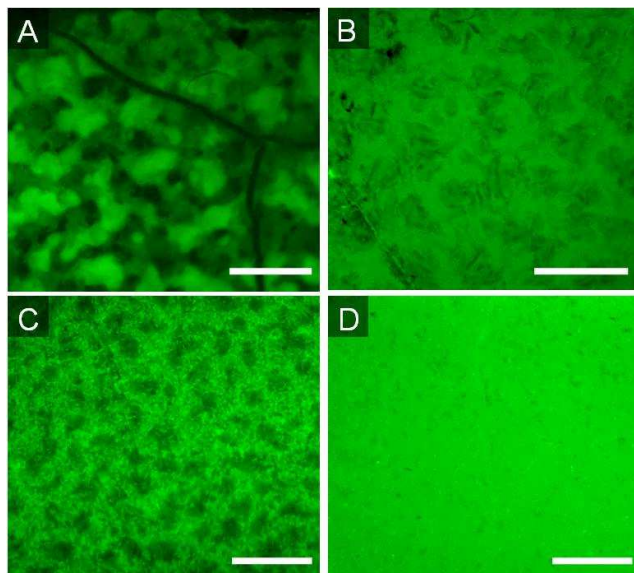


Figure 2.8: Fluorescence images of elastomers prepared with 15% TEOS and A: 1% surfactant (S), 10% catalyst (C), B: 5%(S) and 10% (C), C: 5%(S) and 7% (C), D: 5%(S) and 4%(C) (Table 2.2, entries 24-27). Scale bar = 500 μm .

In the silicone elastomers described above, the use of an atypical (slow) catalyst, aminopropylsilicone, in low viscosity, unfilled RTV systems, alters the cure profile

significantly. Only in cases where water ingress is appreciably faster than either crosslinking or silica formation is a homogeneous silicone formed. Such cases occurred at high RH, low TEOS concentrations and/or low catalyst concentrations. Even in such cases, however, inhomogeneity can result if the water must travel relatively long distances through the silicone. For example, the low surface area/volume sample (1 x 1 x 4.5 cm deep) gave a highly cured elastomer only to a depth of about 0.5 cm even with cure at 90% RH. Thus, in general, crosslinking and silica formation occurred faster, and to a greater extent, at the air interface of these silicones.

The structural features of greatest interest of these asymmetric cured silicones are: interfacial hydrophilicity, roughness, and internal structuring. The synthetic parameters that allowed their control (Table 2.2) are examined in turn. The amine catalyst (Figure 2.3) has a nitrogen content about 4.4 atom%. As seen from Figure 2.4, the surfaces of the cured silicone elastomer can be highly enriched in catalyst (nearly 25% of the material present) at the upper interface.¹⁹ The degree to which the upper interface is populated by amines is a function of the catalyst concentration, and of the TEOS and water concentrations. More rapid cure and higher concentrations of TEOS were associated with decreased catalyst presence at the interface. The catalyst thus diffuses to the interface unless extensive silica formation occurs more rapidly. Amine groups near neutral pH are protonated in aqueous media, which will impact both on the cure chemistry (see below) and the chemistry of the interface.

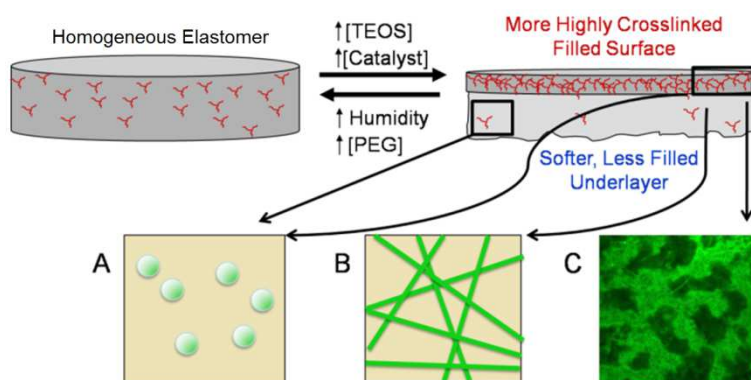


Figure 2.9: Asymmetry caused by increasing crosslinker. With increasing TEOS concentration, A: dispersed PEG droplets, B: then assembled into ribbons and finally, C: into three-dimensional networks.

Higher concentrations of TEOS, and of catalyst, but lower water concentrations led to high degrees of crosslinking and of silica formation at the air interface (Figure 2.9). At ambient humidity, the reactions at the interface, and diffusion of the reagents within the silicone to the surface, occur more rapidly than water vapor can diffuse into the silicone. At the extreme, with high levels of catalyst and TEOS under relatively dry conditions, rough, brittle layers form on top of nearly uncured silicone elastomers. Decreasing concentrations of either TEOS or catalyst, or increased water concentrations enhanced the thickness of the more highly cured and filled upper layer. Note that thicker overlayers were formed when PEG was present in the formulations. The hydrophilic nature of PEG provides a mechanism to deliver water further into the silicone than in its absence. That is, PEG lowers the barrier for water transmission such that the ratio of internal vs. surface crosslinking/silica formation is increased. Thus, as a consequence of the clear differences in reaction rates between cure/silica formation and the diffusion of moisture, it is possible to control both the modulus of the silicone at the air interface and the interfacial hydrophilicity.

At low humidity, very rough surfaces were observed at high concentrations of TEOS. Highly reticulated brittle surfaces, comprised mostly of silica, are unable to anneal during cure, leading to rough, kinetically formed structures. By contrast, when excess water was present, and particularly when PEG was present to deliver water into the core of the elastomer, well-defined waves could be clearly seen even by eye at the external interface. The wavelength (up to nearly 1 mm) and amplitude (up to 250 μm , see SI) of these waves were affiliated with much lower surface crosslink densities, but higher than the underlayers. Such waves, particularly on silicone elastomer surfaces, have previously been examined by a variety of authors.²²⁻²⁶ During cure, two elastomer layers form. The higher modulus elastomer at the air interface shrinks and the resulting waves are a consequence of yielding of the lower modulus underlayer. As seen from Figure 2.5, the amplitude and wavelength of the surface can be manipulated over a large range particularly by changing the TEOS concentration, which directly correlates both with chemical crosslinking, and physical crosslinking via the silica particles.

Internal structural organization

The soft underlayer of the silicone elastomer contained a homogeneous dispersion of silica as isolated or slightly aggregated particles and, when present, of PEG as droplets. By contrast, as shown using fluorescence microscopy, highly organized hydrophilic domains presented in the upper layer except for very lightly crosslinked materials (Figure 2.7A).

Two features in particular controlled the nature of the internal hydrophilic structuring: TEOS concentration and the presence of surface-active species. As the concentration of TEOS increased, isolated particles first became linear ‘ribbons’ and then three-dimensional network structures (Figure 2.7B,C, Figure 2.9, SI). The facility for 3D structuring increased with catalyst concentration (data not shown) and when silicone/PEG surfactants were added (3225C, Figure 2.8).

Two independent but closely related processes are occurring during hydrolysis and condensation: crosslinking of the silicone polymer, and formation of silica due to the large excess of TEOS present. Of course, these processes are not mutually exclusive. While a single TEOS molecule could lead to a 3- or 4-armed branch point (Figure 2.3), condensation of the silicone can occur with silicic acid oligomers or silica ribbons/particles. Reinforcement of the silicone can also occur through physical interactions with silica. We focus now on the formation of silica.

The hydrolysis of TEOS is very slow at neutral pH. By contrast, rates increase rapidly away from pH 7. This pH sensitivity has been exploited to control silica structuring in various ways, perhaps most famously in the formation of model silica colloids by Stöber, in which TEOS is hydrolyzed in ethanol with ammonia catalysis.²⁷ We propose that analogous pH control is provided by the amino group on the aminopropylsilicone catalyst to facilitate hydrolysis/condensation of TEOS, yielding silica, primarily in particulate form.

The organization of the hydrophilic silica/PEG domains can be understood by considering the templated synthesis of meso and macroporous silica from TEOS using surfactants. Perhaps best known of these are the syntheses of zeolites such as MCM-41 in

which surfactants such as CTAB create cylinders around which silica synthesis occurs.²⁸ Normally, such syntheses are undertaken in hydrophilic solvents, which may be aqueous or alcohol based, although strategies for assembly in organic solvents have been elegantly reviewed by Morris and Weigel.²⁹

As with any of the templating processes used to prepare zeolites and other mineral species, a surface-active material guides the assembly of these structures by interactions occurring, in part, between complementary charged species. We propose, in the silicone elastomers formed using aminopropylsilicone catalysts, the ammonium ions on the catalyst can interact with silanolate on silica surfaces (Figure 2.10). The polar silica interface is stabilized in the hydrophobic silicone elastomer matrix by such an interaction. Similar types of interactions, although based on non-ionic/polar interactions can occur when the silicone surfactant 3225C is present (Figure 2.8, Figure 2.10). Such interactions have been used to direct the assembly and porosity of silica particles³⁰ and silica monoliths.³¹ As the concentration of surfactant is increased, the hydrophilic silica domain size is decreased (Figure 2.8).

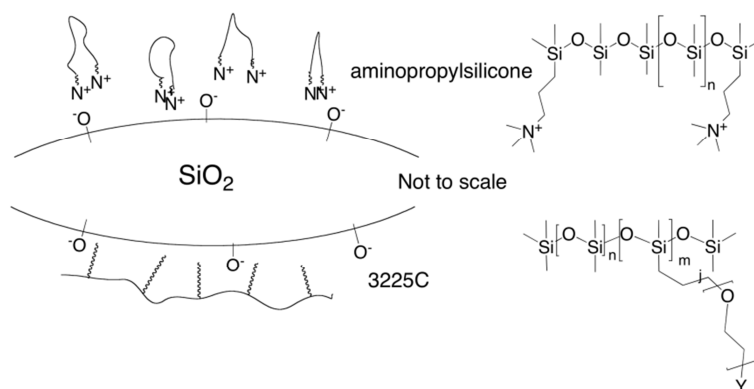


Figure 2.10: Model interfaces between silica/silicone controlled by surface-active materials.

The biocompatibility of silicone species relies on interactions that take place at the interface of the device. As shown above, the use of a surface active catalyst in an RTV system, in combination with control of crosslinker and water concentrations, permits the preparation of elastomer surfaces with controlled geometry and with internal hydrophilic

structuring. We shall report in due course on the biocompatibility of such systems *per se*, and the ability to release hydrophilic bioactive species from the structured silicones.

2.6 Conclusion

The density and organization of hydrophilic silica/PEG domains within silicone RTV elastomers can be controlled by manipulating the relative rates of hydrolysis/condensation with respect to diffusion of water through the matrix. At high TEOS (crosslinker and silica precursor) concentrations, preferential reactions occur proximal to the air interface. Surface-active materials, which include the aminopropylsilicone cure catalyst and, optionally, PEG-modified silicone surfactants act to assemble the hydrophilic domains into ribbons and three-dimensional structures.

2.7 Acknowledgements

We acknowledge with gratitude the financial support of the Natural Sciences and Engineering Research Council of Canada and 20/20: NSERC Ophthalmic Materials Network, and thank Renita D'souza for assistance with the profilometry measurements

2.8 Supplementary Information

Table S 2.1: Phase separated liquid on 5% TEOS elastomer (Table 2.2, entry 6)

Compound	FG	δ , ppm	Integration	J-coupling	Multiplicity
TMB	-OCH ₃	3.78	9.00	-	s
	=CH ₃	6.10	3.00	-	s
PDMS	-OSi(CH ₃) ₂ O-	0.08	5.03	-	s
	SiCH ₂ CH ₂ CH ₂ -	0.49-0.58	0.26	-	m
Aminopropyl-terminated PDMS*	SiCH ₂ CH ₂ CH ₂ -	1.43-1.55	0.26	-	m
	SiCH ₂ CH ₂ CH ₂	2.64-2.71	0.26	7.00	t
PEG	CH ₂ CH ₂ O	3.66	1.55	-	s

* Si = polydimethylsiloxanes

Table S 2.2: Atomic % of nitrogen at 30 for elastomers with PEG (Table 2.2, entries 7-10)

%TEOS	Surface At. %	Bottom At. %
10	1.283	0.846
15	0.433	0.238
20	0.594	0.442
25	0.257	0.006

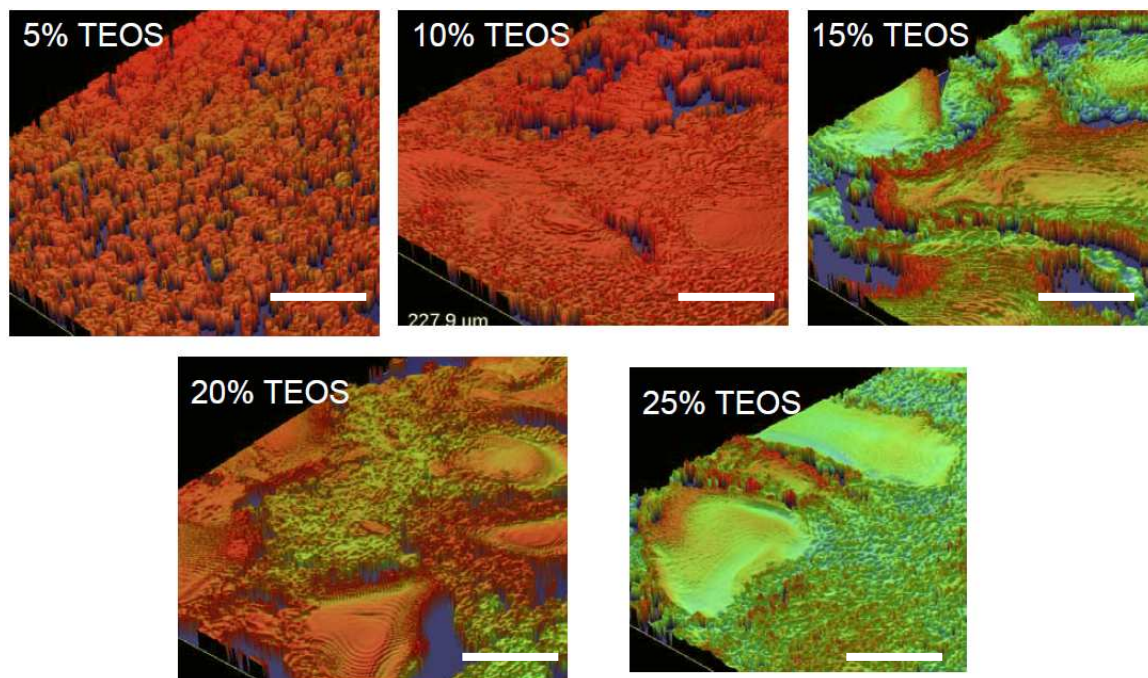


Figure S 2.1: Formation of 'domains' with increasing TEOS. Scale bars = 50 μm .

Experimental for Optical Microscopy Amplitude Measurements of Wave Structures

For the determination of the amplitude of the wave structures found on certain elastomer surfaces, optical microscopy was used by first determining the number of fine tuning units it took to focus on the top and bottom faces of a glass slide of known thickness. Thus the distance travelled in each fine tuning unit was determined to be 1.5 μm /unit and applied.

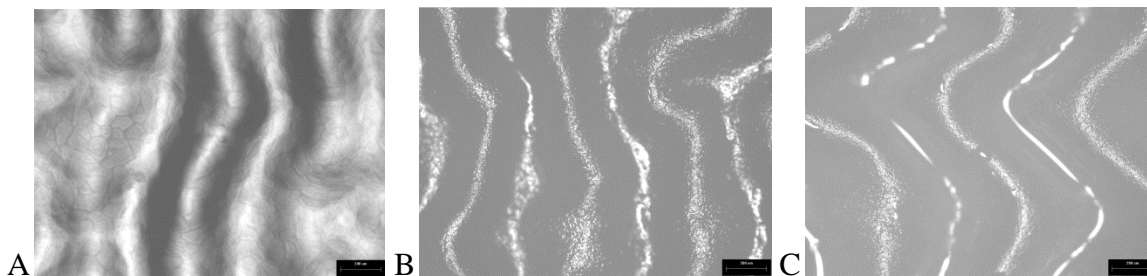


Figure S 2.2: Selected surface images showing wave structures using A: 5% T. B: 10% T and C: 15% T at 90% RH (Table 2.2, entries 19 - 21). Scale bars = 200 μm .

Table S 2.3: Amplitudes of wave structures on elastomer surfaces

Elastomer (Table 2.2 entries)	Rz (μm)
15% T No Peg, 90% RH, Entry 16	173.07
20% T, No PEG, 90% RH, Entry 17	147.97
5% T, 90% RH, Entry 19	39.71
10% T, 90% RH, Entry 19	110.64
15%T, 90% RH Entry 21	165.65
20%T, 90% RH Entry 22	310.15
25%T, 90% RH Entry 23	254.48

Rz is the average maximum height of the profile as it takes the average of the 10 highest and 10 lowest data points. The Rz factor is calculated using the following formula:

$$R_z = \frac{1}{10} \left[\sum_{j=1}^{10} H_j - \sum_{j=1}^{10} L_j \right]$$

Where H_j and L_j are the highest and lowest points respectively.

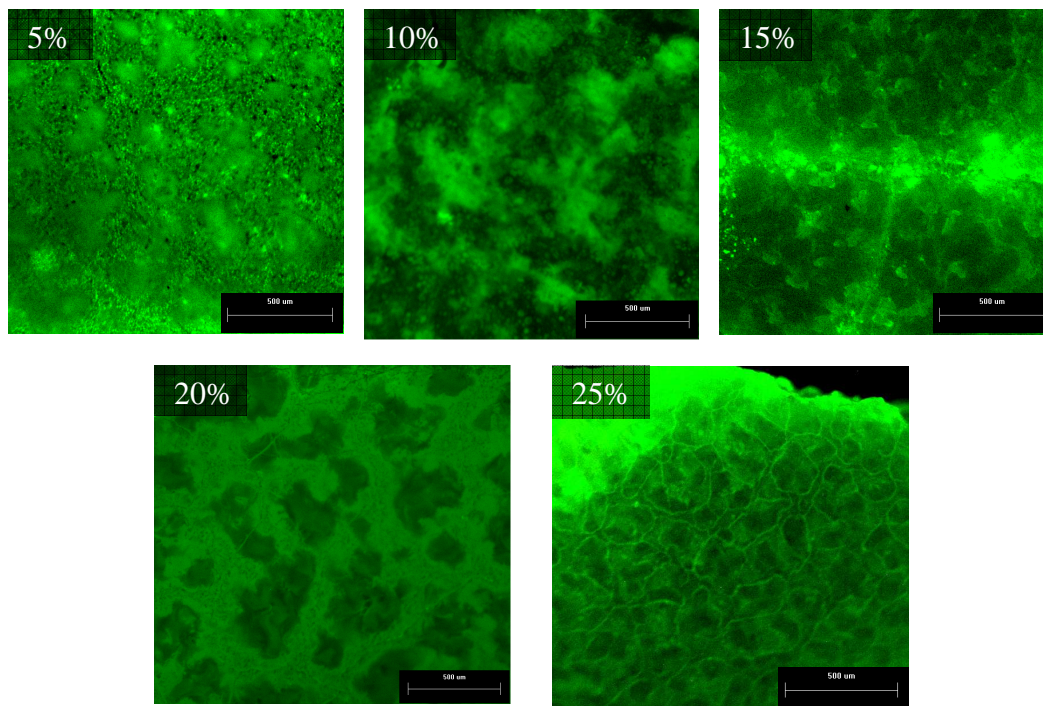


Figure S 2.3: Fluorescence images of elastomers with varied amounts of crosslinker.

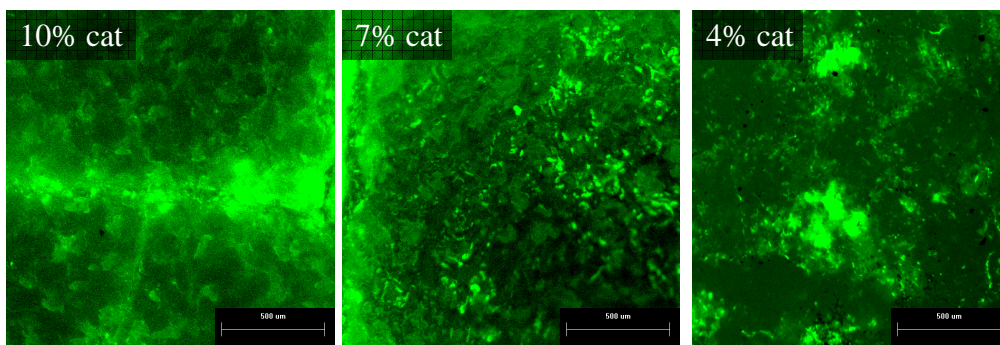


Figure S 2.4: Internal structuring with varying catalyst.

2.9 References

- (1) Jones, R. G. *Elastomerics*, **1988**, 120, 12.
- (2) Ratner, B. D.; Hoffman, A. S.; Schoen, F. J.; Lemons, J. E. *Biomater. Sci.*; Academic Press: New York, 1999.
- (3) Owen, M. J. *Silicon-Based Polymer Science: A Comprehensive Resource*; American Chemical Society: Washington D.C., 1990.
- (4) Owen, M.; Clarson, S. *Siloxane Polymers*, PTR Prentice Hall, Englewood Cliffs, NJ, 1993.
- (5) Sanchez, W.; Evans, J.; George, G. *Aust. J. Chem.*, **2005**, 58, 447.
- (6) Jones, L.; Senchyna, M.; Glasier, M. A.; Schickler, J.; Forbes, I.; Louie, D.; May, C. *Eye Contact Lens*, **2003**, 29, S75.
- (7) Werner, L. *Curr. Opin. Ophthalmol.*, **2008**, 19, 41.
- (8) Kajihara, M.; Sugie, T.; Hojo, T.; Maeda, H.; Maeda, H.; Sano, A.; Fujioka, K.; Sugawara, S.; Urabe, Y. *J. Control. Rel.*, **2001**, 73, 279.
- (9) Brook, M. A.; Holloway, A. C.; Ng, K. K.; Hrynyk, M.; Moore, C.; Lall, R. *Int. J. Pharm.*, **2008**, 358, 121.
- (10) Ratner, B. D.; Kwok, C.; Walline, K.; Johnston, E.; Miller, R. J.; W02004000382, **2003**, *Genzyme Corporation*.
- (11) Dicolo, G. *Biomaterials*, **1992**, 13, 850.
- (12) Lee, J. H.; Lee, H. B.; Andrade, J. D. *Prog. Polym. Sci.*, **1995**, 20, 1043.
- (13) Turner, J. S.; Cheng, Y. L. *Macromolecules*, **2000**, 33, 3714.
- (14) Nicolson, P. C.; Vogt, J. *Biomaterials*, **2001**, 22, 3273.
- (15) Bottom, C. B.; Hanna, S. S.; Siehr, D. J. *Biochem. Ed.*, **1978**, 6, 4.
- (16) Beamson, G.; Briggs, D. *High Resolution XPS of Organic Polymers: The Scienta ESCA300 Database*; Chichester: New York, 1992.
- (17) Clarson, S. J.; Semlyen, J. A. *Siloxane Polymers*; Prentice Hall, 1993.
- (18) Pujol, J. M.; Prebet, C. *J. Adhes. Sci. Technol.*, **2003**, 17, 261.
- (19) Foister, R. T. *J. Colloid Interface Sci.*, **1984**, 99, 568.
- (20) Brook, M. A. *Silicon in Organic, Organometallic, and Polymer Chemistry*; Wiley-VCH Verlag, 2000.
- (21) Noll, W. J. *Chemistry and Technology of Silicones*; Academic Press: New York, 1968.
- (22) Bowden, N.; Brittain, S.; Evans, A. G.; Hutchinson, J. W.; Whitesides, G. M. *Nature*, **1998**, 393, 146.
- (23) Huck, W. T. S.; Bowden, N.; Onck, P.; Pardoën, T.; Hutchinson, J. W.; Whitesides, G. M. *Langmuir*, **2000**, 16, 3497.

- (24) Breid, D.; Crosby, A. J. *Soft Matter*, **2009**, *5*, 425.
- (25) Chan, E. P.; Crosby, A. J. *Soft Matter*, **2006**, *2*, 324.
- (26) Patrito, N.; McCague, C.; Norton, P. R.; Petersen, N. O. *Langmuir*, **2007**, *23*, 715.
- (27) Stöber, W.; Fink, A.; Bohn, E. *J. Colloid Interface Sci.*, **1968**, *26*, 62.
- (28) Brinker, C.; Scherer, G. *Sol-Gel Science: The Physics and Chemistry of Sol-Gel Processing*; Academic Press: New York, 1990.
- (29) Morris, R. E.; Weigel, S. *J. Chem. Soc. Rev.*, **1997**, *26*, 309.
- (30) Cademartiri, R.; Brook, M. A.; Pelton, R.; Brennan, J. D. *J. Mater. Chem.*, **2009**, *19*, 1583.
- (31) Brook, M. A.; Chen, Y.; Guo, K.; Zhang, Z.; Brennan, J. D. *J. Mater. Chem.*, **2004**, *14*, 1469.

Chapter 3 – Nearly Monodisperse Silica Microparticles From Silicone (Pre)elastomer Mixtures[§]

3.1 Abstract

The formation of silica from a tetra-alkoxysilane in a sol-gel process usually requires a highly polar, typically aqueous, medium that aids in the hydrolysis of the silane and leads to electrostatic stabilization of the growing silica particles. Formation of such silica particles in a hydrophobic medium is much more challenging. We report the formation of silica microspheres within silicone oils (hydroxyl-terminated poly(dimethylsiloxane), HO-PDMS) during elastomer cure using atmospheric humidity in a one-pot and one-step synthesis. Using tetraethyl orthosilicate (TEOS) as both cross-linker and silica precursor, and aminopropyl-terminated dimethylsiloxane oligomer (AT-PDMS) as a catalytic surfactant, silica particles of low polydispersity formed near or at the air interface of the elastomer: the presence of a hydrophilic polymer, poly(ethylene glycol) (PEG), had an indirect effect on the particle formation, as it assisted with water transmission into the system, which resulted in particle formation over a wider range of parameters and facilitated silicone elastomer cure further away from the air interface. Depending on the relative humidity during cure, the sizes of particles presenting at the air interface varied from $\sim 6 - 7 \mu\text{m}$ under ambient conditions (20–30% RH) to $\sim 7 - 9 \mu\text{m}$ at high relative humidity (90% RH). The origin of the controlled particle synthesis is ascribed to the relative solubility of the catalyst and the efficiency of water permeation through the silicone matrix. AT-PDMS preferentially migrates to the air interface, as shown by ninhydrin staining, where it both catalyzes alkoxysilane hydrolysis and

[§] The following chapter was reprinted with permission from: Vinodh Rajendra, Ferdinand Gonzaga, Michael A. Brook, *Langmuir*, **2012**, 28, 1470. Copyright 2013 American Chemical Society.

I was responsible for all practical and analytical work. Dr. Gonzaga helped with the Soxhlet extractions and Dr. Brook gave some useful advice and troubleshooting ideas. I wrote the 1st draft of the manuscript and Dr. Brook helped with editing the document for final submission to the above journal.

condensation, and stabilizes the growing silica particles prior to aggregation. Since reactions in the presence of this catalyst are slow, TEOS can migrate from within the pre-elastomer body to the interface faster than water can penetrate the silicone, such that the main locus of hydrolysis/condensation leading both to silica formation and elastomer cross-linking is at the air interface.

3.2 Introduction

The ability to form monodisperse silica particles using sol gel processes has been known for some time, as demonstrated in the seminal paper by Stöber and Fink.¹ $\text{Si}(\text{OEt})_4$ (TEOS) is hydrolyzed in ethanol/water mixtures under basic conditions generated by ammonia. Particle monodispersity is a consequence of the nucleation of primary particles after the growing silica oligomers become insoluble in the alcoholic medium. Particle growth then occurs both by further condensation chemistry on particle surfaces, and by the capture of new particles formed by secondary nucleation. During these processes, electrostatic stabilization in the hydrophilic medium is provided by ammonium silanolates (SiO^-) on the silica surface, maintaining colloidal stability.

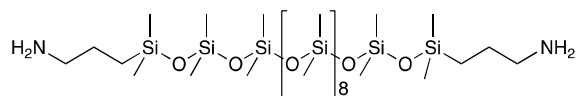
The Stöber process of forming silica particles has been utilized in many investigations for creating narrowly dispersed silica particles, mostly in hydrophilic media. However, its use has rarely been exploited in more hydrophobic media. Condensation of mercaptopropyltrimethoxysilane in the polar but nonhydroxylic solvent DMSO with relatively low concentrations of water led to the formation of distorted spherical silsesquioxane particles of about 60 nm in diameter: the analogous recipe in water/ethanol mixtures gave particles over 800 nm in diameter.² Less polar solvents such as THF can also be used as a medium to grow small (~20–175 nm), distorted spherical silica particles starting from TEOS using relatively large quantities of amine catalysts.³ The amine was shown by NMR experiments to play a role both as catalyst and as a stabilizer for the particles.

The ability to grow silica particles in the presence of even less polar constituents has also been demonstrated. Avnir and coworkers, in an interesting series of papers, described a strategy to incorporate various organic polymers within silica particles. For

example, the inclusion of about 20% of silicone oil of various molecular weights within a classic Stöber formulation, led to the typical monodisperse, spherical particles of diameter from about 160 – 250 nm. The ability to include silicone oil in the silica particles hinged on the use of non-ionic silicone/polyether surfactants.⁴

It is also possible to grow silica particles within a preformed silicone elastomer,⁵ after cross condensation reactions between TEOS and silicone oils (room temperature vulcanization, RTV). After soaking in a TEOS/water solution, very small silica particles ~15 nm in size eventually formed throughout the entire rubber body. Alternatively, silica of undefined structure can be formed in situ during typical condensation (moisture initiated) cure of hydroxy-terminated silicone oils and functional silanes.⁶

During experiments designed to create hydrophilically modified silicones by the addition of poly(ethylene glycol)(PEG) to an RTV formulation,⁷ we were surprised to discover very large (~6–7 μm), narrowly dispersed silica particles exposed at the air interface of (only partly cured) silicone elastomers (Figure 3.1).⁸ The formation of these large, spherical silica particles was a consequence of the catalyst used. Instead of dibutyltin dilaurate, the common commercial catalyst for RTV silicones,⁹⁻¹¹ a less efficient amine catalyst¹² aminopropyl-terminated poly(dimethylsiloxane) (AT-PDMS) was used. These structures are distinct in their size from previously described materials. Perhaps more importantly, the method for their preparation involves no addition of water, except in the form of moisture in the air, involves very low catalyst concentrations, and the absence of classical surfactants to stabilize particles from aggregation. We have therefore examined the role of the silica precursor, catalyst type, humidity, and PEG on this one-step formation of silica particles from alkoxysilanes during silicone elastomer cure.



AT-PDMS

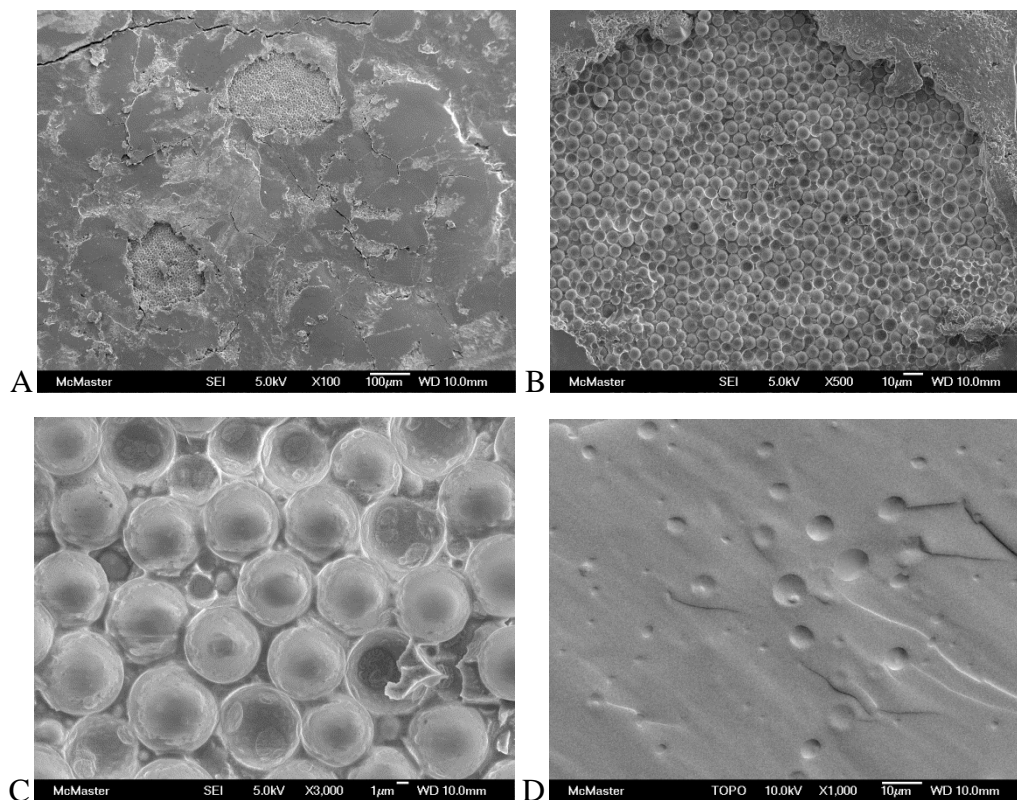


Figure 3.1: A: SEM of 25% TEOS with PEG elastomer cured with AT-PDMS at ambient conditions showing exposed, narrowly dispersed silica particles directly below the elastomer surface. B: Expansion of A. C: Expansion of B. D: SEM cross-section of dibutyltin dilaurate-catalyzed elastomer at 25% TEOS loading.

3.3 Experimental Section

Materials

Hydroxy-terminated PDMS (HO-PDMS, 1800–2200 cSt, ~36 000 g/mol, Aldrich), tetraethylorthosilicate (TEOS, 99.999%, Aldrich), aminopropyl-terminated PDMS (AT-PDMS, 10–15 cSt, ~875 g/mol, Gelest), dibutyltin dilaurate (Aldrich), poly(ethyleneglycol)- (PEG, 1000 g/mol, Aldrich), tetrahydrofuran (THF, reagent grade, Caledon), and hexanes (reagent grade, Caledon) were used as received.

Particle Formation in Silicone Elastomers

Silica microspheres were prepared in silicone oil as the nonaqueous dispersion medium. HO-PDMS, TEOS, the catalyst dibutyltin dilaurate or AT-PDMS; and, optionally, PEG were mixed together in a specific order. First HO-PDMS was measured using a 3 mL plastic syringe and poured into a 20 mL glass vial. Then PEG, when a constituent of the formulation, was added into the glass vial where it was weighed. TEOS was added dropwise and then the mixture was gently heated to a temperature of $\sim 50\text{ }^{\circ}\text{C}$ for approximately 30 s. This step was continued until the PEG liquefied. After the mixture was cooled for 30 s, the amine or tin catalyst was added to the mixture that was manually mixed for approximately 2 min, leading to a cloudy mixture. The mixture was poured into a plastic Petri dish (35 mm diameter, film thickness was approximately 2 mm) lined with a Teflon film and allowed to cure at room temperature ($20\text{ }^{\circ}\text{C}$) for either 2 weeks at ambient humidity (20 – 30% RH) or 1 day at 90% RH inside an ESL-2CA constant humidity chamber (ESPEC). The general experimental details for particle forming formulations are provided in Tables 2 and 3. All individual formulations, including controls, can be found in the Supporting Information.

As seen from Table 2, to make an elastomer containing PEG with a 25% TEOS loading, the following formulation was used: HO-PDMS (1.600 g, 60 wt %, 1.2 mol %), TEOS (0.625 g, 25 wt %, 87 mol %), PEG (0.125 g, 5 wt %, 3.5 mol %), and AT-PDMS (0.250 g, 10 wt %, 8.3 mol %) were mixed together with the procedure shown above and cured for up to 2 weeks at ambient conditions, or 1 day at 90% RH.

Extraction of Samples

Cured samples were first cut into circular disks of ~ 2 mm in thickness using a 0.6 cm diameter coring tool. These were placed in cellulose extraction thimbles and extracted with a Soxhlet apparatus using reagent grade hexanes overnight. Elastomers were then dried in a vacuum oven at room temperature overnight. Extraction was done to remove residual materials that could obscure morphological details on the SEM.

Imaging of Samples

Scanning electron microscope (SEM) images of elastomers were obtained by first gold coating samples for 30 s at a rate of 15 nm/min. Samples were then mounted on aluminum stubs and imaged using a JEOL 7000F SEM at an accelerating voltage of 5 kV. To obtain cross sections, elastomers were initially frozen in liquid nitrogen and then fractured before mounting. Particle sizes and distributions, with a sample size of $n = 50$, were determined using ImageJ software.

Hardness Tests

This test was only performed on the tin cured formulations. The AT-PDMS formulations formed non-homogeneously cured elastomers, which had brittle surfaces but lightly cured bottom halves in many cases (the lightly cured elastomers formed using AT-PDMS were too soft to be characterized by Shore A hardness). First 3 elastomer disks were cut, as mentioned above, and then stacked on top of each other. Measurements utilizing a Shore A durometer (MFG. Co. Inc., U.S. Patent 2453042) were then made on these stacked elastomer disks. Shore A hardness is related to a materials Young's modulus.

X-ray photoelectron Spectroscopy (XPS)

XPS was conducted at the University of Toronto using a Thermo Scientific Theta Probe XPS spectrometer (ThermoFisher, E. Grinstead, U.K.) in standard mode. The angles were taken relative to the surface normal. A monochromatic Al K_{α} X-ray source was used, with a spot area 400 μm . Charge compensation was provided utilizing the combined e^{-}/Ar^{+} flood gun. The position of the energy scale was adjusted to place the main C 1s feature (C-C) in the high resolution spectrum at 284.4 eV, the literature value for PDMS.¹³ Data processing was performed using the software (Avantage) provided with the instrument. There was an approximately linear decrease in the atomic% of nitrogen measured on elastomer surfaces at takeoff angles of 20°, 30°, 50°, 70°, and 90°, respectively, as a function of TEOS concentration. The key results, presented in Table

3.1, show that nitrogen, which is only associated with the AT-PDMS catalyst, preferentially migrates to the air interface.

Attempts to section the silica particles to permit characterization by transmission electron microscopy and EDX were unsuccessful. One particle that fractured during the manipulation showed it to be dense throughout (data not shown), similar to Stöber particles.

Table 3.1: Atomic % of nitrogen from AT-PDMS catalyst on cured elastomers at 20-30% RH as measured by XPS at a takeoff angle of 30°

%TEOS ^a	Surface of Elastomer	Bottom of Elastomer
10	1.283	0.846
15	0.74	0.003
20	0.594	0.442
25	0.257	0.006

^a 5% TEOS elastomers not measured by XPS due to phase separated liquids that contaminated the surface.

3.4 Results and Discussion

Control elastomers were prepared using a traditional RTV silicone formulation catalyzed by dibutyltin dilaurate, but with a high loading of TEOS (25 wt %), the addition of PEG, and under 90% RH for 24 h to give a rigid (Shore A hardness of 55), white silicone elastomer typical of commercial RTV-cured elastomers (Supporting Information). After extraction with hexanes to remove residual silicone oils, PEG, and catalyst, a cross section of the elastomer showed voids, but no evidence of silica particles either at the micro- or nanoscale within the resolution of the instrument (Figure 3.1D). PEG is relatively insoluble in silicone oil and the voids thus indicate the location of insoluble PEG droplets that were present following mixing and during the curing process.¹⁴ The PEG appeared to improve the curing processes by increasing water transmission into the system and had a minor effect on particle size as will be explained below.

Table 3.2: Typical formulations of AT-PDMS catalyzed silicone elastomers with varying TEOS loadings (5 - 25% in 5% increments) (2.5 g total in each formulation)

Parameter	Formulations w/o PEG (g)	Formulations w/ PEG (g)
HO-PDMS	2.125-1.625 ^a (85-65%)	2.000-1.500 ^b (80-60%)
TEOS	0.125-0.625 (5-25%)	0.125-0.625 (5-25%)
AT-PDMS	0.250 (10%)	0.250 (10%)
PEG	0	0.125 (5%)
Relative Humidity (H ₂ O)	20-30%/90%	20-30%/90%
Cure Time (20°C)	2 weeks/1d	2 weeks/1d

^a For example, the formulation containing 15 wt % TEOS (0.375 g) was made with 10% AT-PDMS (0.250 g), 75% HO-PDMS (1.875 g), and cured at 20–30% RH for 2 weeks. ^b For example, the formulation containing 5 wt % TEOS (0.125 g) was made with 10% AT-PDMS (0.250 g), 5% PEG (0.125 g), 80% HO-PDMS (2.000 g), and cured at 90% RH for 1d.

Table 3.3: Typical formulations of silicone elastomers cured with varying amounts of AT-PDMS (4, 7 and 10%) at 15% TEOS (2.5 g)

Parameter	Formulations w/o PEG (g) ^a	Formulations w/ PEG (g) ^b
HO-PDMS	2.025-1.875 (81-75%)	1.900-1.750 (76-70%)
TEOS	0.375 (15%)	0.375 (15%)
AT-PDMS	0.100-0.250 (4-10%)	0.100-0.250 (4-10%)
PEG	0	0.125 (5%)
Relative Humidity (H ₂ O)	20-30%/90%	20-30%/90%
Cure Time (20 °C)	2 weeks/1d	2 weeks/1d

^a For example, the formulation containing 15 wt % TEOS (0.375 g) was made with 10% AT-PDMS (0.250 g), 75% HO-PDMS (1.875 g), and cured at 90% RH for 1d. ^b For example, the formulation containing 15 wt % TEOS (0.375 g) was made with 4% AT-PDMS (0.100 g), 5% PEG (0.125 g), 76% HO-PDMS (1.900 g), and cured at 20–30% RH for 2 weeks.

New RTV formulations, using the atypical amine catalyst AT-PDMS, were prepared under similar conditions to those above. To melted 1000 MW PEG (when included in the formulation) was added high loadings of TEOS (5 – 25 wt % in 5% increments), the silicone base material, hydroxy-terminated poly(dimethylsiloxane) (HO-PDMS, 65–85 wt %) and the catalyst (Table 3.2). The samples were allowed to cure at ambient temperature and humidity (~20–30%) for up to two weeks, or for 1 day at 90% RH.

Effect of TEOS and AT-PDMS Catalyst Concentrations

A series of elastomers were prepared with AT-PDMS as catalyst and TEOS concentrations varying from 5 to 25 wt % in 5% increments under ambient conditions to investigate the effect of cross-linker concentration on silica particle formation. In most cases, except at high TEOS loadings (cured at 90% RH with PEG, see below), thin skins of elastomer covered layers of close packed silica particles. Cross sections of the elastomers prepared with varying amounts of TEOS under ambient conditions were imaged by SEM (Figure 3.3A–C) and showed that layers of particles of approximately the same diameter formed near the air interface (Figure 3.1A–C).

Table 3.4: Particle diameters (μm) with standard deviations in elastomers prepared with varying amounts of TEOS

% TEOS	Ambient w/o PEG ^b	Ambient w/ PEG(μm) ^b	90%RH w/o PEG ^b	90%RH w/ PEG (μm)
5	NP	NP	ID	13.4 \pm 3.8
10	NP	ID	7.0 \pm 1.6	8.5 \pm 1.9
15	7.3 \pm 1.5	6.4 \pm 1.7	7.5 \pm 1.3	8.2 \pm 1.7
20	ID	5.7 \pm 1.3	7.9 \pm 1.7	8.6 \pm 2.1
25	ID	6.7 \pm 0.6	7.5 \pm 1.8	9.1 \pm 2.0
25(S) ^a	NP	NP	NP	12.6 \pm 1.4

^a w/ PEG = with PEG in the formulation; w/o PEG = no PEG in the formulation; NP = no particles observed; ID = ill-defined silica structures formed. ^b Refers to the single layer of particles that grew and presented at the air interface of the elastomer. The previous line in the table refers to particles that were present below this single silica particle layer. The presence of two different layers of particles only occurred with the formulation containing a 25% T loading at 90% RH with PEG (Figure 3.2B, Table 3.2, SI)

Particle sizes were sensitive to the humidity during the reaction, which was effectively moderated by the presence of PEG, particularly when low humidity conditions were used: $\sim 6\text{--}7\ \mu\text{m}$ at low humidity, and $7\text{--}9\ \mu\text{m}$ at higher humidity (Table 3.4). At conditions of low relative humidity, 20–30% RH, elastomers prepared with 5% or 10% TEOS loadings showed essentially no particles or ill-defined silica structures (Figure 3.3A). At higher humidity, particle formation was much more effective even at low TEOS loadings.

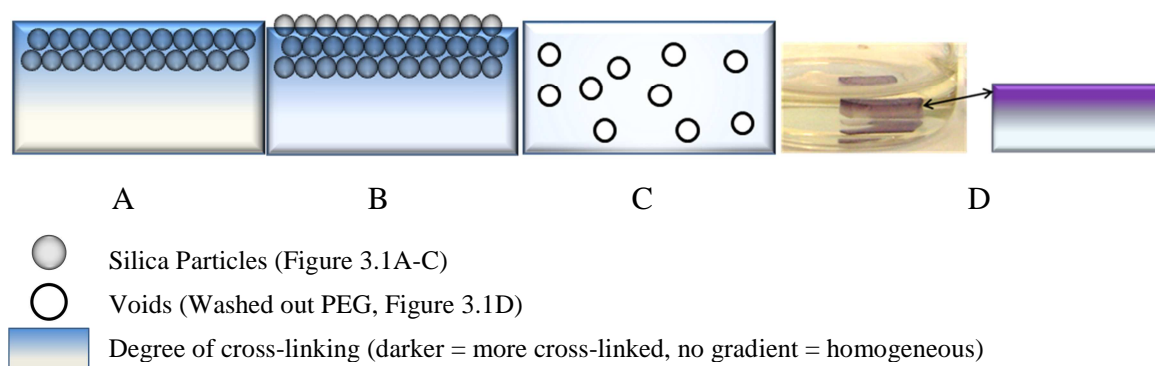


Figure 3.2: Cartoon showing different 3D structural features of elastomer cross-sections prepared using different catalysts. A: AT-PDMS cured elastomers for all formulations that form particles (Table 3.4) except for the formulation in the next pictorial. B: AT-PDMS, humidity 90%, 25% TEOS and with PEG; surface covered with a thin silicone layer interrupted by ‘silica particle pock marks,’ Figure 3.1A. C: Dibutyltin dilaurate, homogeneous elastomer. D: Ninhydrin-stained elastomer showing presence of amine at the air interface.

There was a correlation between the TEOS concentration in the formulation and the thickness of the particle layers. For example, as the TEOS concentration increased from 5 to 25% in the PEG-containing samples cured at 90% RH, the silica layer increased in thickness from $\sim 15\text{--}35\ \mu\text{m}$ (Supporting Information). In general, additional layers of particles formed at higher humidity and when more TEOS was included in the formulation (Table 3.5), but particle size remained relatively invariant (Table 3.4). To summarize, TEOS loadings had only a minor effect on the size or morphology of the particles formed, but played a major role in determining the number of defined spherical particles that formed.

Table 3.5: Summary of parameter effects on particle formation

Parameter	Effect on Particle Formation
HO-PDMS	-
TEOS	[TEOS] \propto number of defined spherical particles and their dispersity
AT-PDMS	Required for surface stabilization and catalysis of particle formation
PEG	Improves water transmission, indirectly allows for particle formation on elastomer surface; increases the degree of cure in the underlying elastomer
Relative Humidity	[H ₂ O] \propto number of particles/minor effect on particle size, and increased cure of elastomer

Cross sections of the cross-linked elastomers stained by ninhydrin (Figure 3.2D) show that the majority of the amine groups associated with the catalyst were present at the air interface and associated with the silica particles. The preferential presence of amines at the air interface, and to a much lower extent at the vessel interface (data not shown), was supported by XPS data (Table 3.1). When the amine concentration was decreased, silica particles were either ill-defined or did not form at all (Figure 3.3D–F). These results seem to indicate that the amine catalyst is a key contributor to particle formation and likely in the stabilization of the particle surface (Table 3.5).

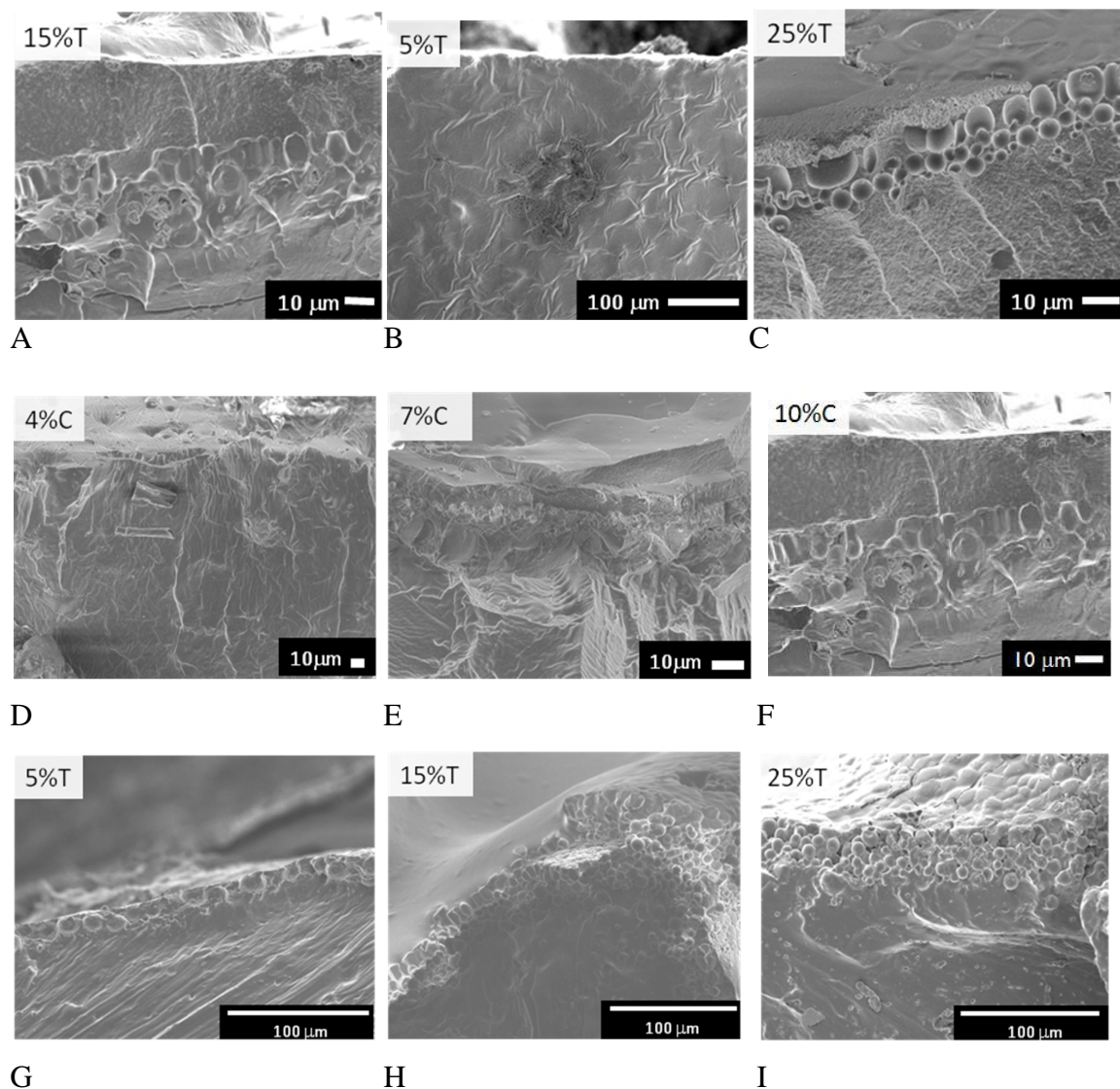


Figure 3.3: SEM cross-sections (air interface is at the top of all images) of AT-PDMS-catalyzed elastomers containing PEG with varying TEOS concentrations (%T) at 20-30% RH (A, B, C); varying catalyst concentration (%C) 4%, 7% and 10% with 15%T at 20-30% RH (D, E, F), and varying TEOS concentrations at 90% RH (G, H, I).

The degree of cross-linking and the formation of a cure gradient of the silicone pre-elastomer depended inversely (surprisingly) on the concentration of TEOS present. For ATPDMS- derived silicones prepared with a 25% TEOS loading and cured under ambient conditions, the top half (1 mm) of the elastomer body was comprised of highly cross-linked silicone with silica, however, the lower part of the silicone was comprised of

very lightly cross-linked viscoelastic materials (Figure 3.2A). The cohesive strength of the lower silicone layer was insufficient to permit clean removal from the Petri dish. With lower TEOS loadings (5–20%), the silicone layers were more homogeneously cured (i.e., there was a less pronounced gradient in cure from the air interface to the bottom of the vessel, Figure 3.2A, B), and the bottom half of the silicone body more highly cross-linked, thus making removal more facile.⁸ Elastomers cured at 90% RH were far more homogeneously cured and slightly more cross-linked (Figure 3.2B). However, none of these soft elastomers exhibited properties like the robust (Shore A hardness 55) and homogeneous silicone elastomers prepared using the dibutyltin dilaurate catalyst (Figure 3.1D, Figure 3.2C, Supporting Information). Elastomers that also contained PEG were more homogeneously cross-linked than formulations without it, that is, AT-PDMS catalyzed formulations cured at 90% RH with PEG, exhibited the smallest cure gradient between the air interface and bottom of the vessel (Figure 3.2A, B).

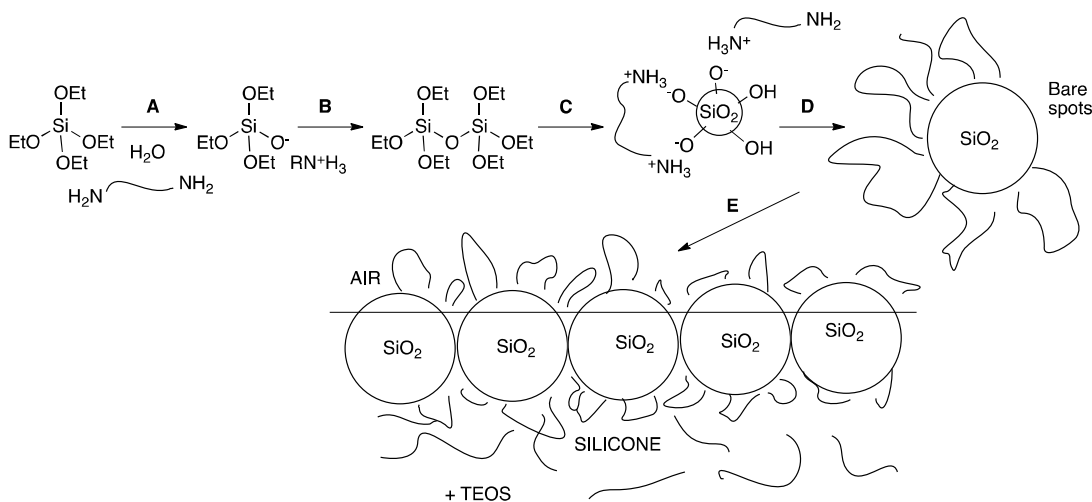


Figure 3.4: Model for steric stabilization of silica by AT-PDMS. A, hydrolysis; B, condensation; C, precipitation of silica oligomers; D, growth of sterically stabilized silica (by particle capture and growth through hydrolysis/condensation); E, aggregation once particle size exceeds available surfactant, liberation of surfactant that can lead to additional particle layers (if TEOS is present).

Effect of Atmospheric Water and PEG

The constituents of the elastomer include HO-PDMS, TEOS and the catalyst. However, water is also a key component for the process, as it plays a catalytic role in

silica and elastomer formation.¹⁵ A comparison was therefore made between the silicone structures formed at ambient humidity (20–30% RH) and at higher humidity (90% RH) (Table 3.2, Table 3.3). Cross sections of the cured elastomers showed that silica microspheres are formed more efficiently at high humidity than under drier conditions (Figure 3.3A–C vs. G–I, Supporting Information): the presence of higher moisture concentrations favors silica particle formation at the interface, and at the expense of silicone cross-linking. For example, a thin monolayer of silica particles formed at the air interface when a 5% TEOS formulation was cured at 90% RH with PEG (Figure 3.3G), whereas at ambient humidity no particles formed (Figure 3.3A). Particle size did increase slightly with the increased water concentration: particles prepared at 90% RH ranged from ~7–9 μm (Table 3.4) compared to ~6–7 μm at ambient conditions (20–30% RH). The presence of slightly larger particles at high humidity could be reconciled by the location of the catalyst and the increased efficiency of hydrolysis of TEOS. There is a concentration gradient in the catalyst: as one moves from the air interface into the silicone the concentration of the AT-PDMS catalyst decreases (Figure 2D).⁸ Less catalyst/stabilizer means particles will aggregate earlier than at higher stabilizer concentrations. At higher humidity and TEOS concentrations, kinetics favor TEOS hydrolysis and condensation into particles at the air interface. Thus, the availability of water plays a minor role in determining the size and shape of the silica particles formed.

One outlier to the particle sizes observed at high humidity was the 5% TEOS formulation which shows a larger average particle size of $13.4 \pm 3.8 \mu\text{m}$. At this TEOS concentration, the system is considerably less well behaved, leading to a more polydisperse set of particles as seen from the larger standard deviation. This indicates that a large molar excess of TEOS is also required to drive the system toward narrowly dispersed silica particles, as TEOS is being used simultaneously for both RTV curing and particle formation.

As shown previously, the presence of PEG did not have a dramatic effect on silica particle sizes or their morphology. However, formulations that included PEG were capable of forming particles over a wider range of TEOS loadings and led to more

homogeneously cured elastomers than formulations without PEG. We believe that PEG aids in atmospheric moisture transmission onto and through the silicone system to increase the rate of hydrolysis for TEOS. As explained above, this increased rate pushes the reaction kinetics in favor of silica formation at the air-surface interface. RTV curing can also take place more efficiently throughout the elastomer as water can be transmitted further into the material. Thus, PEG makes both silica formation at the air interface and RTV curing throughout the silicone body more efficient due to increased water transmission. Figure 3.2B depicts a second outlier. A single layer of silica particles formed directly at the air interface of the elastomer at a high relative humidity, with 25% or higher TEOS loadings, and in the presence of PEG. These particles were larger, with an average particle size of $12.6 \pm 1.4 \mu\text{m}$, than the particles in layers further away from the air interface, or in other elastomer formulations (Table 3.4): the underlying elastomer was better cured in this case. We propose that the PEG/TEOS mixtures can efficiently capture water at the air interface. Such a pool of PEG/TEOS/H₂O/silica may overcome surface reversion by the underlying silicones and account for the open zones (pock marks) on the surfaces of these materials that exhibit the silica particles directly (Figure 3.2B). In addition, this layer can lead to the growth of larger particles than the more poorly hydrated layers beneath.

Origin of the Nearly Monodisperse Silica Particles.

Many studies have been done on the formation and growth of Stöber silica particles with improved techniques emerging over the years to provide a more detailed understanding of the process.¹⁶⁻¹⁸ We found the aggregative growth model that was proposed initially by Zukoski et al. to be a very compelling model for the system described above, even though it was developed to explain silica formation in aqueous solutions. Once primary silica particles nucleate (precipitate from solution during oligomer growth), they can continue to grow either via molecular addition or through aggregation. Larger particles capture newly (secondary) nucleated particles because of van der Waals attractive forces that overwhelm electrostatic repulsion due to silanolate groups (R₃SiO⁻) on the silica surfaces.

Electrostatic stabilization requires a medium that supports ion solvation. While this can sometimes be observed in polar organic solvents,¹⁹ nonaqueous dispersions generally require steric stabilization for stability,^{20,21} particularly in a nonpolar medium such as silicone oil. Pelton et al. demonstrated that silicone chains can stabilize poly(methyl methacrylate) particles in a silicone environment.^{22,23} Vincent et al. have similarly shown that silica particles with polystyrene chains grafted to the surface of the particles can be dispersed within nonaqueous media: in this case, however, the silica particles were pre-formed using the classical Stöber method and then surface modified.²⁴ We have been unable to find reports of silica particle formation in silicone oils without any pre-modification.

The narrow degree of polydispersity of the silica formed in silicones (Figure 3.1 and Figure 3.3) is consistent with particle growth following Zukowski's mechanism. To invoke such a process, however, requires identifying a replacement for the electrostatic stabilization that is provided in hydrophilic solvents. AT-PDMS was shown to preferentially migrate to the air interface, which is also where water vapor – necessary for both cure and silica formation – arrives at the pre-elastomer formulation. We hypothesize that AT-PDMS is acting both as a hydrolysis/condensation catalyst and a steric stabilizer. As silica starts to form from hydrolysis/condensation at the air interface Figure 4A–B, silanols that present on the external silica surface are titrated by the surfactant, generating ammonium silanolate^{12,25} that anchor the surfactant to the surface (Figure 3.4C). Such anchoring may occur at one or both ends of the surfactant chain: at lower catalyst concentrations, looping would be expected. Normally, the stabilization provided by such a few siloxane linkages would not be expected to be very efficacious as a steric stabilizer. The lack of completely efficient stabilization apparently permits larger silica particles to sequester small, secondarily nucleated particles as a growth mechanism in addition to further hydrolysis/condensation of TEOS (Figure 3.4D), similar to the Stöber process. However, the stabilization is sufficient to prevent irreversible aggregation of the large particles only until they reach about 6–7 μm in diameter at ambient conditions or 7–9 μm at 90% RH, at which point the particles are able to assemble into close packed systems

prior to the final elastomer formation (Figure 3.4E). This could be related to the efficiency of AT-PDMS becoming protonated and properly stabilizing the charged particle surface.

This process is therefore analogous to the Stöber silica formation, even though it occurs in a water-deprived hydrophobic medium. The characteristics of the formulation that favor silica formation over silicone oil cross-linking include the migratory aptitude of the catalyst, which prefers the air interface as shown by XPS and ninhydrin staining (Table 3.1, Figure 3.2D), as previously reported.⁸ The presence of water is also important, as it enters the silicone at the air interface, which then becomes the locus of reaction: migration of water through the silicone oil is inherently inefficient. The formation of well-defined silica particles thus reflects a careful kinetic balance. Because hydrolysis/condensation is inherently inefficient with AT-PDMS as a catalyst, migration of TEOS and the catalyst to the air interface, where water is comparatively plentiful, occurs more rapidly than the silicone oil can cure into elastomers. Very little silicone cross-linking, and no observable silica formation, occurs below the silica rich layer within a few days, although a very lightly crosslinked product eventually becomes more cross-linked throughout the elastomer body. The presence of additional water (e.g., 90% RH) facilitates silica formation by favoring surface reactions.²⁶ For example, although formulations containing 5% TEOS did not lead to well-defined silica particles when cured at 20–30% RH, high moisture reaction conditions 90% RH led to silica particle formation even at this low TEOS concentration (Figure 3.3A–C vs. G–I). These observations suggest migration of water at the silicone/silica interface into the silicone is slow compared to migration of TEOS from within the silicone pre-elastomer to the air interface where silica forms: additional humidity illuminates this difference in rates of migration.

This silicone elastomer formulation using AT-PDMS is very different from tin-catalyzed systems that also need water to undergo cure. With tin, a homogeneous cross-linked rigid elastomer formed. In this case, the catalyst does not preferentially diffuse to the air interface, and there are no surfactants present to stabilize silica. As a consequence,

a homogeneous, highly cross-linked elastomer is observed with only very small silica domains that are homogeneously dispersed through the elastomer.

The use of amine RTV catalysts in lieu of traditional titanium or tin-derived compounds does not lead to better silicone elastomers. However, it does provide a surprising ability to synthesize large, nearly monodisperse silica particles in a hydrophobic environment, when forming lightly cured elastomers. With the less effective AT-PDMS catalyst, in particular, it was relatively difficult to achieve homogeneous cure of the elastomer. We are currently examining strategies to better manipulate and exploit these silica structures by varying the system parameters.

3.5 Conclusion

The use of an amine-based catalyst, high concentrations of the cross-linker and silica precursor TEOS and, optionally, PEG as a hydrophilic phase, permits the formation of well-defined silica particles near or at the air interface of silicone elastomer matrices. The surface-active aminopropylsilicone AT-PDMS catalyst dissolves efficiently neither in silicone nor PEG and migrates effectively to the air interface where it facilitates silica formation and stabilizes growing silica particles until they aggregate. The amount of water in the system plays an important role, as slightly different particle sizes can be formed depending on the relative humidity. Particles $\sim 6\text{--}7\ \mu\text{m}$ in diameter form at 20–30% RH whereas particles ranging from $\sim 7\text{--}9\ \mu\text{m}$ can form at 90% RH. This discrepancy can be attributed to increased amount of hydrolyzed TEOS that preferentially takes part in silica formation giving particles stabilized by the amine catalyst at the air-surface interface. PEG containing formulations allowed for silica particles to be formed with wider range of TEOS amounts than those without it, and also gave elastomers that exhibited less gradient cure because of increased water transmission through the silicone body. In a specific formulation that included PEG, particles can be seen growing directly on the surface of the elastomer. By further varying the different parameters in the system, it should be possible to achieve different types of silica structuring and morphologies in the future.

3.6 Acknowledgments

We thank 20/20: NSERC Ophthalmic Materials Research Network for financial support. We also express our thanks to Dr. Robert Pelton for helpful discussions and the use of his humidity chamber and Dr. Yang Chen for help with freeze fracturing of the silicone elastomers.

3.7 Supporting Information

Table S 3.1: Control formulations utilizing dibutyltin catalyzed silicone elastomer formulations with varying TEOS loadings (5-25% in 5% increments) (2.5 g total in each formulation)

F. #	Parameter	Weight (g)	Wt.%	F. #	Parameter	Weight (g)	Wt.%
1	HO-PDMS	2.362	94.5	6	HO-PDMS	2.237	89.5
	TEOS	0.125	5		TEOS	0.125	5
	Dibutyltin Dilaurate	0.013	0.5		Dibutyltin Dilaurate	0.013	0.5
	PEG	0	0		PEG	0.125	5
	Relative Humidity	20-30%/90%			Relative Humidity	20-30%/90%	
	Cure Time (20°C)	2 weeks/1d			Cure Time (20°C)	2 weeks/1d	
2	HO-PDMS	2.238	89.5	7	HO-PDMS	2.113	84.5
	TEOS	0.25	10		TEOS	0.25	10
	Dibutyltin Dilaurate	0.013	0.5		Dibutyltin Dilaurate	0.013	0.5
	PEG	0	0		PEG	0.125	5
	Relative Humidity	20-30%/90%			Relative Humidity	20-30%/90%	
	Cure Time (20°C)	2 weeks/1d			Cure Time (20°C)	2 weeks/1d	
3	HO-PDMS	2.112	84.5	8	HO-PDMS	1.987	79.5
	TEOS	0.375	15		TEOS	0.375	15
	Dibutyltin Dilaurate	0.013	0.5		Dibutyltin Dilaurate	0.013	0.5
	PEG	0	0		PEG	0.125	5
	Relative Humidity	20-30% /90%			Relative Humidity	20-30%/90%	
	Cure Time (20°C)	2 weeks/1d			Cure Time (20°C)	2 weeks/1d	
4	HO-PDMS	1.987	79.5	9	HO-PDMS	1.862	74.5
	TEOS	0.5	20		TEOS	0.5	20
	Dibutyltin Dilaurate	0.013	0.5		Dibutyltin Dilaurate	0.013	0.5
	PEG	0	0		PEG	0.125	5

	Relative Humidity	20-30%/90%			Relative Humidity	20-30%/90%	
	Cure Time (20°C)	2 weeks/1d			Cure Time (20°C)	2 weeks/1d	
5	HO-PDMS	1.862	74.5	10	HO-PDMS	1.737	69.5
	TEOS	0.625	25		TEOS	0.625	25
	Dibutyltin Dilaurate	0.013	0.5		Dibutyltin Dilaurate	0.013	0.5
	PEG	0	0		PEG	0.125	5
	Relative Humidity	20-30%/90%			Relative Humidity	20-30%/90%	
	Cure Time (20°C)	2 weeks/1d			Cure Time (20°C)	2 weeks/1d	

Table S 3.2: AT-PDMS catalyzed formulations (2.5g) with varying TEOS loadings and the thickness of the silica particle layers formed

F. #	Parameter	Weight (g)	Wt.%	F. #	Parameter	Weight (g)	Wt.%
1	HO-PDMS	2.125	85	6	HO-PDMS	2	80
	TEOS	0.125	5		TEOS	0.125	5
	AT-PDMS	0.25	10		AT-PDMS	0.25	10
	PEG	0	0		PEG	0.125	5
	Relative Humidity	20-30%/ 90%			Relative Humidity	20-30% or/ 90%	
	Cure Time (20°C)	2 weeks/1d			Cure Time (20°C)	2 weeks/1d	
	Thickness of SiO ₂ particle layer	-/-			Thickness of SiO ₂ particle layer	-/~15µm	
2	HO-PDMS	2	80	7	HO-PDMS	1.875	75
	TEOS	0.25	10		TEOS	0.25	10
	AT-PDMS	0.25	10		AT-PDMS	0.25	10
	PEG	0	0		PEG	0.125	5
	Relative Humidity	20-30%/ 90%			Relative Humidity	20-30%/ 90%	
	Cure Time (20°C)	2 weeks/1d			Cure Time (20°C)	2 weeks/1d	
	Thickness of SiO ₂ particle layer	-/~25µm			Thickness of SiO ₂ particle layer	-/~23µm	
3	HO-PDMS	1.875	75	8	HO-PDMS	1.75	70
	TEOS	0.375	15		TEOS	0.375	15
	AT-PDMS	0.25	10		AT-PDMS	0.25	10
	PEG	0	0		PEG	0.125	5
	Relative Humidity	20-30%/ 90%			Relative Humidity	20-30%/ 90%	
	Cure Time (20°C)	2 weeks/1d			Cure Time (20°C)	2 weeks/1d	
	Thickness of SiO ₂ particle layer	~20µm/~55µm			Thickness of SiO ₂ particle layer	~27µm/~27µm	

4	HO-PDMS	1.75	70	9	HO-PDMS	1.625	65
	TEOS	0.5	20		TEOS	0.5	20
	AT-PDMS	0.25	10		AT-PDMS	0.25	10
	PEG	0	0		PEG	0.125	5
	Relative Humidity	20-30%/ 90%			Relative Humidity	20-30%/ 90%	
	Cure Time (20°C)	2 weeks/1d			Cure Time (20°C)	2 weeks/1d	
	Thickness of SiO ₂ particle layer	-/~55µm			Thickness of SiO ₂ particle layer	~29µm/~28µm	
5	HO-PDMS	1.625	65	10 ^a	HO-PDMS	1.5	60
	TEOS	0.625	25		TEOS	0.625	25
	AT-PDMS	0.25	10		AT-PDMS	0.25	10
	PEG	0	0		PEG	0.125	5
	Relative Humidity	20-30%/ 90%			Relative Humidity	20-30%/ 90%	
	Cure Time (20°C)	2 weeks/1d			Cure Time (20°C)	2 weeks/1d	
	Thickness of SiO ₂ particle layer	-/~45µm			Thickness of SiO ₂ particle layer	22µm/~35µm	

^a Obtaining silica particles directly on the elastomer surface requires 90% RH over 1d.

Table S 3.3: Silicone elastomers cured with varying amounts of AT-PDMS at 15% TEOS (2.5g)

F. #	Parameter	Weight (g)	Wt. %	F. #	Parameter	Weight (g)	Wt. %
1	HO-PDMS	2.025	81	4	HO-PDMS	1.9	76
	TEOS	0.375	15		TEOS	0.375	15
	AT-PDMS	0.1	4		AT-PDMS	0.1	4
	PEG	0	0		PEG	0.125	5
	Relative Humidity	20-30%			Relative Humidity	20-30%	
	Cure Time (20°C)	2 weeks			Cure Time (20°C)	2 weeks	
	Thickness of SiO ₂ particle layer	-			Thickness of SiO ₂ particle layer	-	
2	HO-PDMS	1.95	78	5	HO-PDMS	1.825	73
	TEOS	0.375	15		TEOS	0.375	15
	AT-PDMS	0.175	7		AT-PDMS	0.175	7
	PEG	0	0		PEG	0.125	5
	Relative Humidity	20-30%			Relative Humidity	20-30%	
	Cure Time (20°C)	2 weeks			Cure Time (20°C)	2 weeks	
	Thickness of SiO ₂	-			Thickness of SiO ₂	-	

particle layer				particle layer			
3	HO-PDMS	1.875	75	6	HO-PDMS	1.75	70
	TEOS	0.375	15		TEOS	0.375	15
	AT-PDMS	0.25	10		AT-PDMS	0.25	10
	PEG	0	0		PEG	0.125	5
	Relative Humidity	20-30%/ 90%			Relative Humidity	20-30%/ 90%	
	Cure Time (20°C)	2 weeks/1d			Cure Time (20°C)	2 weeks/1d	
	Thickness of SiO ₂ particle layer	~20µm/~55µm			Thickness of SiO ₂ particle layer	~27µm/~27µm	

3.8 References

- (1) Stöber, W.; Fink, A.; Bohn, E. *J. Colloid Interface Sci.*, **1968**, *26*, 62.
- (2) Irmukhametova, G. S.; Mun, G. A.; Khutoryanskiy, V. V. *Langmuir*, **2011**, *27*, 9551.
- (3) El Hawi, N.; Nayral, C.; Delpech, F.; Coppel, Y.; Cornejo, A.; Castel, A.; Chaudret, B. *Langmuir*, **2009**, *25*, 7540.
- (4) Sertchook, H.; Elimelech, H.; Avnir, D. *Chem. Mater.*, **2005**, *17*, 4711.
- (5) Dewimille, L.; Bresson, B.; Bokobza, L. *Polymer*, **2005**, *46*, 4135.
- (6) Clarson, S. J.; Mark, J. E. *Polym. Commun.*, **1987**, *28*, 249.
- (7) Brook, M. A.; Holloway, A. C.; Ng, K. K.; Hrynyk, M.; Moore, C.; Lall, R. *Int J Pharm*, **2008**, *358*, 121.
- (8) Rajendra, V.; Chen, Y.; Brook, M. A. *Polym. Chem.*, **2010**, *1*, 312.
- (9) Pujol, J. M.; Prebet, C. *J. Adhes. Sci. Technol.*, **2003**, *17*, 261.
- (10) Scott, E. B.; Shephard, N. E., *GB 2403723*, **2005**, Dow Corning.
- (11) Patel, M.; Skinner, A. R.; Chaudhry, A.; Billingham, N. C.; Mahieu, B. *Polym. Degrad. Stabil.*, **2004**, *83*, 157.
- (12) Wagner, O.; Kenessey, G. *J. Appl. Polym. Sci.*, **1998**, *69*, 1705.
- (13) Beamson, G.; Briggs, D. *High Resolution XPS of Organic Polymers: The Scienta ESCA300 Database*; Chichester: New York, 1992.
- (14) Fawcett, A. S.; So, H. Y.; Brook, M. A. *Soft Matter*, **2010**, *6*, 1229.
- (15) Vanderweij, F. W. *Makromol. Chem.*, **1980**, *181*, 2541.
- (16) Bogush, G. H.; Zukoski, C. F. *J. Colloid Interface Sci.*, **1991**, *142*, 19.
- (17) Van Blaaderen, A.; Van Geest, J.; Vrij, A. *J. Colloid Interface Sci.*, **1992**, *154*, 481.
- (18) Pontoni, D.; Narayanan, T.; Rennie, A. R. *Langmuir*, **2002**, *18*, 56.

- (19) Ketelson, H. A.; Pelton, R.; Brook, M. A. *Langmuir*, **1996**, *12*, 1134.
- (20) *GB 1337022*, **1973**, Dow Corning.
- (21) Everett, D. H.; Stageman, J. F. *Faraday Discuss.*, **1978**, *65*, 230.
- (22) Pelton, R. H.; Osterroth, A.; Brook, M. A. *J. Colloid Interface Sci.*, **1990**, *137*,
120.
- (23) Pelton, R.; Osterroth, A.; Brook, M. A. *J. Colloid Interface Sci.*, **1991**, *147*, 523.
- (24) Bridger, K.; Fairhurst, D.; Vincent, B. *J. Colloid Interface Sci.*, **1979**, *68*, 190.
- (25) Brook, M. A. *Silicon in Organic, Organometallic, and Polymer Chemistry*; Wiley-VCH Verlag, 2000.
- (26) Jang, K. W.; Choi, S. H.; Pyun, S. I.; Jhon, M. S. *Mol. Sim.*, **2001**, *27*, 1.

Chapter 4 – Controlled Formation of Macroporous or Hollow Silica Particles in Non-aqueous Silicone Dispersions^{**}

4.1 Abstract

The formation of silica particles by sol-gel processes from alkoxy silane precursors normally requires an aqueous environment. This study demonstrates that optionally macroporous or hollow silica particles can be formed from $\text{Si}(\text{OEt})_4$ within silicone oil: water, a key element in the process, is provided only from moisture from the atmosphere. Particles grow in or around a non-aqueous dispersion of poly(ethylene glycol) droplets in the silicone, which may be an oil or a curing elastomer. The structures of both the silica and silicone elastomer are established in a one pot / one step methodology. Control of the silica particle morphology is provided simply by choice of the amine catalyst, benzylamine or dodecylamine: benzylamine leads to open, macroporous monolithic particulate structures, where the particles are also mesoporous, while dodecylamine gives hollow particles with highly condensed shells. These differences arise from the relative abilities of the two catalysts to partition between the hydrophilic/ hydrophobic silicone/poly(ethylene glycol) media. The two morphologies release the surrogate drug fluorescein with different profiles.

4.2 Introduction

Porous and hollow silica particles are materials that have promise in drug delivery,¹⁻³ as reinforcing agents,⁴ separation science,^{5,6} in catalysis,^{7,8} as templating agents,⁹ etc. The advantages possessed by these materials include the ability to encapsulate a variety of (bio)molecules, high surface area, controlled porosity, and good

^{**} The following chapter was reproduced by permission of the Royal Society of Chemistry. The paper was published in *RSC Advances* with the following citation: Vinodh Rajendra, Michal A. Brook, *RSC Adv.*, **2013**, 3, 22229-22238.

I was responsible for all practical and analytical work, plus the writing of the 1st draft of the manuscript. Dr. Brook gave some useful advice and helped with editing the document for final submission to the above journal.

biocompatibility. The formation of silica with specific morphologies for use in these applications normally requires control of sol-gel processes.^{10,11} Most processes of this type utilize aqueous solutions of alkoxy silane precursors that react at pHs away from neutrality. For example, the classical Stöber method leads to highly crosslinked particles by hydrolysis of TEOS ($\text{Si}(\text{OEt})_4$) in an ethanol/water solution containing NH_4OH as a basic catalyst with constant stirring.¹²

A variety of strategies exploiting sol-gel processes are used to create structured silicas. Templated silica structures,¹³ for example MCM-41, arise from the formation of silica around pre-assembled surfactants such as cetyl ammonium bromide (CTAB).^{14,15} A different class of meso- and macroporous, monolithic silica structures arise from the acid-catalyzed hydrolysis and condensation of TEOS in the presence of high molecular weight poly(ethylene glycol) as a structuring agent.^{16,17} As the silica structures begin to grow, spinodal decomposition occurs to give a silica rich phase that matures into a highly structured monolithic assembly of fused silica nanoparticles. Both types of processes take place in the presence of water-rich environments.

Textured mesoporous silica particles can be created in analogous aqueous-based processes, for example, in an acidic medium where low concentrations of TEOS and surfactant are used.^{18,19} Hollow silica particles can be formed around a particle template on which the silica is grown. The utilization of particle templates such as polystyrene (PS)²⁰ or poly(methyl methacrylate)²¹ (PMMA) result in good control of particle size and morphology. However, after silica formation, the template has to be removed, usually through solubilization of the organic polymer in a process that is not always convenient. Alternatively, hollow particles can be formed at an interface, typically a 3 phase system where a water-in-oil-in-water (W/O/W) dispersion is utilized with the silica precursor located the inner water phase, and a basic catalyst found in the outer water phase; the organic phase lies between the two.^{22,23} In this case, silica formation takes place at the internal interfaces of the droplets giving a hollow silica particle, and without additional steps required for removing a template. The common thread between these strategies is

the requirement for an aqueous phase both to hydrolyze alkoxy silane precursors and to stabilize the evolving silica particles during their formation.

Previously, we demonstrated that solid, Stöber-like silica particles can be formed within silicone (pre)elastomer mixtures where the only source of water is humidity from the air.²⁴ The objective of the current research was to develop synthetic methods for silica particles with alternative morphologies, including macroporous and hollow structures, which could similarly be formed in situ in a silicone environment. Such particles may hold promise as reinforcing agents in elastomers or, after isolation from non-crosslinkable silicone oils, as carriers for a variety of (bio)molecule payloads.

We report a strategy to prepare controlled-morphology silica within bulk hydrophobic phases based on either hydroxyl-terminated polydimethylsiloxane (PDMS, HO-PDMS) or vinyl-terminated PDMS (VT-PDMS). Of the two, only HO-PDMS can undergo room temperature elastomer vulcanization using TEOS as both silicone crosslinker and silica precursor. Thus, the silica formed is embedded in the elastomer. With VT-PDMS, a condensation reaction cannot occur to form a silicone network, and TEOS only acts as a precursor to silica particles that may be recovered in this system. In either formulation, and atypical for silicones, was the use of low molecular weight poly(ethylene glycol) (PEG) as a hydrophilic phase that can aid in structuring silica,^{16,25} and either benzylamine (**BA**) or dodecylamine (**DDA**) as catalysts (Figure 4.1). By simply switching between the two basic amine catalysts, which exhibit very different solubilities in silicone oil and PEG, respectively, two different silica particle morphologies could be attained.

4.3 Experimental Section

4.3.1 Materials

α,ω -Hydroxy-terminated PDMS (HO-PDMS, 1800–2200 cSt (silicones are commonly sold by their kinematic viscosity in cSt, which may be converted to viscosity by multiplying by the density of the fluid. 2000 cSt is thus 970 mPa s, ~ 36000 g/mol, Aldrich), vinyl-terminated PDMS (VT-PDMS, 2000 cSt, ~ 36000 g/mol, Gelest),

tetraethyl orthosilicate (TEOS, $\text{Si}(\text{OEt})_4$, 99.999%, Aldrich), benzylamine (**BA**, Aldrich), dodecylamine (**DDA**, Aldrich), poly(ethylene glycol)(PEG, 600 & 1000 g/mol, Aldrich), tetraethylene glycol (TEG, Aldrich), fluorescein (Aldrich), human serum albumin (HSA, 97-99%, Aldrich), and sodium dodecyl sulfate (SDS, Bioshop), were used as received.

4.3.2 Preparation of Silica Particles

Silica microspheres were prepared in a silicone environment using either HO-PDMS or VT-PDMS, TEOS, PEG and either **BA** or **DDA**. PEG1000 was utilized in the crosslinkable HO-PDMS samples while PEG600 was added into the VT-PDMS and drug loaded samples. It was important to add the catalyst last once all the elastomer constituents were present. First HO-PDMS or VT-PDMS was measured using a 3 ml plastic syringe and added into a 20 ml glass vial. Then PEG or TEG was added into the glass vial where it was weighed. TEOS was added dropwise and then, depending on the MW of PEG and the catalyst used, the mixture was gently heated to a temperature of 40 °C for approximately 30 s until PEG and the catalyst liquefied. If **BA** was included as the amine catalyst, it was added to the mixture after liquefying PEG1000: no heating was required with PEG600 or TEG. With **DDA** as catalyst, the PEG was added after the addition of the hydrophilic phase and for PEG1000 the mixture was heated to 40 °C until it just liquefied. After all the reagents were added, they were manually mixed for approximately 2 min, leading to a cloudy mixture. The mixture was poured into a plastic Petri dish (35 mm diameter, film thickness was approx. 2 mm) lined with a Teflon film and allowed to cure in an ESL-2CA constant humidity chamber (ESPEC) at room temperature and 90% RH over the course of 1 day.

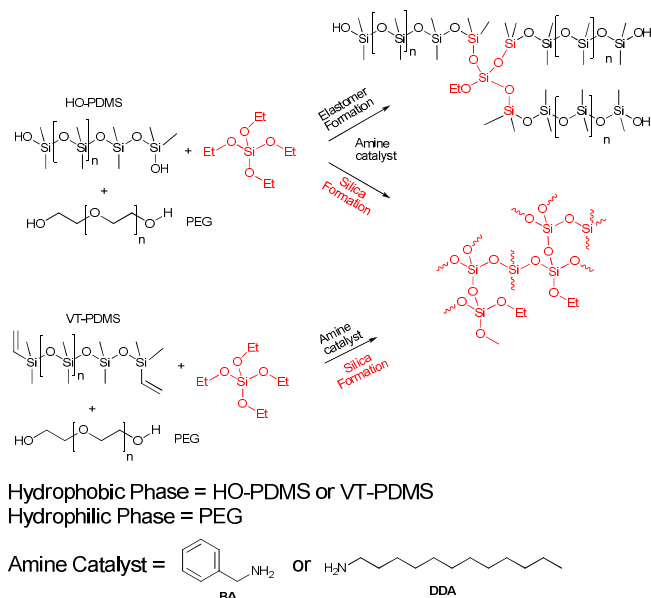


Figure 4.1: Amine-catalyzed reactions lead to both elastomers and silica. Silica particles are entrapped in silicone rubber formed from HO-PDMS, but can be isolated when VT-PDMS is used. PEG is required to form the structured silica structures described below.

The VT-PDMS based mixtures did not cure but were treated identically to those of the HO-PDMS cured silicones except, because 600 g/mol PEG was used, no heating step was required. PEG600 was utilized instead of PEG1000 with the VT-PDMS samples since PEG600 is a liquid, thus for the drug release studies, loading fluorescein or HSA into a liquid PEG phase was simpler than a solid PEG phase. The experimental details for all formulations, including control formulations, are provided in Table 4.1 and Supporting Information (SI). As an example from Table 4.1, to make a **BA**-catalyzed elastomer containing PEG with a 25% TEOS (T) loading: HO-PDMS (1.600g, 60%), TEOS (0.625g, 3.0 mmol, 25%), PEG (0.125g, 5%) and **BA** (0.250g, 0.233 mmol, 10%) were mixed together as mentioned above and cured for 1 day at 90% RH (F#10, SI).

Fluorescein- and HSA-loaded silica particles used slightly modified processes. PEG (600 g/mol) containing 0.6 mM fluorescein replaced pure PEG in the recipe shown above for the 25%T **BA** mixture (F#17, SI) or the 15%T **DDA** mixture (F#35, SI). HSA-loaded particles were prepared by dissolving approximately 20 mg of HSA in just enough water for solubilization, which was then added to 0.3 g of PEG600 with vigorous stirring.

The HSA-PEG mixture was incorporated using the standard protocol into the 25%T **BA** (F#18, SI) mixture.

4.3.3 Soxhlet Extraction of cured Samples

Cured elastomer samples were first cut into circular disks using a 0.6 cm diameter coring tool, giving disks that were ~ 2 mm in thickness, which were then placed in cellulose extraction thimbles and extracted with a Soxhlet apparatus using reagent grade hexanes overnight. Elastomers were then dried in a vacuum oven at room temperature overnight.

4.3.4 Isolation of Silica Particles from Silicone Oil

Silica particles formed in the non-curing silicone oil VT-PDMS were isolated by placing the mixture in 15 mL glass vials. The mixture was initially washed with approximately 10 mL of THF and then centrifuged at 600 RCF (relative centrifugal force) for 4 min. The same washing procedure was repeated 2 times with hexanes and then again with THF as the solvent. With fluorescein or HSA-containing particles, particles were only washed with hexanes (3 times).

4.3.5 Imaging of Samples

Scanning electron microscope (SEM) images of elastomers were obtained using a JEOL 7000F SEM. In order to obtain cross-sections, elastomers were initially frozen in liquid nitrogen and then fractured before mounting; samples isolated from silicone oil were crushed before analysis by placing them in a microtube to which steel ball bearings were added. The sample was then shaken vigorously for approximately 1 min on a mechanical mixer. SEM images of **BA**- and **DDA**-catalyzed systems can be found in Figure 4.2 and ESI†. Particle sizes and distributions were measured manually with a sample size of $n = 50$ using ImageJ software.

Table 4.1: Composition of BA and DDA-catalyzed elastomers and silica particles

Parameter*	Formulations w/o PEG g (wt%)	Formulations with PEG g (wt%)
HO-PDMS	2.125–1.625 (85–65%)	2.000–1.500 (70–60%)
TEOS	0.125–0.625 (5–25%)	0.125–0.625 (5–25%)
Amine catalyst (BA or DDA)	0.250 (10%)	0.250 (10%)
PEG	0	0.125 (5%)

* see also SI.

4.3.6 Porosity Measurements

Nitrogen sorption data was collected with a Quantochrome Nova 2000 utilizing the Novawin v. 1.11 software. All samples were initially degassed at 120 °C overnight and directly measured thereafter. The pore size distribution and surface area of the particles were calculated from the Barrett, Joyner, and Halenda (BJH) model.²⁶ Finally, the total pore volume was measured at a $P/P_0 \approx 1$. Crushed particles were prepared as described in the next section.

4.3.7 Fluorescence Measurements of Fluorescein and HSA-Loaded Silica Particles

Silica particles loaded with fluorescein or HSA were isolated using the method described above. A fraction of these were placed within a 2 mL microtube containing a 1% aqueous solution of SDS (SDS was necessary because, in its absence, residual VT-PDMS led to clumping/aggregation) without any prior treatment to remove PEG.

The microtubes were centrifuged at 600 RCF for 4 min with either silica sample type. Approximately 150 μ l of the supernatant from each microtube was placed within the well of a sterile optically clear bottom 96 well-plate (Nunc, Thermo Fisher Scientific). Fluorescence measurements to follow release of fluorescein were conducted using an Infinite M200 fluorescence plate reader (Tecan) at room temperature and each sample was run in triplicate. The first measurement was taken at about 15 min. The release of fluorescein from the particles was measured using an excitation wavelength of 494 nm and emission of 521 nm. For HSA-loaded particles, an excitation wavelength of 296 nm and an emission wavelength of 314 nm were used for fluorescence measurements. Once

measurements were taken, the 150 μl aliquots were removed from the 96 well-plate and added back into their respective samples. The **BA**- and **DDA**-derived particles were measured approximately every 15 min for 2 h (Figure 4.7).

4.4 Results and Discussion

Silica particles formed in silicone elastomers during cure after reacting HO-PDMS with the tetrafunctional crosslinker, TEOS. In lieu of the normal catalyst for such RTV (room temperature vulcanization) formulations – dibutyltin dilaurate²⁷ – the simple amines **BA** or **DDA**, respectively, were utilized. When TEOS was added in concentrations excess to the requirements for crosslinking, the formation of silica particles within the elastomer was observed. In these cases, two parallel reaction pathways are simultaneously followed: hydrolysis of TEOS and condensation with HO-PDMS to form the network, and, hydrolysis of TEOS and condensation with TEOS-derived silanols to give silica (Figure 4.1). The amine catalysts facilitate both reactions.²⁸ Poly(ethylene glycol) was also incorporated into the formulations as, in the absence of this hydrophilic polymer, structured silica particles were not observed. Instead, a few solid silica particles presented themselves at the air-surface interface non-reproducibly when the process was catalyzed by **BA** (SI); monolithic silica structures formed only in the top $\sim 30\ \mu\text{m}$ of the elastomer surface when the processes were catalyzed by **DDA** (Figure 4.2L). These observations suggest that, in the presence of PEG, silica particle formation takes place in a non-aqueous dispersion of PEG in silicone (see below).

Experiments were also conducted with VT-PDMS (Figure 4.1) to determine if silica particles form and can be isolated from a mobile medium. Vinyl-terminated PDMS cannot undergo a condensation reaction forming new siloxane linkages and thus remains as a viscous liquid during silica formation. Both **BA**- and **DDA**-derived silica particles could still be formed within this non-crosslinkable silicone medium. Since PEG was also required for the formation of the silica particles in these formulations, experiments to load the particles with fluorescent hydrophilic drug surrogates, fluorescein or HSA, and then follow their release in an aqueous solution were conducted.

Particle Size and Morphology

Particles formed using Benzylamine in Crosslinkable HO-PDMS

With **BA** as catalyst, the transparent silicone pre-elastomer mixture was converted to an opaque elastomer, which cured homogeneously with comparable hardness throughout the elastomer body shortly after mixing the 4 constituents of the formulation (HO-PDMS, TEOS, PEG, **BA**). However, the elastomers were not as highly crosslinked (i.e., were softer) than analogous tin-catalyzed silicone elastomers.²⁴ Analysis of the rubbers by optical and electron microscopy showed that polydisperse silica particles of average size approximately 10–11 μm were distributed throughout the cured elastomer body (Figure 4.2A). As seen from low resolution images (Figure 4.2D, SI), all particles exhibited the same open structure of fused silica nanoparticles covered by a thin silica shell in the nanometer range.

At 25%T in the **BA**-catalyzed formulation, the silica particles were covered by an extremely thin silica shell (Figure 4.2G): at 20%T, the microspheres were covered with a somewhat thicker solid silica shell (Figure 4.2J), but which was still only several nanometers thick. The average particle diameters were polydisperse, with diameters of approximately 10–11 μm irrespective of the TEOS concentration used in the formulation (Table 4.2). However, the polydispersity of the particles slightly increased and the shell of the silica particles became less prominent with higher [TEOS] as shown in Figure 4.2J, M and N. Higher concentrations of silica precursor also affected particle morphology as seen in the cross-sections (Figure 4.2G, J, K). The structure of the silica contained within the **BA**-catalyzed particles were macroporous in nature and are reminiscent of those described by Nakanishi¹⁶ and Brennan.^{25,29,30} When comparing Figure 4.2M–O, the pore sizes of the 20%T and 15%T particles appear to be smaller than the 25%T particles. The monolithic silica in the 25%T particles appeared as an open assembly of ~70–100 nm diameter fused silica particles (Figure 4.2M), while the 20%T and 15%T fused particles were even smaller and ranged between ~25–60 nm (Figure 4.2N, O).

All of the SEM images shown above were obtained from formulations containing PEG1000. When very low molecular weight TEG replaced PEG, well defined particles did not form, and instead bulk aggregates resulted (SI).

These results were initially quite surprising since Nakanishi¹⁶ reported that very high molecular weight poly(ethylene oxide) (>100,000 g/mol) is necessary to form macroporous silica structures. It has been reported that PEG of lower molecular weights will also serve to facilitate phase segregation leading to porous silica structures but only if the PEG is capped by small hydrophobes.¹⁷ In both cases, the high viscosities created by these PEGs are important to maintain structure in an aqueous environment. Here, PEG droplets dispersed in a silicone oil can be of lower viscosity because of the slow ingress of the key reagent water: the silica structures are never exposed to a mobile aqueous environment.

Particles formed using Dodecylamine in Crosslinkable HO-PDMS

Using **DDA** as catalyst, a very different outcome was observed under otherwise identical conditions. First, the silicone did not cure homogeneously: preferential curing of the silicone elastomer was always noted near the upper (air) surface (Figure 4.3B–D), which is the locus of entry of the co-reactant water. The silicone at the bottom portion of the elastomers was only lightly crosslinked in many cases and had the consistency of a soft, tacky gel-like material. Over several weeks, the bottom layers of the **DDA**-catalyzed elastomers underwent slight additional cure, but the bottom half of the elastomer body was never as highly crosslinked as the upper half of the elastomer (thickness of the body was ~2 mm).

The type of silica particles that formed within the **DDA**-catalyzed silicone elastomers depended on the presence of PEG, and also on the concentration of TEOS. In the absence of PEG, or at low [TEOS], a monolithic silica layer formed at the air interface (Figure 4.2L). In the presence of PEG, a monolithic silica layer was still observed near the air interface but only at high [TEOS] (25%T), but even in these cases the layers were much thinner than in the absence of PEG.

The silica particles that formed in the presence of PEG with **DDA** catalysts inside the silicone were polydisperse, but less so than the **BA**-derived silica (Table 4.2), and were also smaller in diameter $\sim 4\text{--}5\ \mu\text{m}$: they were dispersed throughout the elastomer body except near the air-interface and the base of the vessel (Figure 4.2B,C). The morphology of the silica particles was completely different from **BA**-derived silica. The particles appeared to be solid and non-porous, but upon freeze fracture were shown to be hollow, with a dense shell that varied slightly with [TEOS]. With 15% TEOS, the particle shell thicknesses were approximately $\sim 310\ \text{nm}$, whereas at 25%T the particles had a shell of $\sim 250\ \text{nm}$ thickness. [TEOS] also affected particle morphology, as at lower [TEOS] (15%T), the particles were hollow but at higher concentrations (25%T) the dense external shells were lined with a layer of porous monolithic silica and a hollow core (Figure 4.2H v I). As with the BA-derived particles, the polydispersity of the particles also increased slightly with higher [TEOS].

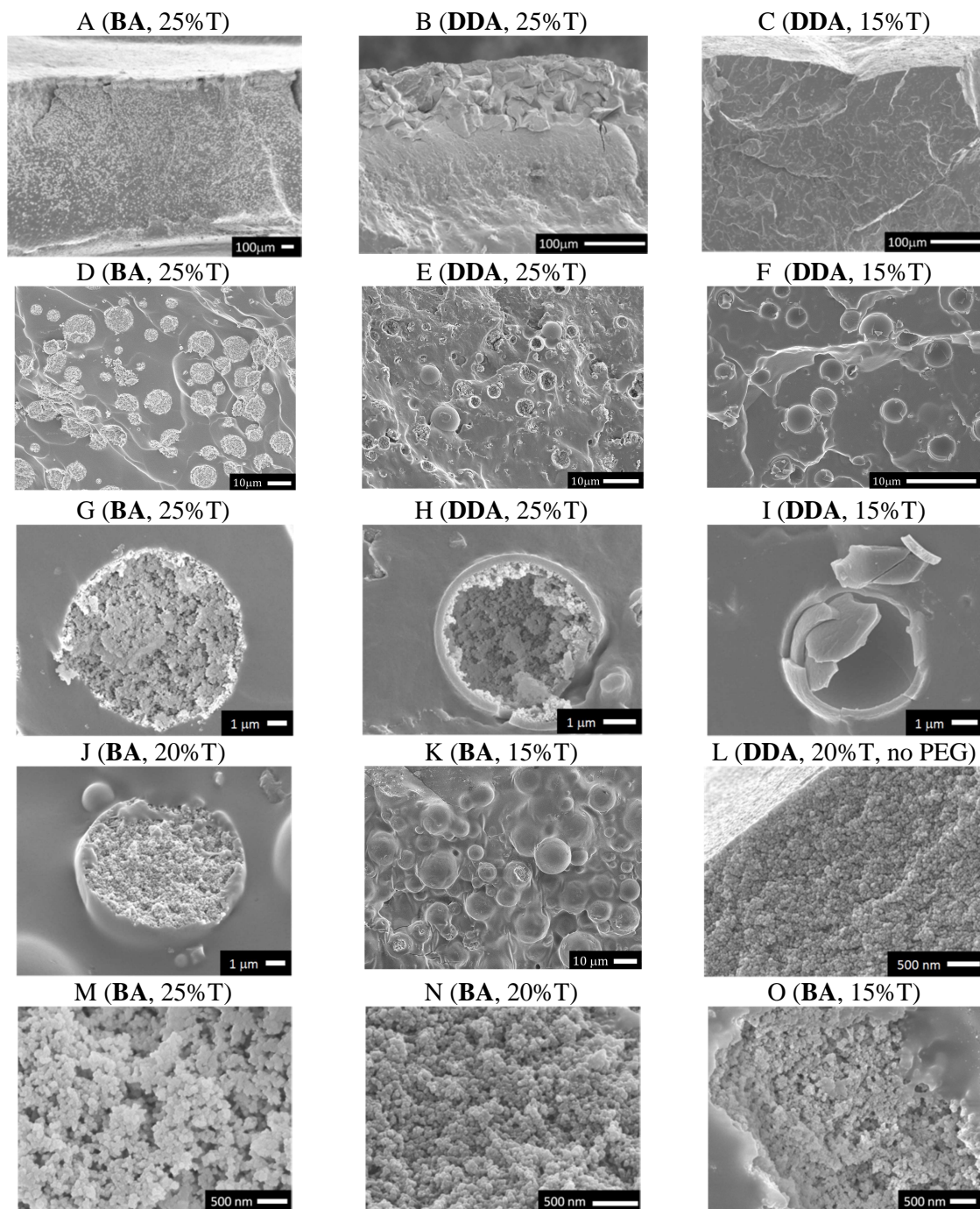


Figure 4.2: SEM Cross-sections of BA- and DDA-derived particles are shown at different TEOS concentrations and magnifications. Images J and K show BA-catalyzed particles at 20%T and 15%T. Image L shows monolithic silica formation at the air-surface interface with DDA in the absence of PEG. Images M–O are expanded images of the BA-catalyzed porous silica at 25%, 20% and 15%T, respectively. Selected additional photos with identical scaling may be found in the SI.

Table 4.2: Average diameter, standard deviation (μm) and polydispersity index (PDI) of BA and DDA-derived particles in HO-PDMS with varying amounts of TEOS^a

% TEOS	BA-catalyzed	PDI	DDA-catalyzed	PDI
15	11.6 \pm 3.6	0.1	3.8 \pm 0.9	0.06
20	11.1 \pm 3.4	0.09	4.9 \pm 1.8	0.13
25	10.6 \pm 4.4	0.17	4.5 \pm 1.4	0.1

^a **BA** and **DDA**-catalyzed formulations at 5–10% TEOS did not give cohesive elastomers for SEM imaging.

BA and DDA-Derived Particles in Non-crosslinkable VT-PDMS

Both macroporous and hollow silica particles could be formed in and isolated from VT-PDMS oil, which does not undergo crosslinking under the condensation conditions used. The morphologies of the particles in VT-PDMS were characterized in the SEM after crushing them with steel ball bearings. As shown in Figure 4.4A–C, the **BA**-derived particles were similar in morphology to their counterparts formed in crosslinked elastomers. By contrast, the **DDA**-derived particles in VT-PDMS were more sensitive to [TEOS]. Clean hollow particles weren't observed: the formulation containing 15%T contained hollow particles but with macroporous silica lining the inside of the shell, similar to the particles observed in the **DDA** 25%T in the elastomer (Figure 4.2H); at higher [TEOS] the shells were filled with monolithic silica (Figure 4.4D, E). The average particle diameters of the isolated particles (Table 4.3) were nearly identical to those obtained in the crosslinkable HO-PDMS system, however, they were slightly more polydisperse compared to their elastomeric counterparts. The shell thicknesses of both **BA** and **DDA** catalyzed were similar to the HO-PDMS counterparts, and the shell of the **BA** catalyzed particles at 25% T can now clearly be seen compared to its crosslinked counterpart. Also unlike the case with crosslinked silicone elastomers, SEM images showed the presence of small amounts aggregated silica in the VT-PDMS samples in addition to the structured particles.

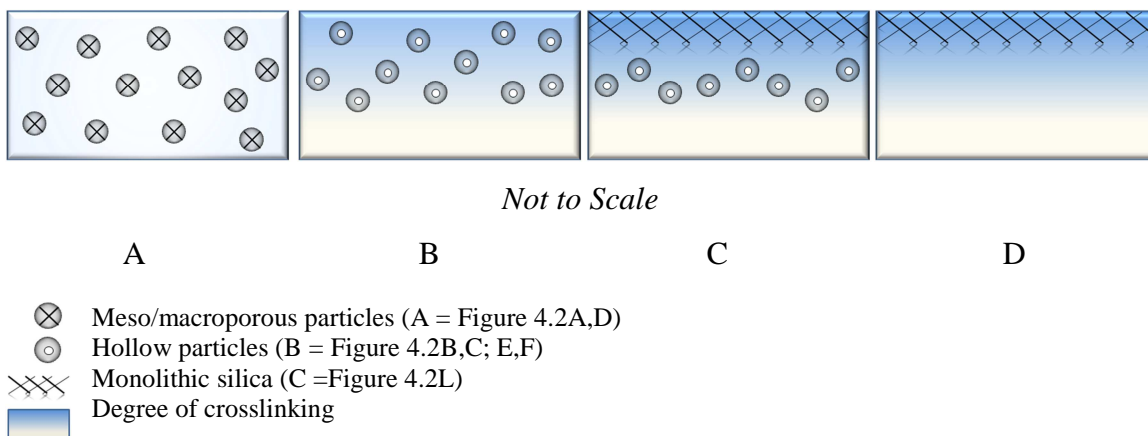


Figure 4.3: Model of silica structuring occurring in A: BA-catalyzed elastomers, B: DDA-catalyzed elastomers with low %TEOS, C: DDA with high %TEOS, D: DDA with high %TEOS and no PEG.

When using either catalyst in VT-PDMS, PEG600 led to particles that were similar to those in the crosslinkable HO-PDMS and PEG1000, but it was not possible to make particles in the presence of a lower molecular weight hydrophilic phase (TEG). Instead, only aggregates resulted (SI).

The amount of available TEOS constitutes one difference between the crosslinking and oil formulations. Since TEOS cannot crosslink VT-PDMS, there is more TEOS available to produce silica than with the HO-PDMS formulations. Silica formation can therefore start more rapidly, and with less well controlled timing of phase separation. More silica precursor also leads to a larger proportion of monolithic silica in the DDA-derived particles in oil. In addition, the size of the final silica particles depend on the PEG droplet sizes. In the VT-PDMS system, PEG droplets can coalesce with each other over time to give a variety of particle sizes. However, within the curing HO-PDMS system, the PEG droplets are eventually locked within a silicone matrix, which reduces the degree of coalescence. For these reasons, dispersed monolithic silica and the increased particle polydispersity is observed in the non-crosslinkable system.

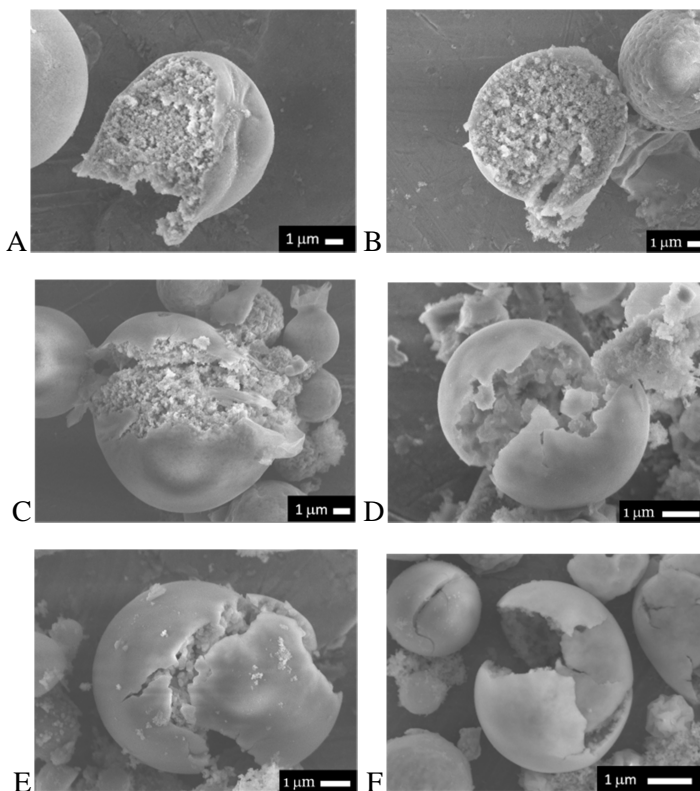


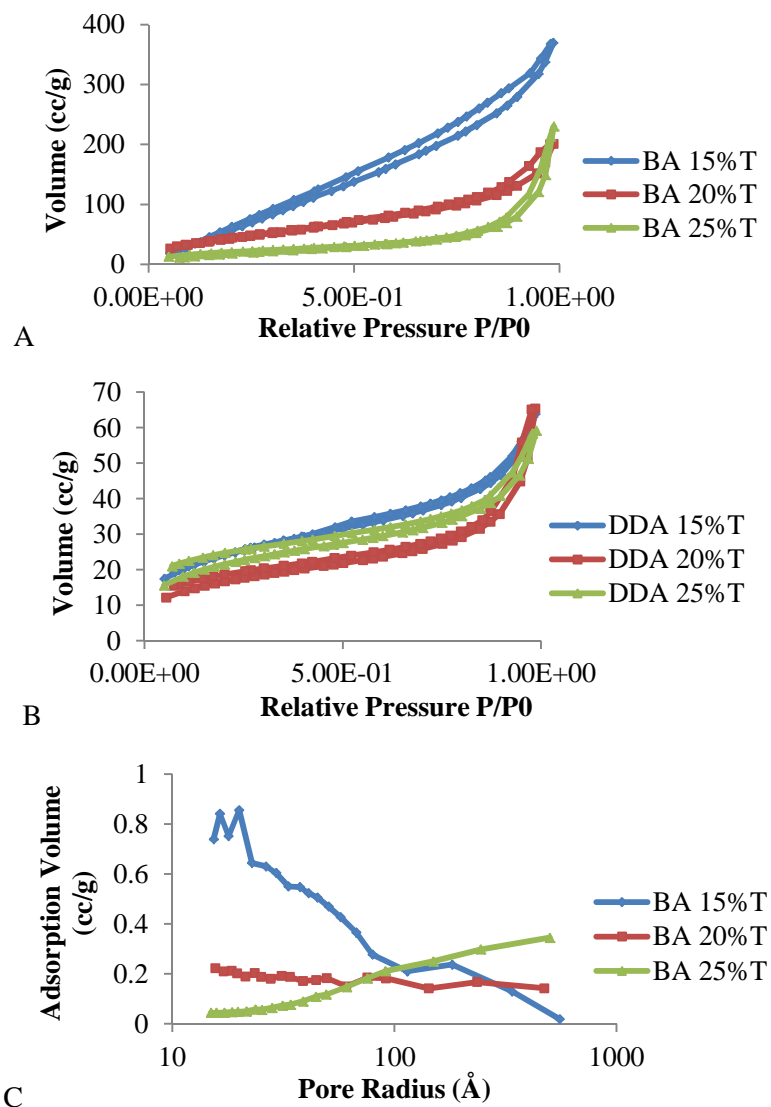
Figure 4.4: SEM images of isolated and crushed silica particles using PEG600 and catalyzed with **BA**-containing 25%T (A), 20%T (B), 15%T (C) and **DDA**-catalyzed particles with 25%T (D), 20%T (E) and 15%T (F).

Table 4.3: Average diameter, standard deviation (μm) and PDI of **BA** and **DDA**-catalyzed particles isolated from VT-PDMS with varying amounts of TEOS

% TEOS	BA -catalyzed	PDI	DDA -catalyzed	PDI
15	10.2 ± 4.7	0.21	3.3 ± 1.5	0.21
20	9.4 ± 4.0	0.18	3.0 ± 1.1	0.13
25	9.6 ± 3.6	0.14	3.5 ± 2.0	0.33

Structural information was also provided by nitrogen adsorption-desorption data for two particles with very different morphologies (see also fluorescein release from these particles below). Figure 4.5A shows that the **BA**-derived particles all have a type V physisorption isotherm whereas the **DDA**-derived particles type IV (Figure 4.5B).³¹ The hysteresis loops for all samples appear as a type H3, consistent with slit-shaped pores.³¹ Utilizing the BJH model, Figure 4.5C and D represent the pore size distributions of the

BA- and **DDA-**derived particles during adsorption. The **BA** particle pore sizes change from predominantly micro and mesoporous at 15%T, to meso-macroporous at 25%T. At 20% T, there is an even distribution of micro to macropores. As expected, the surface area of the **BA** particles calculated by MP-BET decreases with higher [TEOS] as shown in Table 4.4. The **DDA** particles show a similar trend with a greater fraction of smaller pores at a lower [TEOS]. The 15%T particles contain a narrow distribution of micro-mesopores, while the 25%T mainly consists of meso-macropores. The **BA-**derived particles had much higher pore volumes than the **DDA-**derived particles.



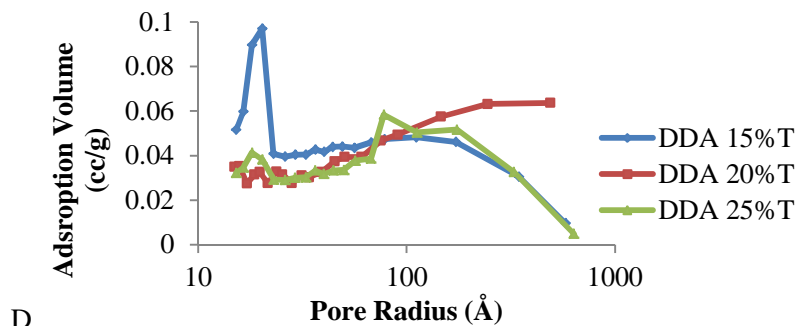


Figure 4.5: Nitrogen adsorption-desorption isotherms of A: **BA** catalyzed B: **DDA** catalyzed particles and BJH pore size distribution data during nitrogen adsorption for C: **BA** catalyzed and D: **DDA** catalyzed particles.

The Role of the Amine Catalysts in Silica Formation

Amines are not particularly efficient catalysts for silicone crosslinking,²⁸ although ammonia is widely utilized to prepare silica from TEOS in the mechanistically related sol-gel Stöber process in hydroxylic solvents.¹² The way in which silica is formed within silicone elastomers in the presence of PEG is clearly dependent on the nature of the catalysts. We propose that structural distinctions in the silica particles arise because of the different solubilities of the two amine catalysts in silicone oil and PEG, respectively, and the facility with which water is transported through the silicone.

Table 4.4: Surface Area and total pore volume of BA and DDA catalyzed particles

Particles	Surface area (m ² /g)	Total Pore Volume (cc/g)
BA 15%T	341	0.572
BA 20% T	165	0.311
BA 25% T	77	0.356
DDA 15%T	88	0.098
DDA 20%T	61	0.101
DDA 25% T	78	0.092

Irrespective of the catalyst used, silica was found to form preferentially within the dispersed PEG droplet, rather than within the silicone environment. An understanding of silica formation requires, therefore, consideration of the behavior of TEOS in PEG when only low levels of water are present. When a catalyst is present in PEG along with TEOS

the sol gel process begins to occur. At relatively early stages in the process, alkoxy silane hydrolysis and silanol condensation begin but, before the silica matrix can solidify, decomposition of the mixture into two phases occurs: PEG/silica-rich and solvent (ethanol)-rich³² phases are stabilized by hydrogen bonding between the ether oxygens and the free silanols on the nucleated silica particles.³²⁻³⁴ The latter phase simply contains solvent or ethanol by-product from hydrolyzed TEOS which can be removed to form pores at the meso and macroporous scales.^{29,30} This behavior is exactly mimicked by the system of TEOS + PEG with **BA** as catalyst.

BA is soluble in both silicone and PEG. Not surprisingly, therefore, silicone crosslinking was relatively efficient, occurring homogeneously through the elastomer matrix. Within the PEG droplet (in the absence of PEG, ill-defined silica aggregates are formed), **BA** effects hydrolysis and condensation at sufficiently low rates that spinodal decomposition occurs prior to complete silica formation within the droplet. As a consequence, the observed silica structure is monolithic and appears to be very similar to those observed in silicone-free systems with PEG, TEOS and small amounts of water.³⁰⁻³⁴ That is, the PEG/TEOS/**BA** droplet is simply a microreactor for monolithic silica formation because the catalyst is also soluble in PEG (Figure 4.6A). In non-crosslinkable VT-PDMS, **BA** is not required for elastomer crosslinking at all, thus it only catalyzes silica formation to form the same porous structures. As seen earlier with Figure 4.2M–O, the size of the pores appear to be marginally larger with higher [TEOS], and this can also be related back to spinodal decomposition. An increase in TEOS leads to an increase in the ethanol by-product, thus phase separation of the ethanol and the PEG/silica phases becomes more pronounced. This allows for phase separation of the PEG/silica and ethanol domains to occur much more efficiently, thus leading to larger pores.

The monolithic silica appears to be comprised of small (~50–100 nm, Figure 4.2K) silica particles that are fused to give a very open structure. The monolithic silica assembly is limited by the size of the PEG droplet within the silicone. Thus, the silica particles are formed in a type of hierarchical assembly controlled by phase separation: PEG/silica phase separation leads to monolithic structures comprised of small, fused

silica particles, while PEG/silicone phase separation controls the size of the monolithic assembly of silica particles in silicone that are about 100 times the size of the fused particles.

PEG plays roles in addition to acting as a silica incubator. Since the polymer is hydrophilic, it acts to sequester water and any silicone soluble PEG can facilitate water transmission through the silicone to the PEG droplets where it can be used to make silica. Without it, transmission of water through the elastomer occurs more slowly and as a result, so does hydrolysis/condensation/cure.

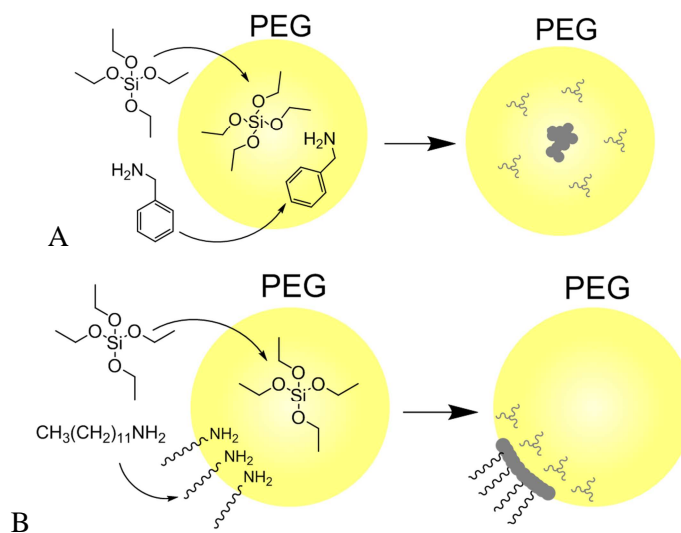


Figure 4.6: General schematic of BA (A) and DDA (B) phase separation from continuous silicone oil phase into PEG droplets for the formation of particles.

DDA-catalyzed silicone elastomers exhibited less crosslinking per se and led to less homogeneously crosslinked elastomer bodies (Figure 4.3B–D). The silica particles within the elastomer or the silicone oil (VT-PDMS) were smaller than with **BA**-catalyzed systems, suggesting the presence of more or better surface-active species to stabilize the PEG droplets. Unlike **BA**, **DDA** with its longer hydrophobic tail is sparingly soluble in either silicone oil (silicones are oleophobic)³⁵ or PEG. The catalyst thus preferentially resides at the PEG/silicone droplet interface with the amine oriented into the PEG phase (Figure 4.6B). This proposal is consistent with the much less efficient curing of the

silicone into elastomers that was observed with this catalyst – the catalyst is tied up at the PEG/silicone interface.

The addition of a surfactant to a formulation increases the surface area of a dispersed phase that can be supported.³⁶ The presence of **DDA** in the PEG-in-silicone dispersion led to much smaller, and less polydisperse, PEG droplet sizes than in analogous **BA**-containing formulations because the **DDA** is acting as a surfactant stabilizing the PEG/silicone interface (Figure 4.6). Within the PEG droplet, hydrolysis and condensation of TEOS will primarily be catalyzed at the PEG/PDMS interface where the **DDA** is located, gradually leading to thick silica shells around the PEG droplet. That is, **DDA** facilitates silica particle structuring by operating as a catalytic surfactant (Figure 4.6B).

In crosslinkable HO-PDMS, **DDA**-derived particles always led to hollow silica particles, however, in VT-PDMS particles filled with porous silica were formed at higher [TEOS] and hollow particles with porous silica lining the shells were formed at low [TEOS]. This suggests that at higher [TEOS] the catalyst can more easily migrate into the PEG droplets. This change in solubility can be understood by the evolving solvent conditions that arise during sol-gel reactions. Ethanol, formed during the sol-gel process, helps solubilize **DDA** in PEG, as shown by Caldararu et al.³⁷ High [TEOS] lead to more ethanol by-product that can solubilize the amine catalyst in the PEG. In this situation, silica forms in three distinct locations: at the PEG/silicone interface leading to the external particle shell, inside the PEG droplet thus forming monolithic porous silica, and adjacent to the silica shell where the EtOH concentration is higher and solubilizes **DDA**.

The dominant process with **DDA**, which is exclusively seen at lower [TEOS], is the formation of a PEG-filled dense silica shell. At high [TEOS], catalyst migration into the PEG droplet increases, thus explaining the different morphologies observed with the **DDA**-derived particles in HO-PDMS and VT-PDMS. In VT-PDMS, crosslinking of the silicone doesn't occur and a much larger amount of silica precursor and ethanol byproduct is available to solubilize the catalyst further into the PEG droplet to form monolithic structures similar to the **BA**-catalyzed particles. That is, with higher EtOH

concentrations the silica forms at the PEG/silicone interface and, by virtue of the EtOH, also in the PEG itself.

For **DDA**-catalyzed elastomer formulations that do not contain PEG, a layer of monolithic silica preferentially forms at the air-surface interface due to the higher rate of hydrolysis and formation of ethanol, and therefore catalyst solubilization, at the locus of entry of water (Figure 4.2L). The same effect was observed in particles formed in non-crosslinkable VT-PDMS formulations, which also led to hollow particles. Since there is a larger quantity of available TEOS, as a silicone network is not being crosslinked, it appears that more TEOS migrates into the PEG droplets to help solvate **DDA** better. Thus, the same macroporous silica lining the interior of the hollowed particles can be achieved at lower [TEOS] compared to the HO-PDMS particles.

TEOS concentration plays an important role in controlling pore volume and surface area (Figure 4.5). With the **BA**-derived particles, surface area dropped sharply with increased TEOS. By contrast, **DDA**-derived particles were much less sensitive. In all cases, dense silica at the PEG/silicone interface formed and at higher TEOS concentrations, was accompanied with monolithic structures inside the droplets.

Fluorescein and HSA Release from Silica Particles

Silica particles of very different morphologies were obtained simply by changing the catalyst for its formation. We reasoned the particles could be very useful for controlled release. Two particles were compared with very different morphologies: the macroporous **BA**-catalyzed particles at 25%T and the hollow **DDA**-derived particles at 15%T, both formed within VT-PDMS. Their potential as drug depots was investigated by formulating silica with PEG that contained either fluorescein or HSA, the release of which were easily followed by fluorescence. A comparison was made between releases into a 1% SDS aqueous solution from the as-isolated particles: the surfactant was required as to avoid coagulation due to residual VT-PDMS.

Figure 4.7 shows the release profiles for fluorescein and HSA-loaded silica particles. For the **BA**-derived particles, release appears complete within the first measurement of the experiment (within 15 minutes), after the burst. By contrast, the

DDA-derived particles show a large initial burst release of fluorescein followed by a slower secondary release.

In previous work with meso/macroporous silica, we observed that small molecules could diffuse through the silica with relatively low resistance.³⁸ Only with certain formulations, which produced small mesopores (< 5 nm) connected by macroporous channels, could proteins be retained. The secondary slow release of fluorescein from the dense shells of **DDA**-derived particles (hollow) is consistent with this behavior. Figure 4.5 demonstrates that **DDA** particles at 15% T have a high fraction of small pores, from which it is proposed the secondary release occurs. That is, the main release is through leakage from the PEG core to the outside through macropores, with slower release through channels in dense silica structures from macropores.

The use of amine RTV catalysts in lieu of traditional titanium- or tin-derived compounds does not lead to better silicone elastomers. Instead either lower levels of cure were observed (**BA**) on inhomogeneous cure (**DDA**) was observed. The use of amine catalysts, however, does provide two distinct levels of morphological control over the silicone elastomer: cure within the silicone, and, morphology of the silica found within the silicone. At high water levels and with **BA** as catalyst, particularly when PEG is present, it is easier to obtain a silicone elastomer body that is homogeneously cured throughout. With the less effective **DDA** catalyst, in particular, it was not possible to achieve homogeneous cure. Thus, these catalysts do not lead to better silicone elastomers.

Of much greater interest is the level of morphological control over the silica formed within silicone oils that is formed within the silicone simply by changing the catalyst. It is possible to create either large macroporous silica particles throughout the elastomer or hollow silica particles. The very different silica structures provide different release profiles of a small molecule and protein.

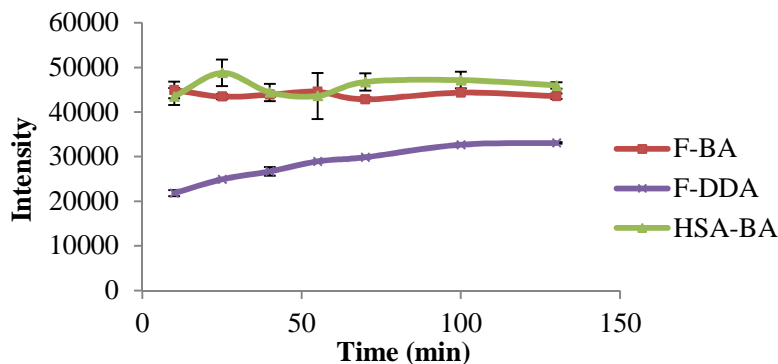


Figure 4.7: Fluorescence profiles of **BA**- and **DDA**-catalyzed particles loaded with fluorescein (**F**) or **HSA** over time.

4.5 Conclusion

The use of amine-based catalysts, high concentrations of the crosslinker and silica precursor TEOS, and PEG as a hydrophilic phase, permits the formation of well-defined silica particles within silicone elastomer matrices and in silicone oil, which can then be isolated. The solubilities of the amine catalysts in silicone and PEG determine the structural morphologies of the resulting silica particles. The soluble amine, **BA**, leads to macroporous silica particles (~10–11 μ m) that are dispersed throughout the elastomer network when using crosslinkable HO-PDMS, or that can be isolated from non-crosslinkable VT-PDMS. Pore sizes of the **BA** particles were found to increase in size with higher [TEOS]. Dodecylamine, which is a catalytic surfactant for PEG, preferentially resides at the PEG/silicone interface (facilitating droplet formation). As a consequence, hollow particles with thick silica shells (~250–310 nm) surround the PEG droplets in the final product. However, **DDA** can penetrate further within the PEG droplet in VT-PDMS at high [TEOS] due to the higher concentration of solubilizing ethanol byproduct, leading to particles with a higher monolithic fraction. Release profiles of fluorescein and HSA-loaded silica particles show slightly different patterns that correspond to a greater fraction of small pores in the **DDA**-derived particles.

4.6 Acknowledgments

We acknowledge with gratitude the financial support of 20/20: NSERC Ophthalmic Materials Research Network. We also thank Dr. Robert Pelton (McMaster University Chemical Engineering) for use of a humidity chamber, Dr. Yang Chen (McMaster, Chemistry) for assistance with freeze fracturing the prepared samples and both for helpful discussions.

4.7 Supporting Information

Table S 4.1: BA-catalyzed formulations (2.5g) with varying TEOS loadings and their average particle sizes (μm)^a

F. #	Parameter	Weight (g)	Wt.%	F. #	Parameter	Weight (g)	Wt.%
1	HO-PDMS	2.125	85	10	HO-PDMS	1.5	60
	TEOS	0.125	5		TEOS	0.625	25
	BA	0.25	10		BA	0.25	10
	PEG1000	0	0		PEG600	0.125	5
	Avg. Particle Size	-			Avg. Particle Size	10.6 ± 4.4	
2	HO-PDMS	2	80	11	VT-PDMS	1.875	75
	TEOS	0.25	10		TEOS	0.375	15
	BA	0.25	10		BA	0.25	10
	PEG1000	0	0		PEG600	0	0
	Avg. Particle Size	-			Avg. Particle Size	-	
3	HO-PDMS	1.875	75	12	VT-PDMS	1.75	70
	TEOS	0.375	15		TEOS	0.5	20
	BA	0.25	10		BA	0.25	10
	PEG1000	0	0		PEG600	0	0
	Avg. Particle Size	-			Avg. Particle Size	-	
4	HO-PDMS	1.75	70	13	VT-PDMS	1.625	65
	TEOS	0.5	20		TEOS	0.625	25
	BA	0.25	10		BA	0.25	10
	PEG1000	0	0		PEG600	0	0
	Avg. Particle Size	-			Avg. Particle Size	-	
5	HO-PDMS	1.625	65	14	VT-PDMS	1.75	70
	TEOS	0.625	25		TEOS	0.375	15
	BA	0.25	10		BA	0.25	10

	PEG1000	0	0		PEG600	0.125	5
	Avg. Particle Size	-			Avg. Particle Size	10.2 ± 4.7	
	HO-PDMS	2	80		VT-PDMS	1.625	65
	TEOS	0.125	5		TEOS	0.5	20
6	BA	0.25	10	15	BA	0.25	10
	PEG1000	0.125	5		PEG600	0.125	5
	Avg. Particle Size	-			Avg. Particle Size	9.4 ± 4.0	
	HO-PDMS	1.875	75		VT-PDMS	1.5	60
	TEOS	0.25	10		TEOS	0.625	25
7	BA	0.25	10	16	BA	0.25	10
	PEG1000	0.125	5		PEG600	0.125	5
	Avg. Particle Size	-			Avg. Particle Size	9.6 ± 3.6	
	HO-PDMS	1.75	70		VT-PDMS	1.5	60
	TEOS	0.375	15		TEOS	0.625	25
8	BA	0.25	10	17	BA	0.25	10
	PEG1000	0.125	5		0.6 mM PEG600 w/ Fluorescein	0.125	5
	Avg. Particle Size	11.6 ± 3.6					
	HO-PDMS	1.625	65		VT-PDMS	1.5	60
	TEOS	0.5	20		TEOS	0.625	25
9	BA	0.25	10	18	BA	0.25	10
	PEG1000	0.125	5		HSA-PEG600	0.125	5
	Avg. Particle Size	11.1 ± 3.4					

^a At 5% and 10%T loadings, cohesive elastomers couldn't be obtained with or without PEG.

Table S 4.2: DDA-catalyzed formulations (2.5g) with varying TEOS loadings and their average particle sizes (μm)^a

F. #	Parameter	Weight (g)	Wt. %	F. #	Parameter	Weight (g)	Wt. %
19	HO-PDMS	2.125	85	28	HO-PDMS	1.5	60
	TEOS	0.125	5		TEOS	0.625	25
	DDA	0.25	10		DDA	0.25	10
	PEG1000	0	0		PEG600	0.125	5
	Avg. Particle Size	-			Avg. Particle Size	4.5 ± 1.4	
20	HO-PDMS	2	80	29	VT-PDMS	1.875	75
	TEOS	0.25	10		TEOS	0.375	15
	DDA	0.25	10		DDA	0.25	10
	PEG1000	0	0		PEG600	0	0
	Avg. Particle Size	-			Avg. Particle Size	-	
21	HO-PDMS	1.875	75	30	VT-PDMS	1.75	70
	TEOS	0.375	15		TEOS	0.5	20
	DDA	0.25	10		DDA	0.25	10
	PEG1000	0	0		PEG600	0	0
	Avg. Particle Size	-			Avg. Particle Size	-	
22	HO-PDMS	1.75	70	31	VT-PDMS	1.625	65
	TEOS	0.5	20		TEOS	0.625	25
	DDA	0.25	10		DDA	0.25	10
	PEG1000	0	0		PEG600	0	0
	Avg. Particle Size	-			Avg. Particle Size	-	
23	HO-PDMS	1.625	65	32	VT-PDMS	1.75	70
	TEOS	0.625	25		TEOS	0.375	15
	DDA	0.25	10		DDA	0.25	10
	PEG1000	0	0		PEG600	0.125	5
	Avg. Particle Size	-			Avg. Particle Size	3.3 ± 1.5	
24	HO-PDMS	2	80	33	VT-PDMS	1.625	65
	TEOS	0.125	5		TEOS	0.5	20
	DDA	0.25	10		DDA	0.25	10
	PEG1000	0.125	5		PEG600	0.125	5
	Avg. Particle Size	-			Avg. Particle Size	3.0 ± 1.1	
25	HO-PDMS	1.875	75	34	VT-PDMS	1.5	60
	TEOS	0.25	10		TEOS	0.625	25
	DDA	0.25	10		DDA	0.25	10

	PEG1000	0.125	5		PEG600	0.125	5
	Avg. Particle Size	-			Avg. Particle Size	3.5 ± 2.0	
26	HO-PDMS	1.75	70	35	VT-PDMS	1.75	70
	TEOS	0.375	15		TEOS	0.375	15
	DDA	0.25	10		DDA	0.25	10
	PEG1000	0.125	5		0.6 mM PEG600 w/ Fluorescein	0.125	5
	Avg. Particle Size	3.8 ± 0.9					
27	HO-PDMS	1.625	65				
	TEOS	0.5	20				
	DDA	0.25	10				
	PEG1000	0.125	5				
	Avg. Particle Size	4.9 ± 1.8					

^a At 5% and 10% T loadings, cohesive elastomers couldn't be obtained with or without PEG

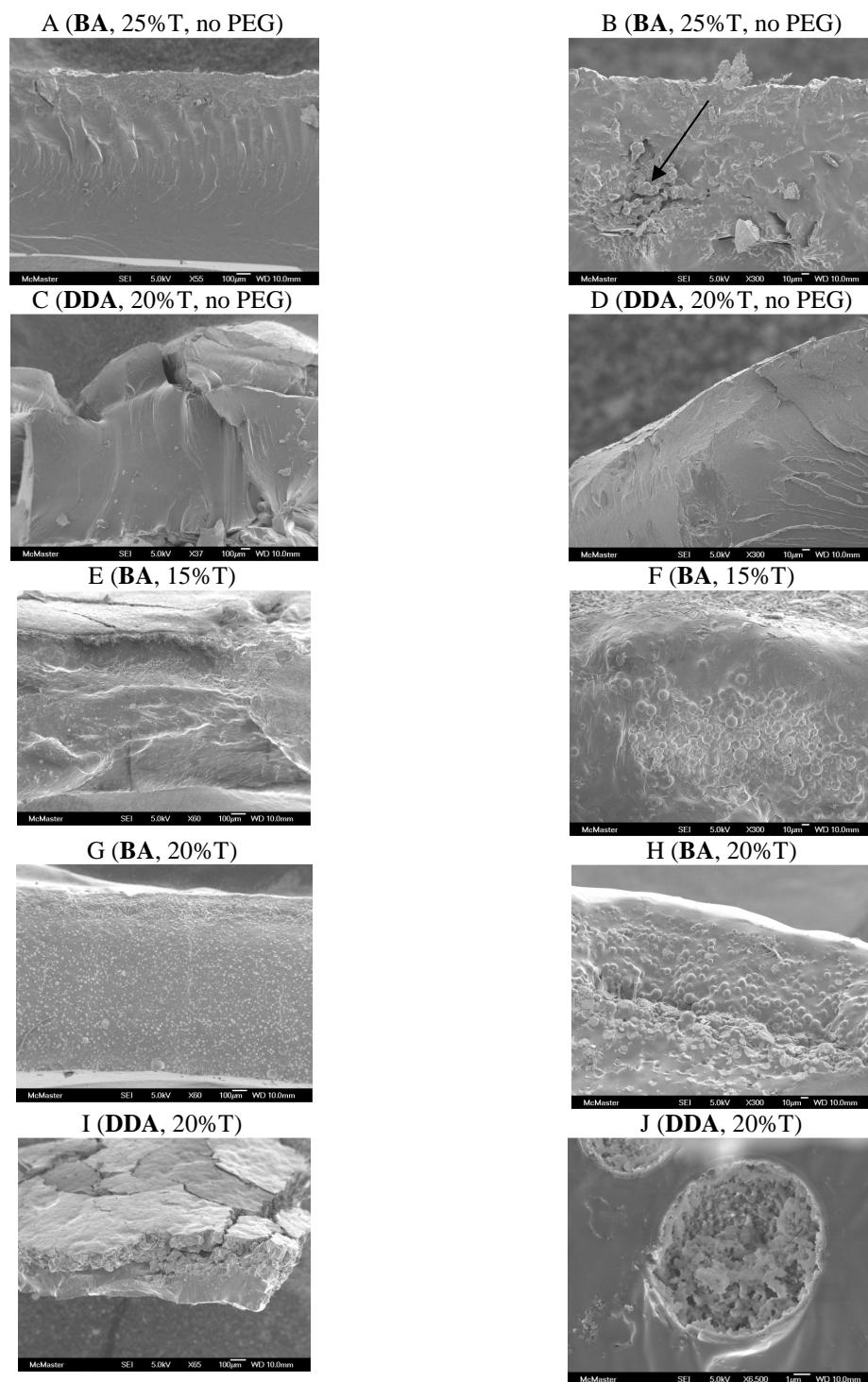


Figure S 4.1: SEM images of various BA and DDA catalyzed elastomers at different magnifications. Arrow in B points out few solid particles that appear non-reproducibly in BA catalyzed systems without PEG.

4.8 References

- (1) Wei, Y.; Xu, J.; Feng, Q.; Dong, H.; Lin, M. *Mater. Lett.*, **2000**, *44*, 6.
- (2) Vallet-Regi, M.; Rámila, A.; del Real, R. P.; Pérez-Pariente, J. *Chem. Mater.*, **2000**, *13*, 308.
- (3) Wang, Y.; Caruso, F. *Chem. Commun.*, **2004**, 1528.
- (4) Ning, Y. P.; Mark, J. E. *Polym. Bull.*, **1984**, *12*, 407.
- (5) Grün, M.; Kurganov, A. A.; Schacht, S.; Schüth, F.; Unger, K. K. *J. Chromatogr. A*, **1996**, *740*, 1.
- (6) Han, A.; Qiao, Y. *J. Am. Chem. Soc.*, **2006**, *128*, 10348.
- (7) Silva, A. R.; Wilson, K.; Whitwood, A. C.; Clark, J. H.; Freire, C. *Eur. J. Inorg. Chem.*, **2006**, *2006*, 1275.
- (8) Hah, H. J.; Um, J. I.; Han, S. H.; Koo, S. M. *Chem. Commun.*, **2004**, *0*, 1012.
- (9) Wang, Y.; Caruso, F. *Adv. Mater.*, **2006**, *18*, 795.
- (10) Brinker, C.; Scherer, G. *Sol-Gel Science: The Physics and Chemistry of Sol-Gel Processing*; Academic Press: New York, 1990.
- (11) Iler, R. K. *The chemistry of silica: solubility, polymerization, colloid and surface properties, and biochemistry*; Wiley New York, 1979.
- (12) Stöber, W.; Fink, A.; Bohn, E. *J. Colloid Interface Sci.*, **1968**, *26*, 62.
- (13) Hoffmann, F.; Cornelius, M.; Morell, J.; Fröba, M. *Angew. Chem. Int. Ed.*, **2006**, *45*, 3216.
- (14) Cai, Q.; Cui, F. Z.; Chen, X. H.; Zhang, Y.; Luo, Z. S. *Chem. Lett.*, **2000**, *29*, 1044.
- (15) Cai, Q.; Luo, Z.-S.; Pang, W.-Q.; Fan, Y.-W.; Chen, X.-H.; Cui, F.-Z. *Chem. Mater.*, **2001**, *13*, 258.
- (16) Nakanishi, K.; Tanaka, N. *Acc. Chem. Res.*, **2007**, *40*, 863.
- (17) Cademartiri, R.; Brook, M. A.; Pelton, R.; Brennan, J. D. *J. Mater. Chem.*, **2009**, *19*, 1583.
- (18) Yang, H.; Coombs, N.; Ozin, G. A. *Nature*, **1997**, *386*, 692.
- (19) Yang, H.; Coombs, N.; Sokolov, I.; Ozin, G. A. *J. Mater. Chem.*, **1997**, *7*, 1285.
- (20) Caruso, F.; Caruso, R. A.; Möhwald, H. *Science*, **1998**, *282*, 1111.
- (21) Hwang, H. S.; Lee, S. B.; Park, I. *Mater. Lett.*, **2010**, *64*, 2159.
- (22) Fujiwara, M.; Shiokawa, K.; Tanaka, Y.; Nakahara, Y. *Chem. Mater.*, **2004**, *16*, 5420.
- (23) Fujiwara, M.; Shiokawa, K.; Sakakura, I.; Nakahara, Y. *Nano Lett.*, **2006**, *6*, 2925.
- (24) Rajendra, V.; Gonzaga, F.; Brook, M. A. *Langmuir*, **2011**, *28*, 1470.

- (25) Cruz-Aguado, J. A.; Chen, Y.; Zhang, Z.; Brook, M. A.; Brennan, J. D. *Anal. Chem.*, **2004**, *76*, 4182.
- (26) Barrett, E. P.; Joyner, L. G.; Halenda, P. P. *J. Am. Chem. Soc.*, **1951**, *73*, 373.
- (27) Thomas, D. R. In *Siloxane Polymers*; Clarson, S. J., Semlyen, J. A., Eds.; Prentice Hall: Englewood Cliffs, 1993.
- (28) Brook, M. A. *Silicon in Organic, Organometallic, and Polymer Chemistry*; Wiley-VCH Verlag, 2000.
- (29) Brook, M. A.; Chen, Y.; Guo, K.; Zhang, Z.; Brennan, J. D. *J. Mater. Chem.*, **2004**, *14*, 1469.
- (30) Hodgson, R. J.; Chen, Y.; Zhang, Z.; Tleugabulova, D.; Long, H.; Zhao, X.; Organ, M.; Brook, M. A.; Brennan, J. D. *Anal. Chem.*, **2004**, *76*, 2780.
- (31) Sing, K. S. W.; Everett, D. H.; Haul, R. A. W.; Moscou, L.; Pierotti, R. A.; Rouquerol, J.; Siemieniewska, T. *Pure Appl. Chem.*, **1985**, *57*, 603.
- (32) Takahashi, R.; Nakanishi, K.; Soga, N. *J. Non-Cryst. Solids*, **1995**, *189*, 66.
- (33) Takahashi, R.; Sato, S.; Sodesawa, T.; Yabuki, M. *J. Catal.*, **2001**, *200*, 197.
- (34) Nakanishi, K.; Komura, H.; Takahashi, R.; Soga, N. *Chem. Soc. Jpn*, **1994**, *67*, 1327.
- (35) Haidara, H.; Chaudhury, M. K.; Owen, M. J. *J. Phys. Chem.*, **1995**, *99*, 8681.
- (36) Hunter, R. J. *Introduction to modern colloid science*; Oxford University Press Oxford, 1993; Vol. 7.
- (37) Caldararu, H.; Caragheorgheopol, A.; Savonea, F.; Macquarrie, D. J.; Gilbert, B. *C. J. Phys. Chem. B*, **2003**, *107*, 6032.
- (38) Hodgson, R. J.; Besanger, T. R.; Brook, M. A.; Brennan, J. D. *Anal. Chem.*, **2005**, *77*, 7512.

Chapter 5 – Silicone Resin Films from Reactive Siloxane-in Water Emulsions^{††}

5.1 Abstract

The Piers Rubinsztajn (PR) reaction has gained a considerable amount of attention because of efficient formation of siloxanes under mild conditions. This report explores the utilization of the PR reaction to form siloxane based films from surfactant free siloxane-in-water (S/W) emulsions as a convenient alternative to traditional sol-gel chemistry. Typically the PR reaction is extremely rapid and exothermic, however, since the $B(C_6F_5)_3$ catalyst used is a good Lewis acid, water, which acts as a Lewis base, coordinates to the catalyst to greatly moderate the reaction. The emulsions were formed within seconds by sonication and their stability and droplet sizes were investigated over 2 weeks. During this time depending on the concentration of the catalyst, which also acted as an electrostatic stabilizer, droplets underwent growth and coalescence, or crosslinking to form elastomeric systems. Depending on the age and catalyst concentration in the dispersion, it was possible to form rigid hydrophobic foam, dense films, or films of particles that fuse but do not coalesce. The film characteristics also depended on the cure temperature: more control was observed when cure occurred at RT rather than 100 °C on a glass substrate. The higher surface area particulate films formed may be of interest as separation media such as in gas chromatography (GC) columns. It was possible to deposit fused particulate films on the inside of glass capillary tubes or fused silica GC columns.

^{††} Portions of the following chapter were submitted to ACS Applied Materials and Interfaces with the citation: Vinodh Rajendra, Michael A. Brook, *ACS Appl. Mater. Interfaces*, 2014.

I was responsible for all synthesis and analysis. Dr. Brook gave some useful advice and troubleshooting ideas. I wrote the 1st draft of the manuscript and Dr. Brook helped with editing the document for final submission to the above journal.

5.2 Introduction

The formation of films of siloxane-based resins traditionally utilized sol-gel methodology. This process involves the condensation of alkoxy silanes such as tetraethyl orthosilicate (TEOS), or methyltrimethoxysilane, or other functional silanes, commonly under acidic or basic conditions. Over time and optionally with heating a network of siloxanes Si-O-Si forms. Once the solution has been prepared, substrates can then be dip coated to form thin silica films,¹⁻⁴ porosity of the films can be controlled with surfactants,^{2,3,5,6} particle templates,^{7,8} modified silica particles,⁹ electro-assisted deposition,¹⁰ the ordering of porous silica films can be controlled,^{3,11} and many other different studies. Such films are used in a variety of applications, including as catalytic supports and in electronics as interlayer dielectrics.¹²

The Piers Rubinsztajn (PR) reaction can be used to form Si-O-Si linkages by utilizing alkoxy silanes, hydrosilanes and the Lewis acidic catalyst $B(C_6F_5)_3$ (Figure 5.1A).¹³⁻¹⁵ Reactions occur rapidly under mild and can be used to prepare precisely structured small silicones,^{16,17} large polymers or well defined 3D structures.¹⁸⁻²⁰ It has been applied in organic media or without solvents, for example, to prepare foamed elastomers²¹ or aqueous solutions, including cationic silicone polymerizations in solution.²² Rubinsztajn et al. have reported the formation of silanol free resins using this method.²³ Ganachaud et al. described the formation of surfactant free siloxane-in-water emulsions which were used as microreactors to give large molecular weight silicone polymers and small cyclics from difunctional monomers.²⁴ The study also reported that the emulsions were colloidal stable for up to 1 week, whereafter precipitation occurred. Piers et al. have extended the control of this reaction. By synthesizing a carbamate borate salt, the catalyst remains inactive until irradiation with a 254 nm UV source that releases the carbamate group, thus reactivating the catalyst.²⁵ They noted that the PR reaction under these conditions leads to thin silica-based films using much milder conditions compared to the standard polycondensation method.

Our group was interested in forming hydrophobic films using this chemistry. One challenge involved finding conditions under which the reaction was controllable both in

terms of the exothermicity of the reaction and the structures of the resulting crosslinked products. It was also necessary to develop methodologies that had dispersions with reasonable pot lives. To address all these issues, we utilized the Ganachaud et al. emulsion methodology.^{22,24} Water is a Lewis base that co-ordinates to the boron catalyst to greatly inhibit catalysis: polymer synthesis could take up to several days to complete according to Ganachaud's findings because most of the catalyst was located in the water.

This report investigates the condensation of tetrafunctional siloxanes in a silicone-in-water emulsion by utilizing the PR reaction to form siloxane-based films upon drying. We note that the reaction conditions had to be designed to avoid competing reactions of boron-catalyzed silanol formation and the coupling of hydrosilanes and silanol groups (Figure 5.1B, C).

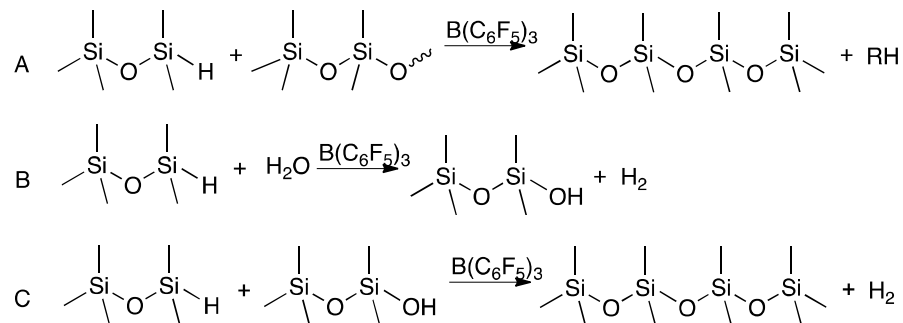


Figure 5.1: General reaction scheme of A: Piers-Rubinsztajn, B: hydrosilane with water and C: silanol coupling with a hydrosilane.

5.3 Experimental

Materials

Tetraethyl orthosilicate (TEOS, 95%, Aldrich), tetrakis(dimethylsiloxy)silane $\text{Si}(\text{OSiMe}_2\text{H})_4$ (QM^{H}_4 , Gelest), $\text{B}(\text{C}_6\text{F}_5)_3$ (95%, Aldrich), and de-ionized water (DI) was used to produce emulsions. All reagents were used as received. RT = 21-23 °C.

Characterization

^1H nuclear magnetic resonance (NMR) experiments were performed on a Bruker 600 spectrometer and ^{29}Si NMR with Si-H cross-polarization and magic angle spinning (CP-MAS) studies were conducted on a Bruker 300 or DRX500 spectrometer.

ATR-IR spectra were recorded on either a Thermo Scientific Nicolet 6700 FT-IR or a Bruker Vector 22, which was then processed by Omnic software and Excel. S/W emulsions were dropped onto the ATR crystal (ZnSe) at ambient conditions and were measured for their composition. In certain experiments, the emulsions were allowed to dry on to the crystal to form a film. The films were then removed from the crystal by physically scrapping them off.

Scanning electron microscopy (SEM) was conducted using a JEOL 7000F microscope with samples coated in gold for 1 min at $\sim 15 \text{ nm min}^{-1}$. Particle size and distributions were then measured manually from the micrograph using ImageJ software with $n = 50$.

Zeta potential measurements were performed with a ZetaPlus Zeta Potential Analyzer by Brookhaven Instruments. Measurements were carried by diluting samples (3 separate samples) in a 2mM NaCl solution at RT with 10 measurements and 15 cycles for each.

A Melles Griot 05-LHP-928 instrument with 75mW HeNe laser at 633 nm wavelength at RT was utilized for dynamic light scattering (DLS) measurements for average particle size measurements of the emulsions. 3 separate samples were utilized to determine an average.

Catalyst Stock Solutions

Three different stock solutions of TEOS/B(C₆F₅)₃ were created using 1 mg (0.002 mmol, 0.016 mM), 4 mg (0.008 mmol, 0.063 mM), or 12 mg (0.024 mmol, 0.19 mM) of the boron catalyst in 0.125 g of TEOS. Under dry conditions, the catalyst stock solutions could be stored for several hours or days.

Aqueous Emulsions

QM^H₄ (0.2 g, 0.6 mmol) was added to DI water (3 mL) in a glass vial that was immersed in an AquaSonic Model 50HT sonicator (VWR) for approximately 10 s to facilitate dispersion. Immediately thereafter, one of the TEOS + catalyst stock solutions (0.125g of TEOS and either 1, 4 or 12 mg of B(C₆F₅)₃) was added to the water mixture during sonication, which was continued for an additional 20 s to form the dispersion

(Figure 5.2). The sample could be used at once, or stored on the bench for up to several weeks. The particle size changed over this time (see below). An additional experiment was performed using a higher $\text{QM}^{\text{H}}_4/\text{B}(\text{C}_6\text{F}_5)_3$ ratio: QM^{H}_4 (0.26 g, 0.8 mmol) and $\text{B}(\text{C}_6\text{F}_5)_3$ (4 mg TEOS (0.08 g, 0.4 mmol)) were dissolved/dispersed in 3 mL of water to give a 2:1 molar ratio between QM^{H}_4 and TEOS, respectively (**W4**, Table 5.1). The dispersions were turbid.

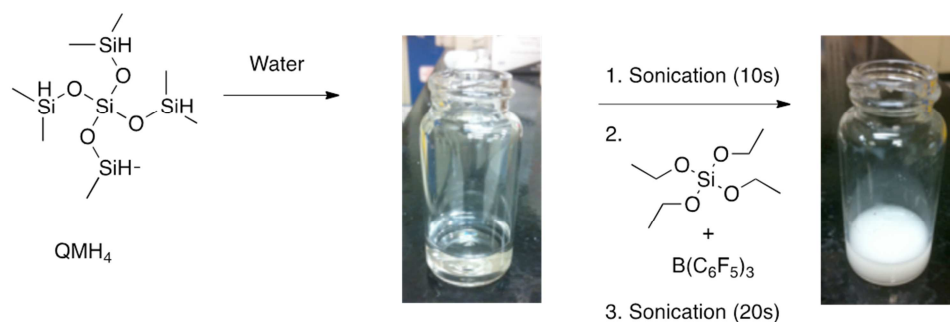


Figure 5.2: General procedure for forming S/W emulsions.

Film Formation

Films could be formed from the aqueous dispersion by placing approximately 0.3 mL of the emulsions dropwise with a pipette on clean glass slides and then drying at either $\sim 100\text{ }^\circ\text{C}$ on a hot plate or at RT. Emulsions dried within 2-4 min at $\sim 100\text{ }^\circ\text{C}$. At RT, the drying process was dependent on humidity: it could take several hours for films to form and dry.

Coating of Capillary Tubes and GC columns

90 mm melting point capillary tubes (Fisher Scientific) were used as received and were cut into 2 cm pieces with both ends open. Emulsions **W2A7** or **W3A10** (100 μL) were loaded into the cut capillary tubes and were then taped to steel rollers of a modified ‘hot dog roller’ with temperature control. The capillary tubes were rolled at a constant 4 rpm under ambient conditions and allowed to dry overnight and then broken for SEM analysis. A fused silica GC column (untreated, 99 μm internal diameter) was provided by Restek and used as received. Approximately 3 cm of the GC column was cut and then

loaded with the **W2A7** emulsion, which was then dried at ambient conditions on the bench.

Table 5.1: S/W emulsion formulations

Recipe ^a	TEOS	QM ^H ₄	B(C ₆ F ₅) ₃	Aged (d)	Temp. Dried
W1	0.6	0.6	0.002	-	-
W2	0.6	0.6	0.008	-	RT
W2T	0.6	0.6	0.008	-	~100 °C
W2A3	0.6	0.6	0.008	3	RT
W2A3T	0.6	0.6	0.008	3	~100 °C
W2A7	0.6	0.6	0.008	7	RT
W2A7T	0.6	0.6	0.008	7	~100 °C
W3	0.6	0.6	0.024	-	RT
W3T	0.6	0.6	0.024	-	~100 °C
W3A3	0.6	0.6	0.024	3	RT
W3A3T	0.6	0.6	0.024	3	~100 °C
W3A10	0.6	0.6	0.024	10	RT
W3A10T	0.6	0.6	0.024	10	~100 °C

^a Recipe code shows the solvent, days emulsion is aged and temperature dried. For example, W3A3T: W = water, A3= aged 3 days, T = dried at ~100 °C (no T in code means RT).

5.4 Results

Colloidal Stability

Alkoxysilanes such as tetraethoxysilanes undergo relatively rapid hydrolysis at pHs away from neutrality.²⁶ This is a classic route to the formation of silica dispersions in water.²⁷ B(C₆F₅)₃ forms a strong Brønsted acid in water. We were surprised, therefore, to learn that it was possible to create relatively stable TEOS/QM^H₄ emulsions in the presence of B(C₆F₅)₃ in water: silica formation was not observed but, consistent with B(C₆F₅)₃:H₂O complex formation, pHs of the aqueous continuous phase became slightly more acidic (pH = 6.5-6.8) as the dispersion formed.

Initially, attempts to form a stable silicone O/W (oil-in-water) emulsion by stirring the tetrafunctional reagents in water were problematic and irreproducible. Even with the

slow addition of TEOS and $B(C_6F_5)_3$ catalyst to a dispersion of QM^H_4 in water, the mixture *frequently reacted violently releasing ethane gas and/or gave precipitate/coagulate*. The violent reaction was attributed to the direct PR reaction of a phase separated QM^H_4 layer with TEOS generating ethane. However, a homogenous oil-in-water dispersion was readily formed if QM^H_4 was first added to water and dispersed briefly by sonication to give a hazy dispersion. After addition of a mixture of TEOS and $B(C_6F_5)_3$ the dispersion became milky white (Figure 5.2). Some gas bubbles could be observed at the air/water interface once sonication was complete. We have not established if the gas is H_2 resulting from the hydrolysis of hydrosilane groups (Si-H) giving polar silanols (Si-OH)(Figure 5.1B) or the PR reaction¹⁵ with TEOS giving ethane (Figure 5.1A).

Ganachaud et al. have suggested that colloidal stabilization arises from boronate water complexes that present at the oil/water interface in emulsions containing $B(C_6F_5)_3$ (Figure 5.3).^{22,24} The decrease in pH observed during dispersion formation is consistent with this proposal. Control experiments for dispersing the siloxane agents in water were conducted by sonicating QM^H_4 and TEOS both individually and together using a sonicator for 10 s in the absence of catalyst to determine if sonication alone could lead to the formation of stable emulsions: surfactants were not used to aid the dispersion. In the absence of $B(C_6F_5)_3$, complete phase separation of any of the oil/water mixtures occurred within 1-2 minutes.

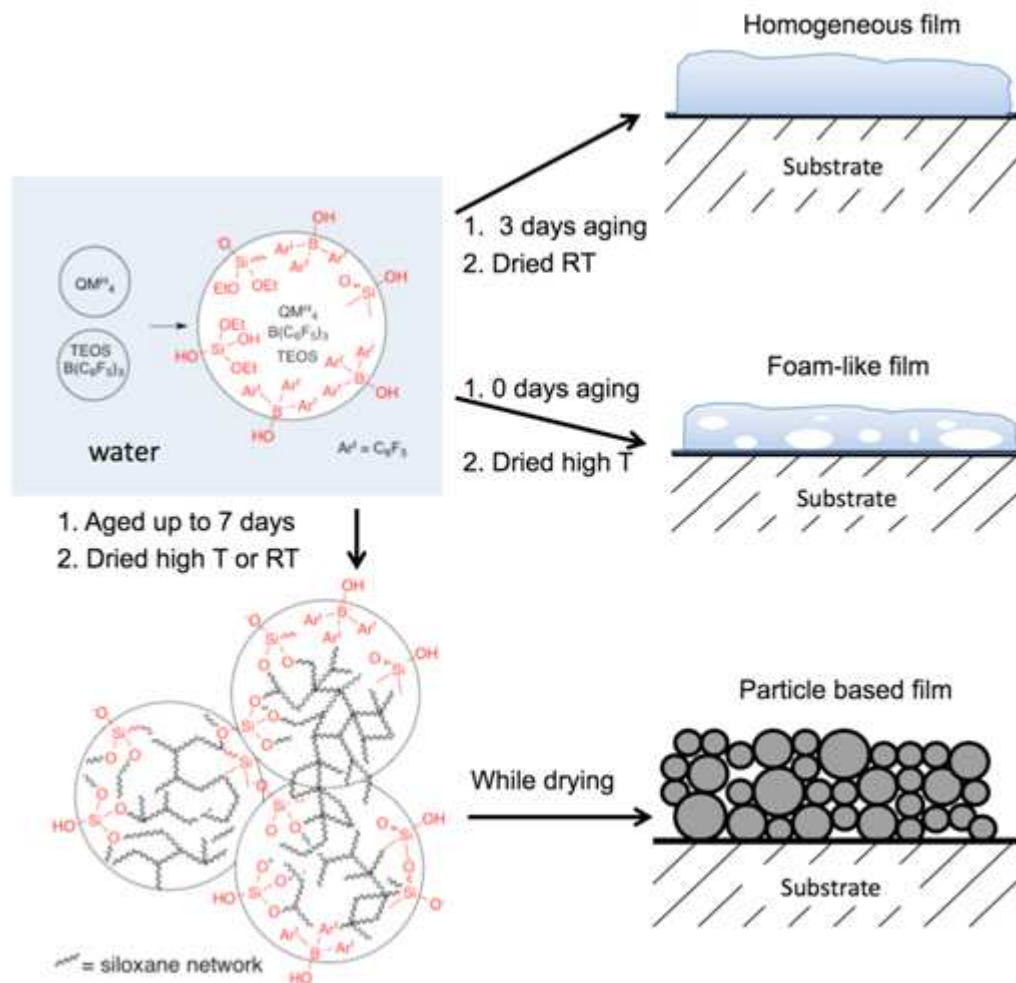


Figure 5.3: Model for the formation of stable siloxane-in water emulsions that can be aged and dried to give 3 distinct film structures.

To examine in more detail the role of $B(C_6F_5)_3$ in stabilizing the emulsions, solutions were prepared with three different catalyst solutions (1 mg, 4 mg and 12 mg of catalyst in 125 mg of TEOS to give **W1**, **W2** and **W3**, respectively). Zeta potential measurements of the dispersions formed from the three catalyst solutions with TEOS and QM^H_4 showed an initial sharp increase in the zeta potential values after the addition of catalyst, and then a slower, steady increase over time: the magnitude of the increase depended on the catalyst concentrations (Figure 5.4). Of the three samples tested, zeta

potential measurements indicated that **W2** had the largest negative values throughout the 1 week study. This result was unexpected, as greater surface charge was expected with **W3**, which had the highest concentration of catalyst and, therefore, of potential interface-stabilizing ionic groups.

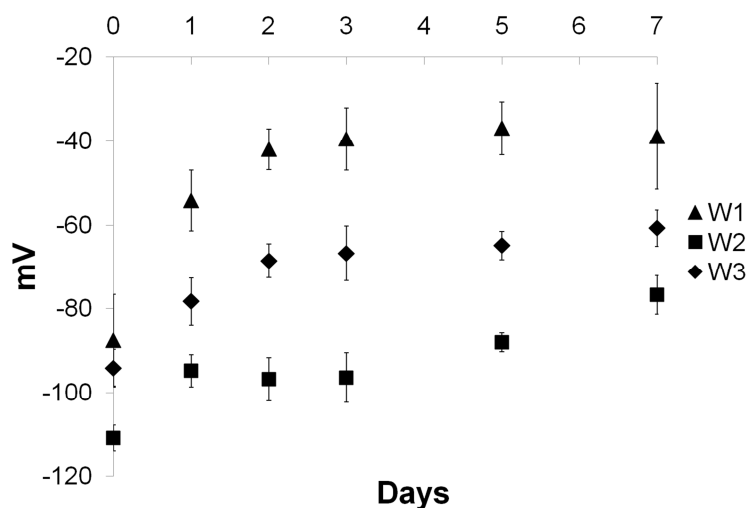


Figure 5.4: Zeta potential measurements over 1 week of QM^H_4 and TEOS with varying concentrations of catalyst.

The three dispersions underwent sedimentation to varying degrees. The larger particles in **W1** (Table 5.2) sedimented most rapidly, to be followed by **W3** and **W2**. The latter two dispersions could be resuspended quickly by agitation for up to two weeks. By contrast, after 1 week, **W1** had aggregated (aggregate sizes ranging from ~ 800 nm-7400 nm).

Table 5.2: Particle size measurements (nm) of S/W emulsions after 1 week using DLS.

Day	Formulation and Catalyst loading (mg)		
	W1 (1)	W2 (4)	W3 (12)
0	325 ± 132	241 ± 88	267 ± 103
7	Aggregate	445 ± 128	294 ± 77

Table 5.2 shows that dispersion **W2** initially formed the smallest particles as determined by dynamic light scattering (DLS): even though it did not have the highest catalyst concentration, it did have the highest initial surface charge (Figure 5.4).

However, the particles increased in size after aging for one week. By contrast **W3**, with the highest $B(C_6F_5)_3$ concentration, had comparably sized particles on synthesis that did not change very much over one week. These data clarify that nominal particle size and stability could be controlled by the amount of catalyst present and the degree of aging.

Normally, with electrostatic stabilization, higher charged particles would be expected to be the most colloiddally stable. Although enhanced stability was observed with **W3**, the surface charge was less than expected and less than **W2**. We do not have an explanation at this time for the greater charge. A model that is consistent with the colloidal behavior is shown in Figure 5.5. Low catalyst levels **W1** lead to unstable larger particles that readily coalesce. An intermediate catalyst loading **W2** gave electrostatically stabilized particles, with some of the catalyst resident at the water/silicone interface to give particles of intermediate stability that increase in size over one week. At the highest catalyst loadings **W3**, more stable particles are formed. We ascribe enhanced particle stability in this case to the partition of catalyst between the external interface and interior of the drop. The internal catalyst initiates crosslinking, which obviates Ostwald ripening as a viable mechanism for particle growth: the monomers become linked into the particle network.^{28,29}

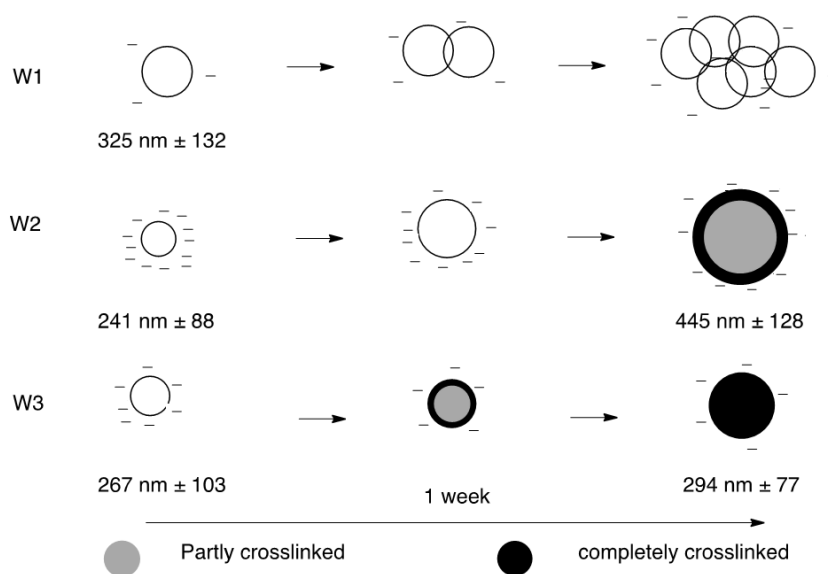


Figure 5.5: Model showing changes in particles over time as a function of catalyst concentration.

The compositional change of emulsions **W2** was tracked utilizing ATR-IR over the course of a week (Figure 5.6A). The Si-H functionality, which has an intense absorption at $\sim 2130\text{ cm}^{-1}$, was monitored, as it is a key reactive component in the PR reaction. It was found to slowly disappear over the course of a week due to the crosslinking PR reaction occurring slowly within the emulsions. It is less likely that the alternative mechanism for Si-H loss, hydrolysis of the Si-H group, is a major contributing factor to the loss of Si-H, as the zeta potential measurements indicated that the emulsions became less stable over time. Conversion of Si-H to Si-OH should increase the surface polarity and facilitate droplet stabilization: by contrast, the **W2** particles were destabilized over time.

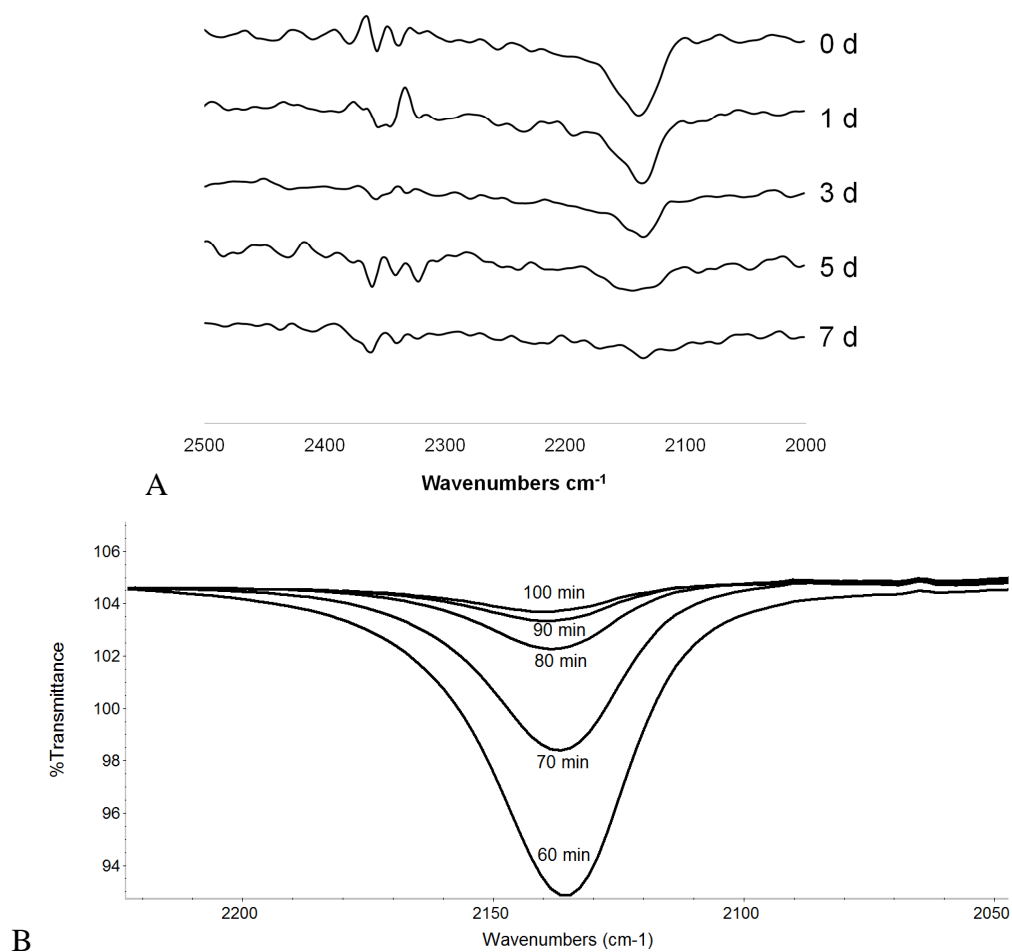


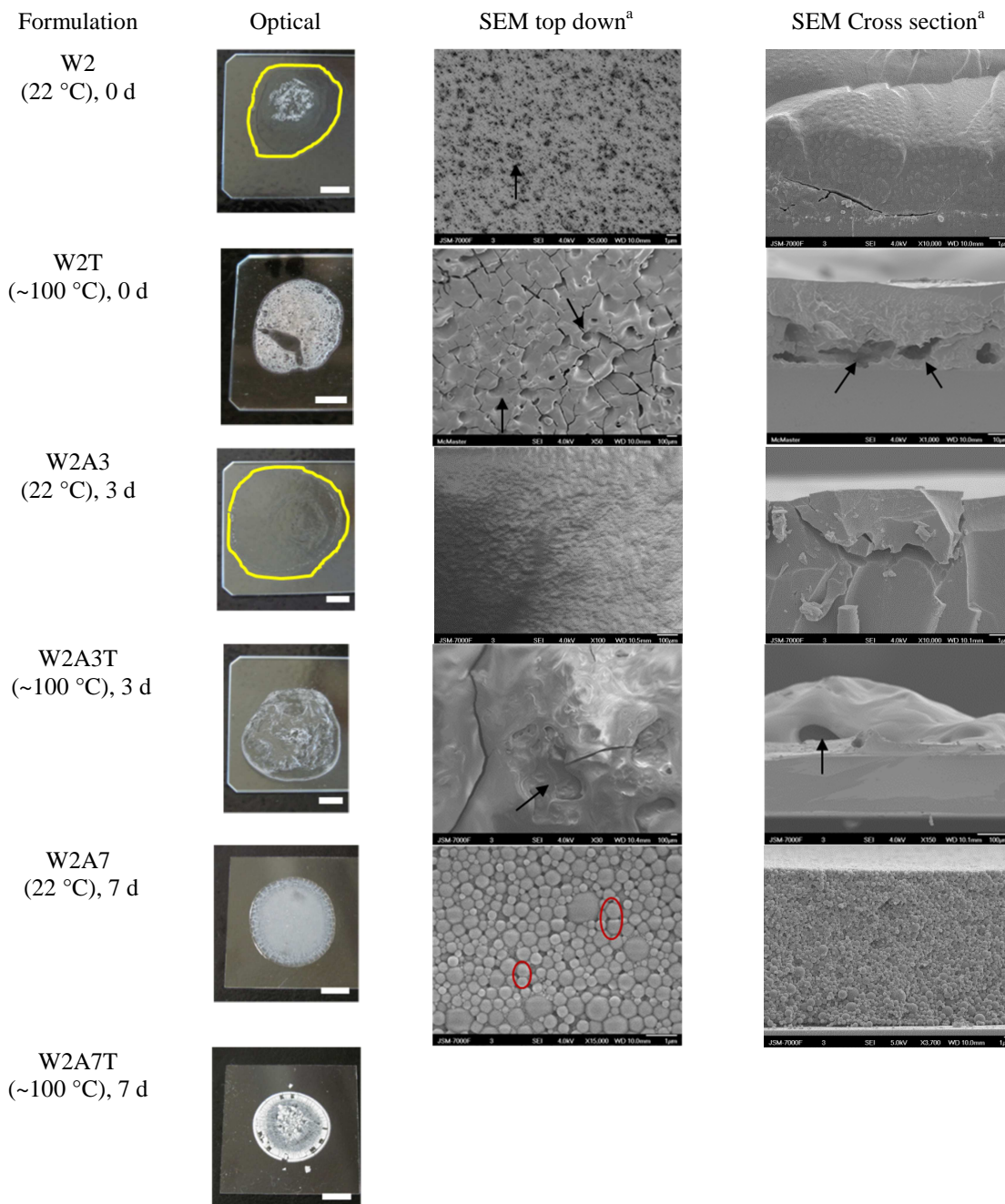
Figure 5.6: ATR-IR data of W2 A: over 1 week in solution, B: drying on the instrument after 60-100 mins in ambient conditions.

Film Formation

Crosslinked siloxane films formed from **W2** and **W3** emulsions after drying: **W1** led to sticky, improperly crosslinked materials. The absorption of the Si-H groups in the IR was used to follow curing by the PR reaction during the drying of emulsion **W2** under ambient conditions to form a film. Figure 5.6B shows that the PR reaction only occurs after most of the water has evaporated (60 minutes after being placed on the slide) and proceeded to form a crosslinked film with the majority of the Si-H having disappeared within an additional 40 minutes.

The film character depended on the chemical makeup and age of the dispersion at the time of deposition on a surface. Films varying from dense and transparent homogeneous films, to opaque aggregates of particles, foam-like structures or mixtures thereof were formed from **W2**, **W3**. As shown in Figure 5.7, higher drying temperatures with freshly prepared emulsions led to an increased rate of the PR reaction and formation of foam-like films blown by release of the alkane byproduct. By contrast, drying at RT led to films with far fewer voids.

Aging the dispersions for a few days before film casting initially led to films with fewer voids or pockets when dried either at RT or at ~100 °C. For example, after 3 days drying at RT, **W2A3** was a transparent cohesive film with few voids pockets (Figure 5.7). However, films formed from dispersions aged 7 days were opaque and highly friable when formed heated at ~100 °C, or simply cloudy when dried at RT. The cloudiness proved to be a consequence of the presence of large, crosslinked particles in the dispersion prior to deposition.



^a Arrows indicate the presence of small voids or air pockets in **W2** and red circles (**W2A7**) show “necking” of particles. The outline of the film is provided in yellow.

Figure 5.7: Dried films from both ageing the S/W emulsions and then by drying them at RT or ~100 °C using optical and scanning electron microscopy (SEM). Scale bars for optical images = 5 mm.

SEM images (Figure 5.7) of the films above facilitated interpretation of the optical images of the films and provided greater morphological detail. For example, curing the freshly prepared **W2** dispersion at elevated temperatures (**W2T**) led to pores on the surface and/or internal voids ranging from a few microns to a few hundred microns in diameter. These voids are probably the result of ethane (or less likely hydrogen, Figure 5.1) gas evolving during the condensation reaction as has been reported elsewhere.²¹ Fewer voids and greater homogeneity were observed when cure was performed at lower temperatures **W2**. The cross-sectional image of the homogeneously dense region of **W2** reveals a dense siloxane based film that is formed with small structures of up to a few hundred nanometers diameter throughout, which proved to be hollow pockets of a smaller dimension than those found in **W2T** film (see arrow, Figure 5.7). These data suggest rapid evolution and coalescence of ethane bubbles to give large voids at elevated temperatures, but low gas concentrations, and smaller scale voids, at the time of gelation at lower temperatures.

SEM images of films derived from emulsions aged for 3 days show a slightly different outcome. Although large voids up to several hundred microns formed (fewer than from a freshly made dispersion) when the emulsion was dried at elevated temperatures (**W2A3T**), a void free film was observed when the dispersion was dried at room temperature. This suggests that crosslinking was occurring during the three days and, by the time gelation was initiated at room temperature, the gas that formed did not effectively coalesce into bubbles.

The films formed from dispersions aged 7 days and cured at room temperature were comprised of crosslinked particles (**W2A7**): the film cured at ~100 °C was too friable to collect good SEM pictures. The cross-sectional image of **W2A7** shows that the entire film is comprised of tightly packed, fused particles with an average particle size of 529 ± 307 nm, comparable to the size of the precursor dispersed particles. The films are thus assemblies of crosslinked particles that fused to each other during the drying process.

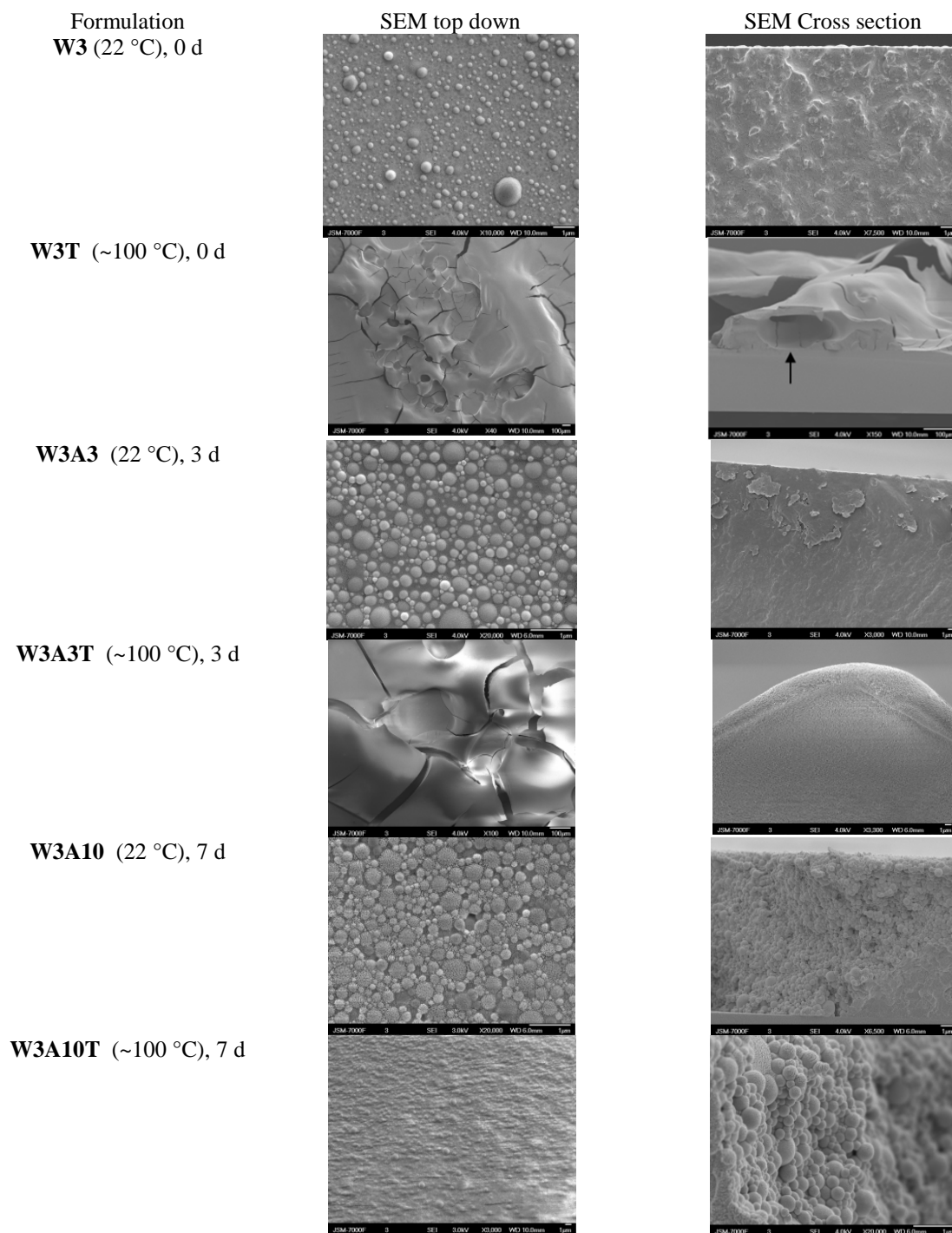


Figure 5.8: SEM images of W3 samples (highest catalyst concentration) as a function of dispersion age and drying temperature.

With higher catalyst concentrations, **W3** underwent more rapid crosslinking than the other particles. As a consequence, even only after aging for 3 days (**W3A3**) particles were sufficiently crosslinked that they did not merge during film formation, unlike **W2** (Figure 5.8). Particle sizes in the cured films, obtained from the SEM images appear to show only small changes over time: average sizes of 292 ± 223 nm, 266 ± 111 nm and 338 ± 147 nm were observed for the films derived from **W3**, **W3A3** and **W3A10**, which were dried at RT.

The effect of catalyst concentration on film morphology was also investigated for the **W2** (0.008 mmol/0.6 mmol silane) and **W3** formulations (0.024 mmol of boron catalyst) (Figure 5.8). As shown in Figure 5.7, **W2** formulations can form foamed, homogeneously dense and particulate films depending on the age of the dispersion. The **W3** formulations only formed foamed and particulate films or a combination thereof (Figure 5.8). With the higher catalyst concentration crosslinking of the particles is efficient and drying the dispersion does not lead to smooth/homogenous films. Instead films of fused crosslinked particles resulted.

The solid state ^{29}Si NMR data (Figure 5.9) shows differences between the films dried at different temperatures from emulsions that are 0, 3 or 7 days old. Films dried at $\sim 100^\circ\text{C}$ are more highly cross-linked as shown by the smaller peaks for M^{H} (SiMe_2H), M^{OH} (SiMe_2OH) and Q^2 ($\text{Si}(\text{OH})_2(\text{OSi})_2$). At RT, water evaporates much more slowly, thus the PR reaction is less efficient and condensation is less complete.

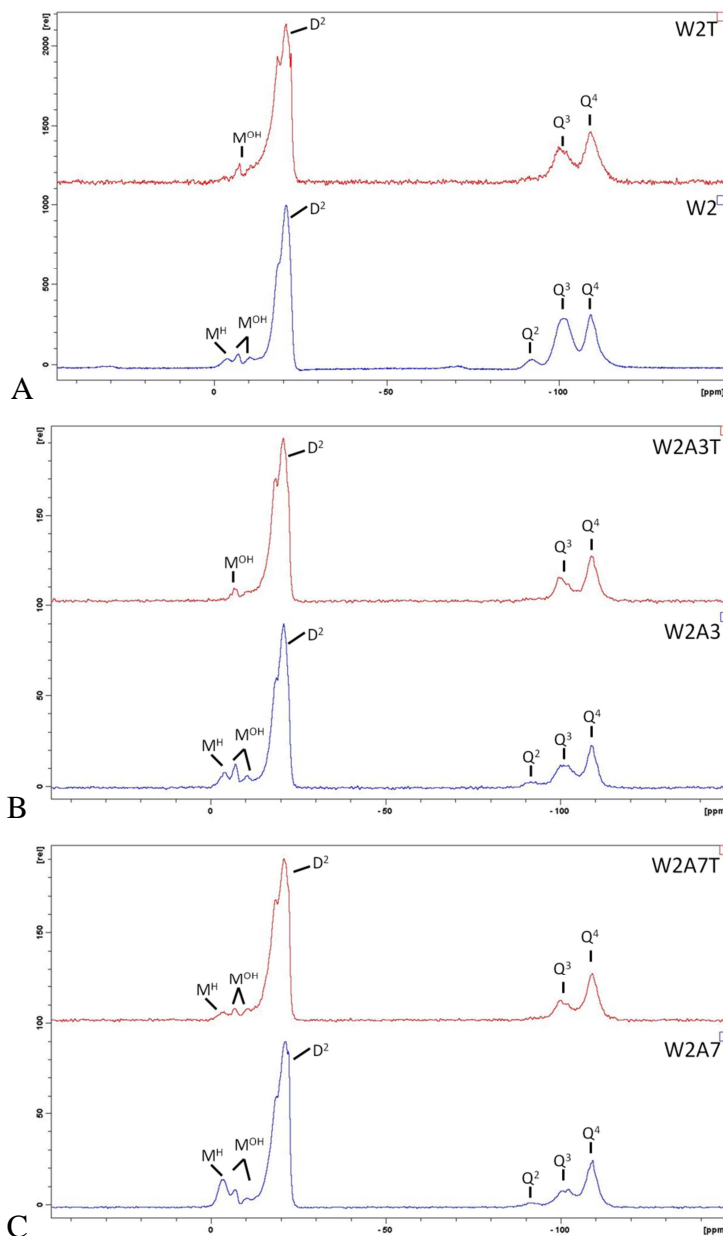


Figure 5.9: Solid state ^{29}Si NMR spectra of dried S/W emulsions at A: 0d (W2T & W2), B: 3d (W2A3T & W2A3) and C: 7d (W2A7T & W2A7).

These data permit a discussion of the processes taking place during film formation. Particles form in newly created dispersions that are electrostatically stabilized by catalyst/water complexes. At lower catalyst concentrations (**W1**) insufficient charge was available to stabilize particles, which underwent relatively rapid aggregation. At higher catalyst concentrations (**W2**), particles were stabilized by sol/charged groups (Si-

OH, Si-O⁻ and ⁻B-OH) at the interface. At yet higher concentrations (**W3**) there is sufficient catalyst to stabilize the particle at the interface (and if it is at the interface complexed to water, it will not be a catalyst for the PR reaction) and facilitate cure within the particle. However, as shown in Figure 5.3, catalyst that isn't bound to water resides at the siloxane droplet core, thus able to undergo the PR reaction. This results in a crosslink density gradient between the interior of the particles (highest crosslink density) and at the siloxane-water interface (lowest crosslink density). The lower crosslink density at the interface is evidenced by drying of the emulsions to reveal the coalescence of particles by “necking” (Figure 5.7, **W2A7**). Thus, films contained particulate structures at much earlier time points for **W3** than **W2**. The effects were amplified at higher temperatures. Voids were also found in some of the films, which was caused by release of gas from the PR reaction.

Although TEOS crosslinks with hydrosilanes, it can also migrate into the water phase over time³⁰ and undergo condensation (traditional sol-gel methodology) to act as a silica “glue” between silica particles during film formation during drying of the dispersion Figure 5.3.

High Surface Area Coatings

A variety of applications require high surface area, hydrophobic coatings. For example, gas chromatography (GC) columns will benefit from higher surface area coatings that lead to an increase in the number of theoretical plates. Currently, the gold standard for GC is fused silica columns coated with silicone elastomers.³¹ To test the ability to coat the interior of glass cylinders, first standard capillary tubes (e.g., a melting point tube) and then an untreated fused silica column were coated with emulsions **W2A7** and **W3A10**, respectively. Emulsions were placed in the capillary tubes that were allowed to dry while rolling on a modified hot dog roller. A thin coating (of a few microns thick) of hydrophobic silica particles formed on the inside surface of the capillary tube, (Figure 5.10A-D). These films cracked and delaminated from the surface only adjacent to the fracture in the glass (that was required to allow imaging). Otherwise, in both cases the films was comprised of fused polydisperse particles, with a smaller particle size observed

for **W3A10**. In neither case was perfect coverage observed as there were bare patches: the origins of this will be examined in future work.

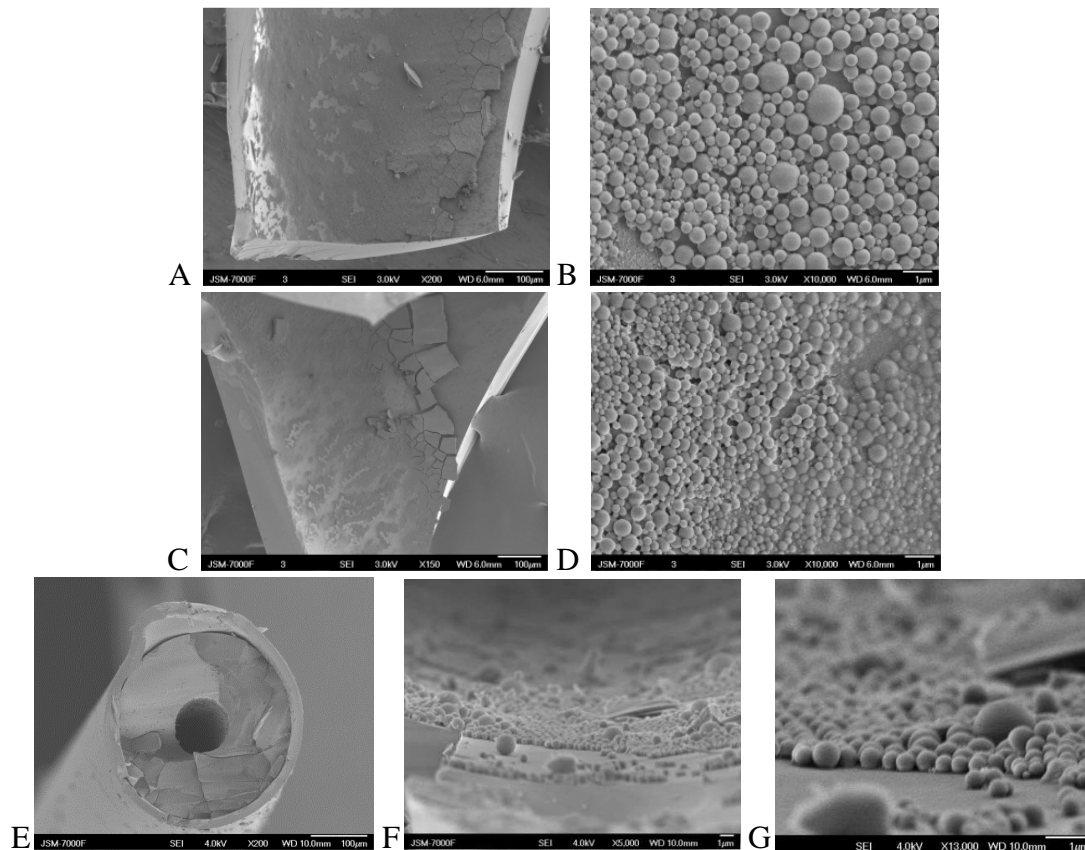


Figure 5.10: SEM images of W2A7 (A,B) and W3A10 (C,D) emulsions dried within standard capillary tubes coated with hydrophobic silica particles. E, F, G: Fused silica GC column coated with W2A7 was allowed to dry.

Using more dilute solutions, it was possible to achieve a submonolayer coverage of particles by allowing **W2A7** to dry inside a fused silica column typical of those used for GC (Figure 5.10E-F). Further studies to correlate particle size, dispersity and film thickness with particle density and separation performance are underway.

5.5 Conclusion

Slow crosslinking silicone-in-water emulsions can be formed from tetrafunctional hydrosilane and alkoxy silanes in the presence of $B(C_6F_5)_3$. The stability of the surfactant-free emulsions was discovered to be a function of the boron catalyst concentration, which also provides charge to the particle surface. An optimal amount of catalyst is required to

achieve the highest stability, which can then remain stable for over 1 week. Various film morphologies could be produced by drying the emulsions, which include foamed, homogeneously dense and particulate films from the same emulsion by optionally ageing it over several days and by drying it at either RT or ~100 °C. These morphologies depend on the available hydrosilane (Si-H) available and degree of crosslinking that has occurred in the siloxane droplets. The hydrophobic particulate films are of greater interest due to their ability to form cohesive films, thus investigated for their ability to coat capillary tubes for applications in GC columns. Although optimization for coating the capillary tubes are necessary, the initial results demonstrated that the emulsions could be easily applied and dried to form a thin silica particle coating. Further studies and optimizations to demonstrate their efficacy as GC column will be done in the future.

5.6 Acknowledgments

Funding from the Natural Sciences and Engineering Research Council (NSERC) and the Sentinel: NSERC Bioactive Paper Network is acknowledged with gratitude. We also wish to thank Dr. John Grande for useful discussions, Prof. Robert Pelton for access to their zeta potential analyzer and DLS and Prof. Harald Stöver for access to a modified ‘hot dog roller’. We thank Dr. Shawn Reese and Restek Corp. for providing an untreated fused silica chromatography column.

5.7 References

- (1) Strawbridge, I.; James, P. F., *J. Non-Cryst. Solids*, **1986**, 82, 366.
- (2) Grosso, D.; Babonneau, F.; Albouy, P.-A.; Amenitsch, H.; Balkenende, A. R.; Brunet-Bruneau, A.; Rivory, J., *Chem. Mater.*, **2002**, 14, 931.
- (3) Lu, Y.; Ganguli, R.; Drewien, C. A.; Anderson, M. T.; Brinker, C. J.; Gong, W.; Guo, Y.; Soye, H.; Dunn, B.; Huang, M. H.; Zink, J. I., *Nature*, **1997**, 389, 364.
- (4) Morikawa, A.; Iyoku, Y.; Kakimoto, M.-a.; Imai, Y., *Polym. J.*, **1992**, 24, 107.
- (5) Yang, H.; Coombs, N.; Sokolov, I.; Ozin, G. A., *Nature*, **1996**, 381, 589.
- (6) Yang, H.; Coombs, N.; Sokolov, I.; Ozin, G. A., *J. Mater. Chem.*, **1997**, 7, 1285.
- (7) Khramov, A. N.; Collinson, M. M., *Chem. Commun.*, **2001**, 767.
- (8) Kanungo, M.; Collinson, M. M., *Chem. Commun.*, **2004**, 548.

- (9) Ohno, K.; Morinaga, T.; Koh, K.; Tsujii, Y.; Fukuda, T., *Macromolecules*, **2005**, *38*, 2137.
- (10) Etienne, M.; Sallard, S. b.; Schröder, M.; Guillemain, Y.; Mascotto, S.; Smarsly, B. M.; Walcarius, A., *Chem. Mater.*, **2010**, *22*, 3426.
- (11) Alberius, P. C. A.; Frindell, K. L.; Hayward, R. C.; Kramer, E. J.; Stucky, G. D.; Chmelka, B. F., *Chem. Mater.*, **2002**, *14*, 3284.
- (12) Muraka, S. P., *Interlayer Dielectrics for Semiconductor Technologies*; Academic Press, 2003.
- (13) Rubinsztajn, S.; Cella, J. A., *WO2005118682*, **2005**, *General Electric Company*.
- (14) Rubinsztajn, S.; Cella, J. A., *US 7064173*, **2006**, *General Electric Company*.
- (15) Brook, M. A.; Grande, J.; Ganachaud, F., *New Synthetic Strategies for Structured Silicones Using B(C₆F₅)₃ Silicone Polymers*; Springer Berlin, 2011; Vol. 235.
- (16) Grande, J. B.; Thompson, D. B.; Gonzaga, F.; Brook, M. A., *Chem. Commun.*, **2010**, *46*, 4988.
- (17) Grande, J. B.; Gonzaga, F.; Brook, M. A., *Dalton Trans.*, **2010**, *39*, 9369.
- (18) Cella, J.; Rubinsztajn, S., *Macromolecules*, **2008**, *41*, 6965.
- (19) Thompson, D. B.; Brook, M. A., *J. Am. Chem. Soc.*, **2007**, *130*, 32.
- (20) Keddie, D. J.; Grande, J. B.; Gonzaga, F.; Brook, M. A.; Dargaville, T. R., *Organic Letters*, **2011**, *13*, 6006.
- (21) Grande, J. B.; Fawcett, A. S.; McLaughlin, A. J.; Gonzaga, F.; Bender, T. P.; Brook, M. A., *Polymer*, **2012**, *53*, 3135.
- (22) Kostjuk, S. V.; Radchenko, A. V.; Ganachaud, F., *Macromolecules*, **2007**, *40*, 482.
- (23) Chojnowski, J.; Rubinsztajn, S.; Fortuniak, W.; Kurjata, J., *Macromolecules*, **2008**, *41*, 7352.
- (24) Longuet, C.; Joly-Duhamel, C.; Ganachaud, F., *Macromol. Chem. Phys.*, **2007**, *208*, 1883.
- (25) Khalimon, A. Y.; Piers, W. E.; Blackwell, J. M.; Michalak, D. J.; Parvez, M., *J. Am. Chem. Soc.*, **2012**, *134*, 9601.
- (26) Brook, M. A., *Silicon in Organic, Organometallic, and Polymer Chemistry*; Wiley-VCH Verlag, 2000.
- (27) Brinker, C. J.; Keefer, K. D.; Schaefer, D. W.; Ashley, C. S., *J. Non-Cryst. Solids*, **1982**, *48*, 47.
- (28) Dickinson, E.; Ritzoulis, C.; Yamamoto, Y.; Logan, H., *Colloid Surf. B*, **1999**, *12*, 139.
- (29) Zeeb, B.; Gibis, M.; Fischer, L.; Weiss, J., *J. Colloid Interface Sci.*
- (30) Schacht, S.; Huo, Q.; VoigtMartin, I. G.; Stucky, G. D.; Schuth, F., *Science*, **1996**, *273*, 768.
- (31) McNair, H. M.; Miller, J. M., In *Basic Gas Chromatography*; John Wiley & Sons, Inc.: 2008, p 156.

Chapter 6 – Inkjet Printed Siloxane-Based Hydrophobic Barriers on Paper for Microfluidic Assays^{‡‡}

6.1 Abstract

Paper-based microfluidic devices exhibit many advantages for biological assays. Normally, the assays are localized on certain areas of paper by hydrophobic barriers comprised of wax or following cellulose functionalization by alkyl ketene dimers. Neither hydrophobic barrier is able to constrain aqueous solutions of good surfactants, which are frequently used in biological assays. We demonstrate that rapidly curing silicone resins can be inkjet printed onto pure cellulose paper. The Piers-Rubinsztajn (PR) reaction dominates the cure chemistry leading to cellulose fibers that are surface coated with a silicone resin. The resulting barriers are better able to resist penetration by surfactant solutions and by the solvents DMF and DMSO. The utility of the barrier is demonstrated using a coliform assay based on β -galactosidase detection.

6.2 Introduction

Microfluidic, paper-based analytical devices (μ PAD) offer a variety of advantages over traditional laboratory-based bioassays as a platform for the detection of various analytes in qualitative or quantitative assays. The most common paper sensor is, of course, pH paper that informs the user of the pH of a given solution by colorimetric detection. Detection of various other analytes have also been developed on paper sensors, including Fe(III) and Au (III),¹ glucose,²⁻⁵ infectious bacteria⁶ and many others.⁷

^{‡‡} Portions of the following chapter will be submitted to Journal of Materials Chemistry: B with the following citation: Vinodh Rajendra, Clémence Sicard, John D. Brennan, Michael A. Brook, J. Mat. Chem. B, 2014.

I was responsible for the majority of the practical and analytical work, plus the writing of the 1st draft of the manuscript. Dr. Sicard gave useful advice, performed a few of the experiments (surface tension measurements and the detection of β -galactisodase biosensor) and wrote the detection of β -galactisodase section of the paper. Dr Brennan gave some useful advice and Dr. Brook also gave useful advice and helped with editing the document for final submission to the above journal.

The availability, cost effectiveness, biocompatibility, and ability to move liquids by wicking rather than external pumping has made these paper-based devices very attractive.⁸ In addition, many of the paper-based sensors developed to date do not require highly skilled technicians to operate, which is important in countries with limited resources.

The ability to print hydrophobic barriers on paper for the formation of paper-based microfluidic devices for diagnostics has recently received a lot of attention. The hydrophobic barrier is designed to localize assays in a region of the paper, or direct flow, using capillary forces, in certain directions. Several methodologies for forming paper-based microfluidic and diagnostic devices have been reported, including wax printing,^{2,9} ink-jet printing,¹⁰ laser ablation,¹¹ and plasma treatment¹² among others.

Methods such as inkjet printing and thermal printing utilize hydrophobizing agents to form hydrophobic barriers. There are only a handful of available agents available to do so. The two most common materials are wax and alkyl ketene dimers (AKD, Figure 6.1), since they are cost-effective materials and can be implemented in a number of printing techniques.¹³ The major limitation with both of these materials is their ability to withstand liquids with low surface tensions: surfactants are frequently utilized for biological samples and assay processes for them.

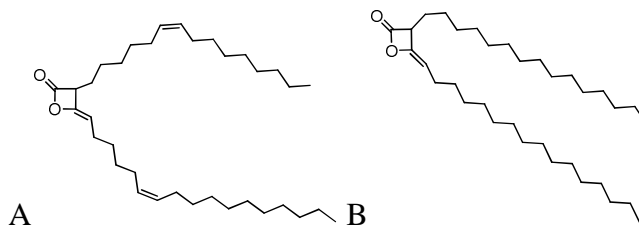


Figure 6.1: Structure of two AKD compounds, A: *Precis* and B: *Aquapel*.¹⁴

We have been exploring the utility of a different cure chemistry for silicone elastomers. The Piers-Rubinsztajn (PR) reaction utilizes a Lewis acidic boron catalyst [$B(C_6F_5)_3$] to facilitate the condensation of hydrosilanes (R_3-Si-H) to alkoxy silanes ($R_3-Si-OR'$) to form new Si-O-Si bonds and an alkane byproduct (Figure 6.2A).^{15,16} This chemistry is extremely rapid (seconds to minutes at room temperature) and is capable of forming various silicone elastomers,^{17,18} resins,¹⁹ and other materials.²⁰

Silicones have a lower surface energy than hydrocarbons and, we reasoned, might be better able to contain aqueous solutions, on paper, particularly those containing surfactants. We describe the printing of silicone precursors (siloxanes) onto pure cellulose (filter paper) that are rapidly converted into hydrophobic siloxane barriers (silicone barriers), and their ability to localize aqueous solutions. The beneficial attributes of this approach is demonstrated using a previously reported paper sensor for coliform detection developed by Hossain et al.²¹

6.3 Experimental

Materials

Tetraethyl orthosilicate (TEOS, Aldrich), tetrakis(dimethylsiloxy)silane (QM^H₄, Gelest), tris(pentafluorophenyl)borane [B(C₆F₅)₃, 95%, Aldrich], 1,3-dimethyltetramethoxysilane (DMTMDS) (Gelest), cetyltrimethylammonium bromide (CTAB, Sigma-Aldrich), Triton X-100 (poly(ethylene glycol) *p*-(1,1,3,3-tetramethylbutyl)-phenyl ether, Sigma-Aldrich), sodium dodecylsulfate (SDS, BioShop), B-PER® direct bacterial protein extraction reagent (Product #1861465, Thermo Scientific), chlorophenol red (CPR, Sigma-Aldrich), isopropyl-β-D-thiogalactopyranoside (IPTG, Bioshop), WhatmanTM qualitative paper grade 1 and quantitative ashless paper grade 41 paper (Whatman) were obtained from the indicated suppliers and used as received. Tryptic soy broth (TSB) media was composed of bacto tryptone (BD), potassium phosphate (Caledon), dextrose (D-glucose, Caledon), sodium chloride (Bioshop) and peptone (BD). All alcohols used were reagent grade and used as received.

Siloxane formulations

Printable formulations were produced by first preparing catalyst stock solutions. B(C₆F₅)₃ was added to TEOS (0.125 g, 0.6 mmol) or DMTMDS (136 mg, 0.6 mmol) to give stock solutions of 0.016 M (2 mg, 0.004 mmol) and 0.063 M (4 mg, 0.008 mmol), respectively. For the P4A formulation (Table 6.1), 40 mg of catalyst was dissolved in 1 mL of a 1:1 MeOH and IPA mixture. Stock solutions could be kept for several hours or days if stored under relatively dry conditions. The printable formulations were then

prepared in a very specific order by first combining the stock solutions with the appropriate alcohols and finally with QM^H₄. Full details for each formulation are shown in Table 6.1.

Table 6.1: Key siloxane formulations to form silicone barriers on paper. Siloxanes and catalyst amounts are reported in mmol and alcohols are reported in mL.

Reagents	Recipe					
	M1	P1	P2	P3	P4A	P4B
TEOS	0.6	0.6	0.6	-	-	-
DMTMDS	-	-	-	0.6	-	0.6
QM ^H ₄	0.6	0.6	0.6	0.6	-	0.6
B(C ₆ F ₅) ₃	0.008	0.008	0.008	0.004	0.08	-
MeOH	1	0.1	0.05	0.05	0.5	0.05
IPA			0.05	0.05	0.5	0.05
Printer Method ^a	-	1P	1P	1P		2P
App ^b	-	4	4	4	2 ^c	2 ^c

^a Printer Method = Number of printers used to form silicone barriers (e.g. P4A and P4B used together utilizing the 2 printer methodology (2P)).

^b App = number of applications or printing passes.

^c P4A and P4B were printed once on each side of the paper, thus a total of 2 applications/printing passes.

Printing hydrophobic siloxane barriers

Ink-jet printing siloxane barriers from a single printer

A Canon Pixma MP280 was used to ink-jet print the siloxane containing solutions (P1-P3) onto WhatmanTM filter paper grade 1, which was cut into 8.5 x 11 inch pieces. PG-210 black ink cartridges that can dispense ink droplets of 25 pL (picoliters), were reconstructed in the following manner. The sponges inside the cartridge and the tank cover slip were removed. The black ink was removed and the cartridge was thoroughly cleaned with water and air dried to reduce the amount of residual water. Once dry, the siloxane-containing solutions were loaded into the cartridge. The printer was controlled by a personal computer and hollowed out circles (like the letter “O”) of 1.1 cm diameter were constructed using Microsoft Word and were printed onto the paper. Up to 4 printing

passes (Table 6.1) were performed with the printing formulations to optimize the amount of siloxane deposited on paper, and then rapidly cured with a heat gun for 10 s.

Ink-jet printing siloxane barriers from two printers

Two Canon Pixma MP280 printers were used to keep the catalyst separate from the other ingredients. The first printer was used to print only the catalyst mixture P4A, while the second printer was used to lay the siloxane mixture P4B on top of the dried catalyst solution: cure began once the two solutions mixed leading to a siloxane-based barrier. It was not possible to use a single printer with two separate ink cartridges, as the automatic cartridge cleaning protocol performed by the printer (which cannot be shut down) leads first to cross contamination followed by clogging. To print two solutions on the same page location (with proper registration) from two different printers, 4 document templates in Microsoft Word were devised: 1 template was used to print the front side and 1 for the back side of the paper for each printer. Once the front and back side templates were properly aligned, formulations P4A and P4B, respectively, were loaded into their respective printers. P4A was first printed on both the front and the back side of the paper with 1 pass each. Then P4B was printed on the front and back sides with 2 passes each and the treated surface. Although cure was relatively rapid at room temperature, greater reproducibility in barrier formation was observed when the samples were heated with a heat gun for 10 s.

Wax printed hydrophobic barriers

For comparative studies with the most commonly used hydrophobic barrier, wax, identical hollowed circles were printed on Whatman filter paper grade 1 as previously described^{9,22} with one pass through a Xerox Phaser 8560 wax printer and then heated at 120 °C in an oven for approximately 2 min and allowed to cool. In one case, the process was repeated 4 times to load extra wax onto the paper.

Surface tension measurements

The surface tension of the tested surfactant solutions were measured with Optical Contact Angle OCA20 (Future Digital Scientific Corp) using the pendant drop method with a 500 μ L Hamilton syringe and a 1.65 mm needle.

Testing the robustness of the hydrophobic barriers

Distilled water (DI) was utilized on its own and in solutions of 1% w/v SDS, 1% v/v Triton X-100 and 1% w/v CTAB in 75 mM phosphate buffer at pH 6.8. The concentrations of all surfactant solutions were chosen to be well above their critical micelle concentrations.²³⁻²⁵ A commonly used cell lysing solution, 10% v/v B-PER was also prepared. The B-PER concentration was chosen to correspond to standard concentrations used for cell lysing experiments. Chlorophenol red (CPR) was then added to each solution as a colorimetric and fluorescent dye for both optical and fluorescent imaging. Each surfactant solution (15 μ L) was added into the printed hollowed circles of either siloxane- or wax-based barriers for comparative studies. Solvents were used as received and were tested against the hydrophobic barriers by placing 15 μ L of the given solvent into the printed hollowed circles. The color observed for the CPR solutions are pH sensitive and can be affected once dried, hence the observed color variations.

Paper sensor: Detecting β -galactosidase from lysed *E. coli* cells within the hydrophobic barriers

Total coliform test strips were adapted from the previously reported tests strips for total coliform detection.²¹ Circles of 1.1 cm in diameter were delimited by a printed wax-based hydrophobic barrier or a siloxane-based hydrophobic barrier, using the 2 printer method explained above. A sensing zone was printed inside the circle with a Canon Pixma MP280 printer. A layer of poly-L-arginine hydrochloride (P-Arg, 2% w/v in Milli-Q water) was first printed, followed by one layer of chlorophenol red β -galactopyranoside (9 mM in MilliQ water). In the original article by Hossain et al.,²¹ poly(vinylamine) (PVAm) instead of P-Arg was utilized as a capturing agent to concentrate the formed dye. However, due to challenges with printability with poly(vinylamine), P-Arg was used instead. *E. coli* ATCC 25922 cells were grown

overnight at 37 °C in TSB media. IPTG (2 $\mu\text{L}/\text{mL}$) was added to the media to induce the β -galactosidase enzymatic production. Cells were lysed with B-PER® direct bacterial protein extraction reagent following the manufacturer protocol (9:1 ratio of cells in suspension to B-PER). 15 μL of cell lysate was dropped onto the circle test strips.

Imaging of hydrophobic barriers

Optical and fluorescent images were obtained with an Olympus BX51 microscope fitted with a Q-imaging Retiga EXi camera and with the Image Pro-Plus software. By utilizing a rhodamine fluorescent filter with an excitation wavelength from 530-550 nm and a long pass emission filter at 590 nm, fluorescence images of CPR were obtained.

Scanning electron microscopy (SEM) images were taken with a JEOL 7000f FE-SEM after coating samples with 15 nm of gold.

6.4 Results

The chemistry used to prepare the hydrophobic siloxane barriers involves the condensation of alkoxy silanes with hydrosilanes in the presence of small quantities of $\text{B}(\text{C}_6\text{F}_5)_3$ (~0.3 mol %) to produce new siloxanes and a hydrocarbon by-product, usually in the form of a gas: the Piers-Rubinsztajn (PR) reaction (Figure 6.2A).²⁶⁻²⁸ By selecting from the wide variety of available siloxanes, it is straightforward to tune the physical properties of the oil, foam²⁰ or elastomer²⁹ produced, including modulus, by manipulating the chain lengths between crosslinks.

Preliminary survey experiments demonstrated that printable formulations required low viscosity starting materials. In addition, it proved beneficial to create highly reticulated silicone resins on the paper. The preferred starting materials were found to be a tetrafunctional hydrosilane QM^{H}_4 and tetrafunctional alkoxy silane (Figure 6.2C). As is discussed in more detail below, when a mixture of the three compounds is placed on cellulose, a hydrophobic domain rapidly forms, which is tightly anchored to the substrate. As a starting point, siloxane ink M1 (Table 6.1), which used TEOS as the alkoxy silane, was applied dropwise to Whatman paper using a pipette and then heat dried with a heat

gun. This experiment demonstrated that Whatman paper could be completely hydrophobized using this chemistry.

Pure siloxane mixtures cured too quickly to be printed. It was necessary to dilute the mixtures with a solvent that slowed reaction by dilution and also by sequestering the $B(C_6F_5)_3$ catalyst by complexation. Any Lewis base, including alcohols and water, can reversibly complex with the boron.³⁰ These interactions serve to retard the rate of the PR reaction. $B(C_6F_5)_3$ can also catalyse the reaction of SiH-containing compounds with phenols,^{31,32} and, to a lesser degree, aliphatic alcohols to form a new silyl ether bond (Figure 6.2B).³³ Since the rate of the alcohol reaction is far slower – the PR reaction occurs within minutes,¹⁷ while silyl ether synthesis may take several hours or days depending on the alcohol³³ – combinations of methanol and isopropanol could be used as diluents. The final solvent mixture was chosen based on surface tension.

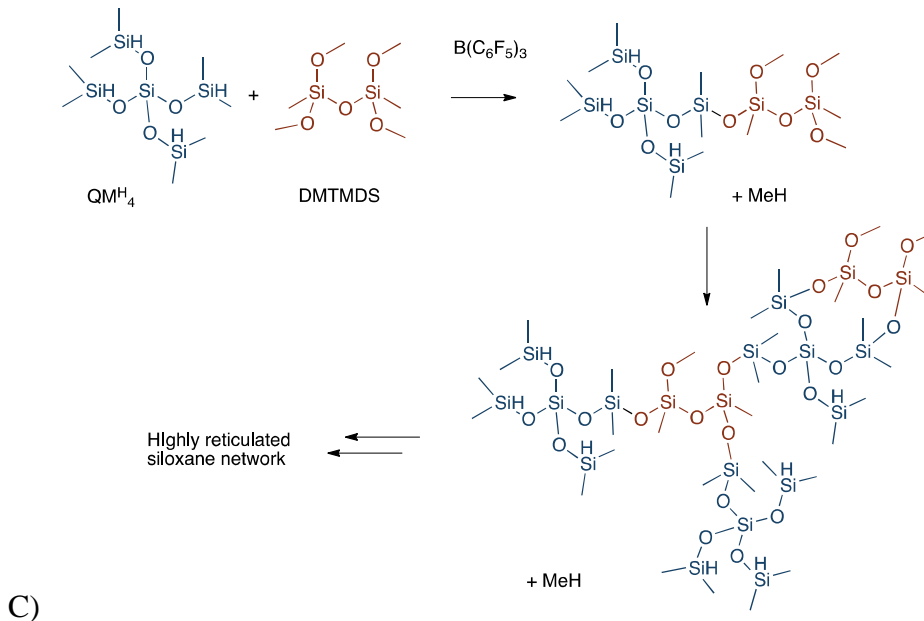
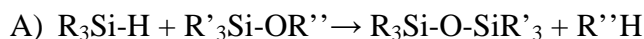


Figure 6.2: General schemes of: A) the PR reaction to form new siloxanes; B) silyl ether synthesis of alcohols with hydrosilanes, with $B(C_6F_5)_3$ as the catalyst in all of the reactions; and C) the PR reaction with tetrafunctional precursors.

We chose to use a very inexpensive inkjet printer to prepare silicone barriers on paper. Three main issues had to be addressed when formulating inks for such a printer: (i) the solution surface tension, (ii) clogging of the ink cartridge, and (iii) the choice of paper. Thermal ink-jet printers commonly use inks with both low surface tension (30-40 mN/m) and viscosities (1-5 cP).^{34,35}

Inks formulated from QM^{H}_4 and TEOS in methanol (P1, Table 6.1) initially had too low a surface tension for consistent printing, which led to dripping issues. A wide range of formulations were screened and a 50:50 methanol:propanol ratio was found to allow for P2 (Table 6.1) to be printed without dripping while retaining its reactivity on paper.

For certain combinations of paper and surfactant solutions, the barrier created by QM^{H}_4 and TEOS was not sufficiently robust and a more effective hydrophobic formulation had to be prepared. Attempts to use nonpolar low molecular weight silicone hydrides or alkoxy-terminated poly(dimethylsiloxane) (PDMS) proved to be unsuccessful. Larger molecular weight silicones increased the viscosity of the solution, which was not desirable with respect to printability. More effective was a combination of the low molecular weight siloxanes QM^{H}_4 (the hydrosilane), and DMTMDS (P3, Table 6.1, Figure 6.2C). It was possible to use less catalyst with this formulation (2 mg), which also helped reduce the incidence of the ink cartridge clogging (see next section).

The desired reaction between alkoxy- and hydrosilanes occurred slowly after the addition of the $\text{B}(\text{C}_6\text{F}_5)_3$ catalyst to the methanolic solution. As a consequence, there was a limited ‘pot life’. More problematic was cure that took place at the nozzle, which led to clogging, a problem that was greatly mitigated by immediately washing and storing the cartridge in isopropanol after use. To completely avoid the clogging issue, two separate inks were prepared (P4A and P4B, Table 6.1, Figure 6.2C) that could be printed from two separate printers and ink cartridges. While in principle keeping these inks as separate ‘colors’ should remove the need for 2 printers, the automatic cleaning routine of the printer still led to cross contamination and clogging. The use of two printers obviated

problems with pot life and printer clogging and led to a highly reproducible printing protocol.

The final parameter that needed to be optimized was the nature of the paper to be printed, for which the ink needed to be tuned. Subtle interplays were observed between paper characteristics and printability. For example, using a pipette to drop the dilute ink M1 (Table 6.1) onto Whatman filter paper grade 41, and briefly heating it, led to a silicone barrier that could resist water penetration (note that small amounts of gas may be observed during heating – this is evidence of alkane release during the PR reaction). By contrast, under the same conditions on Whatman filter paper grade 1 a barrier was not achieved. The most notable difference between the two Whatman papers is the pore size of the cellulosic network: 11 μm and 20 μm for Whatman #1 and Whatman #41, respectively. The larger surface area on Whatman #1 paper required more siloxanes delivered from a more concentrated ink (P1-P3 or P4A and P4B, Table 6.1). The resulting printed barriers were quite resilient: crumpling of the modified paper appeared to have no discernible difference in the ability of the hydrophobic siloxane barriers to withstand water, even after several washings of hexanes.

As noted above, alcohols and water are parasitic reagents for hydrosilanes in the presence of $\text{B}(\text{C}_6\text{F}_5)_3$. Inconsistency in performance of the inks could be attributed to days on which the humidity in the atmosphere (>75% relative humidity), and therefore water in the paper, was high. Inconsistency due to side reactions between hydrosilanes and alcohol/water could be avoided by keeping the reagents and boron catalyst relatively dry (stored as stock solutions under a nitrogen blanket) and by pre-drying out the Whatman #1 paper in an oven at 100 °C for several minutes immediately before printing. Such pre-treatment was not necessary in drier weather periods (e.g., Canadian winter).

Testing barrier robustness to surfactant solutions

After formulations of the siloxane “inks” were loaded into clean and dry ‘black ink’ cartridges, hollowed circles were printed on Whatman #1 paper. Distilled water was initially utilized to test the robustness of the different silicone barriers formed from the various siloxane inks. Consistent barriers after 4 printing passes to contain water could

not always be formed using the P1 formulation (Table 6.1), due to the low surface tension issues mentioned earlier. Inks P2 and P3 also required at least 4 printing passes to fully hydrophobize the paper, that is, to prevent water (15 μ L) placed in the centre of the circle from penetrating through or under the barrier. For inks P4A and P4B, two printers were utilized to create the silicone barriers. P4A (catalyst mixture) was first printed once on each side of the Whatman paper, with a subsequent printing of P4B (siloxane mixture) once on each side of the paper using a separate printer. With a total of 4 printing passes (2 for each ink), barriers that would contain water were formed.

Afterwards, a comparative study between wax printed barriers and the inkjet printed silicone barriers were done using surfactant solutions. Standard surfactant solutions representing different classes of molecules were prepared from anionic (SDS), non-ionic (Triton X-100) and cationic (CTAB) surfactants, respectively. In addition, B-PER, which is commonly used for cell lysis²¹ (the exact composition is a trade secret of Thermo Scientific), was investigated: the ability to retain cell lysates in a defined area of the paper would validate its use for paper-based biological analysis. Neither silicone barriers formed from P2 (data not shown), nor the wax-based barriers (Figure 6.3A), could resist breach by any of the surfactant solutions over time. Note that a surfactant solution could breach a barrier derived from 4 separate applications of wax (Figure 6.3B). By contrast, robust barriers could be prepared using 4 printing passes with ink P3. When surfactant solutions (15 μ L) were added by drops into the circles (Figure 6.3C, D) there was no breaching of the hydrophobic barrier. However, the surfactant solutions penetrated further on the bottom side, which appeared as a lightly colored corona on the printed side of the paper. This indicates that the alcoholic siloxane solution that was always printed on the ‘top’ side of the paper sheet did not penetrate the paper evenly. The cross-sectional image likely has a rhombus-like shape similar to that reported by Shen et al.³⁶ rather than a rectangular shape (Figure 6.4).

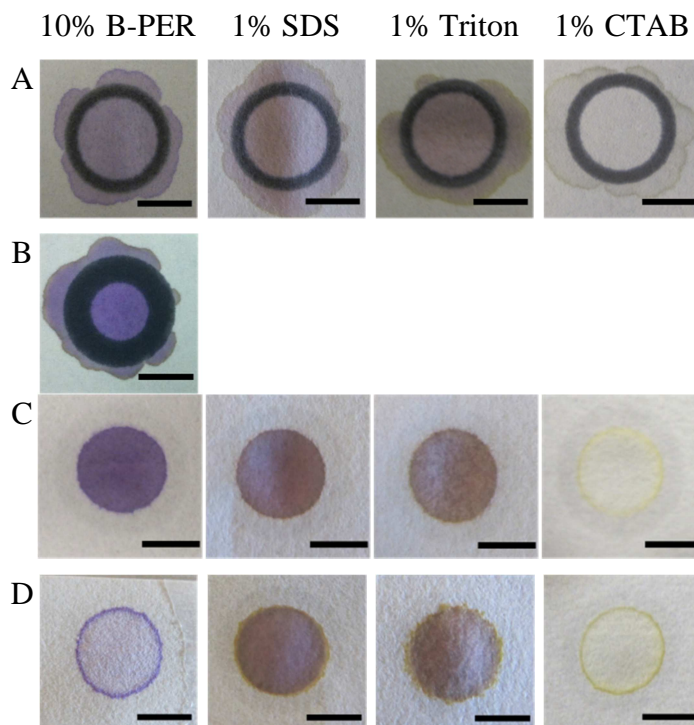


Figure 6.3: Wax based hollow circles stained with CPR surfactant solutions from the printed side (A). 4 wax layers were breached by the same solutions (B). P3 printed hollowed circles on Whatman #1 paper with CPR surfactant solutions on the printed side (C) and back side (D). Scale bars = 5 mm.

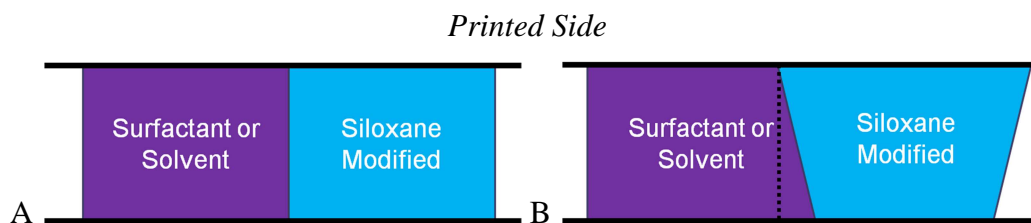


Figure 6.4: Cross-sectional representation of Whatman 1 paper with a surfactant solution/solvent contained by a silicone barrier that is rectangular (A) or rhombus (B) shaped. The dotted line in B represents the triangular slice that appears as a light corona from the printed side.

Analogous silicone barriers could be printed using 2 printers: one with a cartridge containing the catalyst and the other a mixture of the hydro- and alkoxy-silanes. Although the initial setup is slightly more complicated, the two printer method is preferred: both mixing and chemistry occur directly on the paper. Since formulations P4A and P4B (Table 6.1) do not react over time, they can be stored for much longer time periods than

the mixture P3. Using this protocol, both sides of the paper were printed (once on each side for each ink formulation). The two ink formulation approach avoided the clogging of ink cartridges and led to consistent to silicone barriers. It also permitted printing full pages of hollowed out circles as shown in Figure 6.5A within a relatively short time frame (~2-3 mins). Of course, slightly more complex silicone barrier shapes could be printed such as the one shown in Figure 6.5B, which contains 2 mm wide unmodified cellulose channels loaded with the 10% B-PER solution (darker region). The robustness of the barriers derived from P4A and P4B was demonstrated with the different surfactant solutions (Figure 6.5C, D). In no case was the barrier breached and unlike those described with P3 using the one printer method, they appeared uniform on both sides of the paper: no corona was observed by eye.

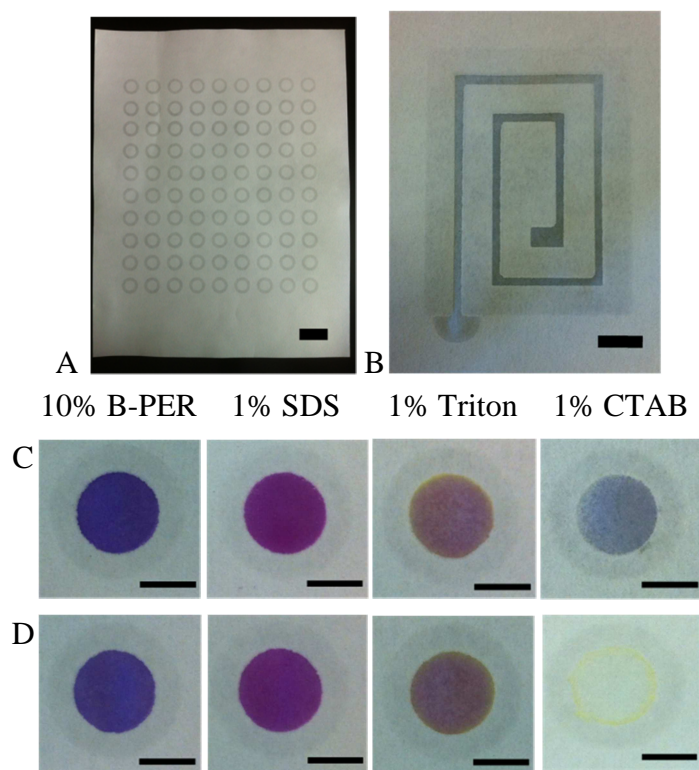


Figure 6.5: P4A and P4B silicone barriers using the 2 printer method in the form of A: 90 hollowed circles, B: rectangular blocks with unmodified paper channels loaded with a 10% B-PER solution (darker region). Images of one printed side (C) and the other printed side (D) of the hollowed circles with the added surfactant solutions. Scale bars = 2 cm (A), 1 cm (B) and 5 mm (C, D).

The wax-based barriers and the silicone barriers formed with both P3 (1 printer method) and P4A/P4B (2 printer method) were also exposed to several solvents to discern any differences in their barrier properties. Like the surfactant solutions, 15 μL of a given solvent was added to the hollowed circles. Neither the siloxane nor wax-based barriers were capable of containing alcohol-based solvents (methanol, ethanol) or nonpolar solvents such as toluene or hexanes (Table 6.2). However, the silicone barriers were capable of containing both DMSO and DMF while the wax barriers could not. DMSO has a surface tension value of 42.92 mN/m while DMF has a value of 35.74 mN/m.³⁷ 1,4-Dioxane was just above the limit that the silicone barriers could contain; only the P4A/P4B silicone barriers could contain this solvent. However, after several seconds of adding dioxane, it would slowly creep into the P4A/P4B barrier, but would not breach it: there was no breaching even after addition of a second 15 μL of solvent.

Table 6.2: Solvents tested against wax and siloxane based barriers (P3 and P4A/P4B) to determine if they are contained (Y), not contained (N) or partially contained (P)^a. Surface tension values are reported at 25 °C.³⁷

Solvent	Wax	Silicone barrier	Surface Tension (mN/m)
Hexanes	N	N	17.89
Isopropanol	N	N	20.93
Ethanol	N	N	21.97
Methanol	N	N	22.07
Acetone	N	N	22.72
Tetrahydrofuran	N	N	26.40
Toluene	N	N	29.46
Dioxane	N	P ^a	32.75
Dimethylformamide	N	Y	35.74
Dimethyl sulfoxide	N	Y	42.94
Water	Y	Y	71.99

^a The P3 silicone barriers could not contain the solvent, whereas the P4A/P4B derived ones could with some solvent penetrating into the barrier.

The wax and silicone barriers were characterized using a variety of techniques. Fluorescent images after exposure to either B-PER or SDS chlorophenol red dye solutions are shown in Figure 6.6. A B-PER/CPR surfactant solution was added to the wax

hollowed circles and was able to breach it (black line) by creeping along the cellulose fibers (Figure 6.6B). Surfactant migration may be associated with wax dissolution once the surfactants come in contact with the barriers, rather than a consequence of exposed fibers that were not sufficiently coated with wax. By contrast, the surfactant solution was shown to be well contained within the P3 silicone barriers when imaged on the printed side of the paper (Figure 6.6C). Figure 6.6C also shows a corona that is ~200-400 μm thick, which contains a lower concentration of CPR (darker region) compared to the rest of the surfactant treated area. The back side of the paper appears to show a thick interlayer (Figure 6.6D) that corresponds to the corona seen by eye on the printed side of the paper. This further suggests that the cross-sectional modification has a rhombus-like shape.³⁶ In other words, the surfactant actually does not penetrate the hydrophobic siloxane barrier: the observed corona is the CPR dye appearing from the backside of the paper as depicted by the dashed triangular slice in Figure 6.4B. The more resilient silicone barriers provided by the P4A/P4B inks contained the CPR surfactant solutions, but do not have an observable corona on either printed side of paper. Printing both sides ensures the siloxane ink doesn't have to wick through the entire thickness of the paper. Unsurprisingly, a much smaller corona was observed on either side (Figure 6.6E, F), which probably results from slight printing misalignments, gradients in hydrophobization, etc. Thus, the cross-sectional silicone resin modification of paper with printing on both sides more closely resembles a rectangular shape, which is shown in Figure 6.4A.

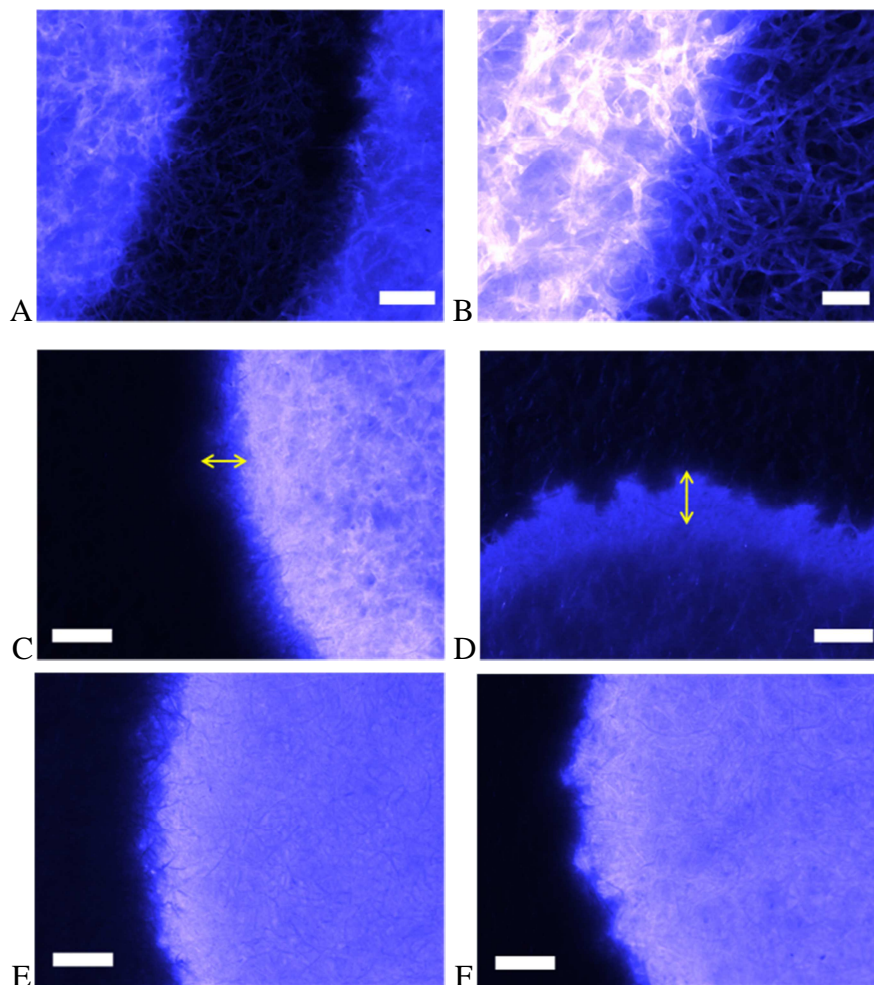


Figure 6.6: Fluorescent images of a 10% B-PER (A – D) and 1% SDS solution (E,F) with a CPR dye added to the wax (A,B), P3- (C,D) and P4A/P4B-s (E,F), respectively. Image C shows the printed side and D shows the backside of the Whatman #1 paper, while E and F show both printed sides of the paper. Arrows indicate the observed corona that corresponds to the thick interlayer on the backside of the paper. Scale bars = 500 μm (A, C – F) and 200 μm (B).

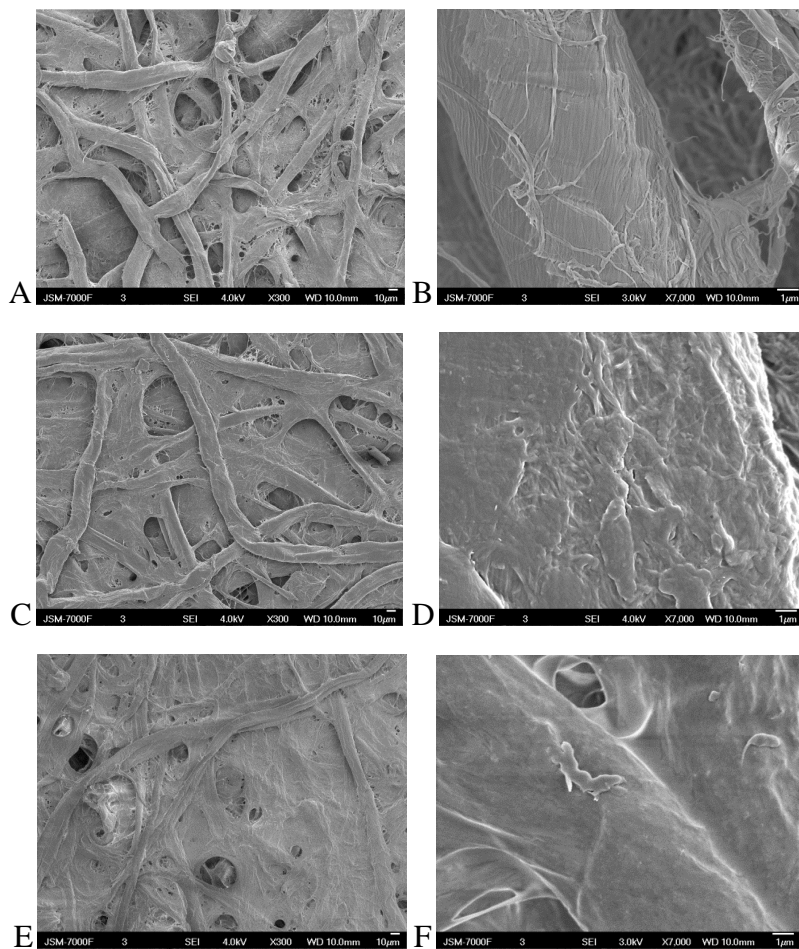


Figure 6.7: SEM images of Whatman #1 paper that is unmodified (A, B), wax modified (C, D) and siloxane-modified with P3 (E, F).

The hydrophobization of paper typically involves coating a hydrophobic layer on the paper surface by chemical modification, physical deposition or physical blocking of the paper pores.¹³ Wax physically deposits on the cellulose fibers without blocking pores and can be compared to unmodified Whatman #1 paper (Figure 6.7A-D). Only at high magnifications can the physical deposition of wax be noticed – discrete fibrils can't be seen. Superficially, the silicone barriers on the Whatman #1 paper appear to be similar to those of wax, as the pores of the paper are not completely blocked. However, at high magnifications modification of the individual cellulose fibers can be seen as shown by the 'blurring' of striations arising from fibrils (Figure 6.7B vs. F). Thus, it appears that the crosslinked hydrophobic siloxane cures around the cellulose fibers

When hydrosilane, alkoxy silane, cellulose and $B(C_6F_5)_3$ are all in contact on the paper surface, where the alcohol concentration is comparatively high both from cellulose and the solvent (MeOH + IPA Table 6.1), competitive reactions occur between the hydrosilane and either the alkoxy silane or the alcohols: the partition between the reaction pathways is unknown. Based on reaction rates in solution, it is expected that chemical anchoring of the silicone resin to the paper via silyl ether formations (in analogy with direct binding found with AKD) is less likely than a layer of silicone resin coating the exposed fibers during a PR reaction (Figure 6.8A < B).

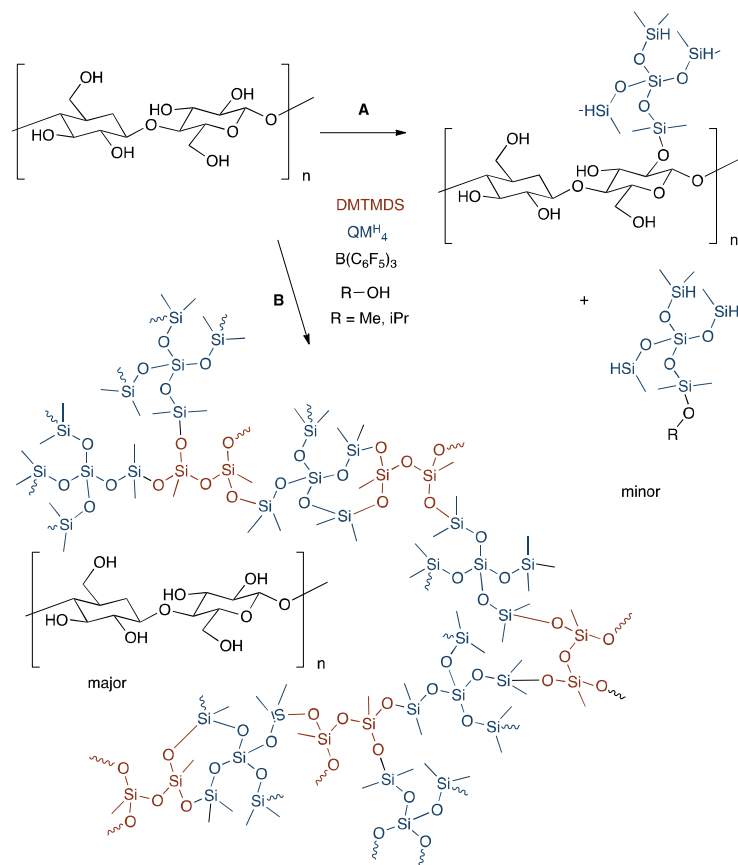


Figure 6.8: Potential chemical modification of cellulose fibers (A) and the cross-sectional diagram of siloxane modified cellulose fibers (B).

The ability of the siloxane barrier to contain surfactant solutions with low surface tension values was surprising: surface tension values were 31.3 ± 0.2 mN/m, 36.6 ± 0.2 , 31.4 ± 0.2 , 35.5 ± 0.2 and for B-PER, SDS, Triton X-100, CTAB and respectively. With

the tested solvents, DMF and DMSO were also contained within the siloxane barriers but 1,4-dioxane, which has a surface tension value of 32.75 mN/m was only partially contained. This value is larger than some of the contained surfactant solutions, thus, the ability of a barrier to contain a solvent or surfactant solution is not exclusively reliant on its surface tension. It is clear that wax cannot contain these surfactants, and AKD (Figure 6.1) is reported only to withstand liquids with surface tensions >35 mN/m.¹⁰ Thus, these siloxane inks form more robust hydrophobic barriers than either wax or AKD.

Applications of printed silicone barriers for diagnostics

Hossain et al. previously reported a paper-based sensor for total coliform detection.²¹ The sensor relied on the colorimetric detection of a commonly used marker for total coliform, the intracellular enzyme β -galactosidase. The test strips contained a yellow substrate, chlorophenol red β -galactopyranoside, which in the presence of β -galactosidase, was hydrolyzed into a red-magenta product, chlorophenol red. The color change from yellow to red-magenta was thus indicative of the presence of β -galactosidase and, therefore, of coliform. A chemical lysing step was performed prior to the assay to release the enzyme, as β -galactosidase is an intracellular enzyme. The lysed samples were, then, assayed via a lateral flow (LF) format.

As part of optimization studies, the strip design was modified to replace the LF format by a direct drop format. Additionally, a purple color change was observed instead of red-magenta for the presence of β -galactosidase, which could have been the result of using of P-Arg instead of PVAm as the capturing agent. When the circles were delimited by a wax barrier, the sample leached outside of the sensing zone, rendering the results hard to analyze and quantify (Figure 6.9A). The P4A/P4B silicone barriers, when using in lieu of wax, allowed the containment of the assay in a well-defined zone on the paper and did not interfere with the assay. The cell lysate did not leach outside of the circle and an intense color change was readily observed (Figure 6.9B and C) demonstrating the potential of such a barrier to be utilized for a biologically relevant assay.

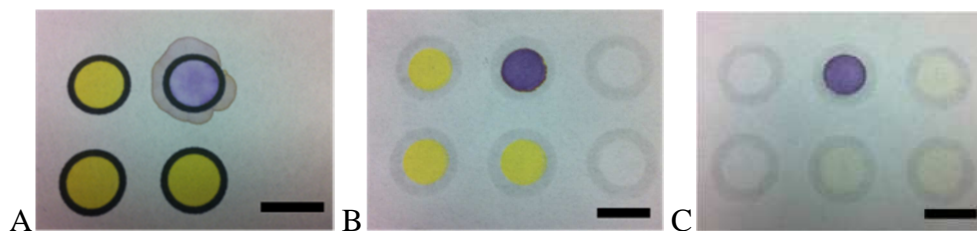


Figure 6.9: Inkjet printed P-Arg and CPR/ β -galactopyranoside solutions (yellow) within wax barriers (A) and P4A/P4B-barrier (B, C) with the addition of lysed *E. coli* cells in a 10% B-PER solution (purple) for total coliform detection. Image C shows the back side of the printed sensor. Scale bars = 1 cm.

Siloxane barriers offer advantages over conventional barriers derived from wax or alkyl ketene dimers in challenging assays on paper based microfluidic devices. Localization of the assays into specific locations is important both because migration leads to dilution of colors needed for assay development and, in the worst case, will lead to mixing of adjacent spots. The silicone barriers are able to resist migration of the surfactants commonly found in biological assays. Simple or complicated hydrophobic patterns can be readily printed using an inexpensive inkjet printer.

6.5 Conclusions

Siloxane-based hydrophobizing agents are readily ink-jet printed onto Whatman paper for use in paper-based diagnostics and microfluidic devices: the paper typically does not require any pre-treatment before printing or post-treatment after the silicone resins have cured. The best reaction found involved the PR condensation of QM^H₄ (the hydrosilane) with DMTMDS catalyzed by B(C₆F₅)₃ using either the 1 printer or the preferred 2 printer methodology. The silicone barriers, unlike wax or AKD hydrophobic layers, were able to withstand low surface tension surfactant solutions (10% B-PER, 1% SDS, 1% Triton X-100, 1% CTAB), which can have values as low as 31.3 mN/m (B-PER). The barriers were also capable of containing solvents such as DMSO and DMF. SEM images of the unmodified and modified paper suggest the silicone resin is able to encase cellulose fibers, although direct grafting to cellulose alcohols cannot be eliminated as a mechanism. The detection and containment of β -galactosidase from lysed *E. coli* cells in a B-PER surfactant solution demonstrates the utility of this protocol. Both the

silicone barriers and the biosensor utilized in this study demonstrated that a low cost inkjet printer can be utilized to form both robust barriers and a colorimetric biosensor for surfactant based mixtures.

6.6 Acknowledgments

The authors thank the Natural Sciences and Engineering Research Council of Canada for funding this work through a Network Grant-SENTINEL Canadian Network for the Development and Use of Bioactive Paper. The authors also thank Norman Shek for providing the *E. coli* cells for β -galactosidase detection. J.D.B. holds the Canada Research Chair in Bioanalytical Chemistry.

6.7 References

- (1) Apilux, A.; Dungchai, W.; Siangproh, W.; Praphairaksit, N.; Henry, C. S.; Chailapakul, O. *Anal. Chem.*, **2010**, *82*, 1727.
- (2) Martinez, A. W.; Phillips, S. T.; Butte, M. J.; Whitesides, G. M. *Angew. Chem. Int. Ed.*, **2007**, *46*, 1318.
- (3) Martinez, A. W.; Phillips, S. T.; Whitesides, G. M. *PNAS*, **2008**, *105*, 19606.
- (4) Olkkonen, J.; Lehtinen, K.; Erho, T. *Anal. Chem.*, **2010**, *82*, 10246.
- (5) Dungchai, W.; Chailapakul, O.; Henry, C. S. *Anal. Chem.*, **2009**, *81*, 5821.
- (6) Li, C.-Z.; Vandenberg, K.; Prabhulkar, S.; Zhu, X.; Schneper, L.; Methee, K.; Rosser, C. J.; Almeida, E. *Biosensors and Bioelectronics*, **2011**, *26*, 4342.
- (7) Yetisen, A. K.; Akram, M. S.; Lowe, C. R. *Lab Chip*, **2013**, *13*, 2210.
- (8) Chin, C. D.; Linder, V.; Sia, S. K. *Lab Chip*, **2007**, *7*, 41.
- (9) Carrilho, E.; Martinez, A. W.; Whitesides, G. M. *Anal. Chem.*, **2009**, *81*, 7091.
- (10) Li, X.; Tian, J.; Shen, W. *Cellulose*, **2010**, *17*, 649.
- (11) Chitnis, G.; Ding, Z.; Chang, C.-L.; Savran, C. A.; Ziaie, B. *Lab Chip*, **2011**, *11*, 1161.
- (12) Li, X.; Tian, J.; Nguyen, T.; Shen, W. *Anal. Chem.*, **2008**, *80*, 9131.
- (13) Li, X.; Ballerini, D. R.; Shen, W. *Biomicrofluidics*, **2012**, *6*, 011301.
- (14) Qiao, L.; Gu, Q.-M.; Cheng, H. N. *Carbohydr. Polym.*, **2006**, *66*, 135.
- (15) Chojnowski, J.; Rubinsztajn, S.; Cella, J. A.; Fortuniak, W.; Cypryk, M.; Kurjata, J.; Kaźmierski, K. *Organometallics*, **2005**, *24*, 6077.
- (16) Brook, M.; Grande, J.; Ganachaud, F.; Muzafarov, A. M., Ed.; Springer Berlin: 2011; Vol. 235, p 161.

- (17) Grande, J. B.; Thompson, D. B.; Gonzaga, F.; Brook, M. A. *Chem Commun*, **2010**, 46, 4988.
- (18) Grande, J. B.; Gonzaga, F.; Brook, M. A. *Dalton Trans.*, **2010**, 39, 9369.
- (19) Kurjata, J.; Fortuniak, W.; Rubinsztajn, S.; Chojnowski, J. *Eur. Polym. J.*, **2009**, 45, 3372.
- (20) Grande, J. B.; Fawcett, A. S.; McLaughlin, A. J.; Gonzaga, F.; Bender, T. P.; Brook, M. A. *Polymer*, **2012**, 53, 3135.
- (21) Hossain, S. M. Z.; Ozimok, C.; Sicard, C.; Aguirre, S.; Ali, M. M.; Li, Y.; Brennan, J. *Anal. Bioanal. Chem.*, **2012**, 403, 1567.
- (22) Carrilho, E.; Martinez, A. W.; Whitesides, G. M. *WO2010102294A1*, **2010**, *President and Fellows of Harvard College*
- (23) Regalado, E. J.; Selb, J.; Candau, F. *Macromolecules*, **1999**, 32, 8580.
- (24) Cuypers, C.; Pancras, T.; Grotenhuis, T.; Rulkens, W. *Chemosphere*, **2002**, 46, 1235.
- (25) Li, N.; Liu, S.; Luo, H. *Anal. Lett.*, **2002**, 35, 1229.
- (26) Rubinsztajn, S.; Cella, J. A. *WO2005118682*, **2005**, *General Electric Company*.
- (27) Rubinsztajn, S.; Cella, J. A. *US 7064173*, **2006**, *General Electric Company*.
- (28) Brook, M.; Grande, J.; Ganachaud, F. o. In *Silicon Polymers*; Muzafarov, A. M., Ed.; Springer Berlin: 2011; Vol. 235, p 161.
- (29) Fawcett, A. S.; Grande, J. B.; Brook, M. A. *J. Polym. Sci., Part A: Polym. Chem.*, **2013**, 51, 644.
- (30) Piers, W. E. *Adv. Organomet. Chem.*, **2004**, 52, 1.
- (31) Zhou, D. Q.; Kawakami, Y. *Macromolecules*, **2005**, 38, 6902.
- (32) Cella, J.; Rubinsztajn, S. *Macromolecules*, **2008**, 41, 6965.
- (33) Blackwell, J. M.; Foster, K. L.; Beck, V. H.; Piers, W. E. *J. Org. Chem.*, **1999**, 64, 4887.
- (34) Kang, H. R. *J. Imaging Sci.*, **1991**, 35, 179.
- (35) Calvert, P. *Chem. Mater.*, **2001**, 13, 3299.
- (36) Li, X.; Tian, J.; Garnier, G.; Shen, W. *Colloids Surf. B*, **2010**, 76, 564.
- (37) Haynes, W. M. *CRC Handbook of Chemistry and Physics 2011-2012*; Taylor & Francis, 2011.

Chapter 7 – Summary

This thesis has demonstrated the formation of silicone elastomers and silica-based colloids, films and foams by controlling a variety of interfaces. The chemistry utilized to form these different materials varied from conventional basic catalysis of siloxane bonds (Chapters 2-4) to the relatively recent Piers-Rubinsztajn (PR) reaction (Chapters 5, 6). These investigations have led to new methods to form silicone/silica based materials that were either unknown or not considered possible previously. Additionally, the materials prepared could be exploited in a number of different applications, as the processes for their preparation is either simplified, compared to existing methods or leads to more robust materials than what is currently available.

The beginning of the thesis described the formation of silicone elastomers with hydrophilic PEG structured within the elastomer, without the need to covalently link the two phases. These elastomers were formed using the slightly basic AT-PDMS catalyst, thus avoiding the use of highly toxic tin and platinum based catalysts. By varying the different parameters of the elastomer, surface roughness, homogeneity of cure, location of catalyst, different internal structures of PEG could also be realized. The hydrophilic PEG structures were controllably localized at the air-surface interface and could form isolated droplets, interconnected channels and even be homogeneously distributed throughout the upper interface of the elastomer. The surface roughness of the elastomers formed could also be varied from several hundreds of nanometers to tens of microns as judged by the root mean square roughness values (R_q).

This directly led into the third chapter, which discusses the formation of silica particles within a silicone pre-elastomer matrix. As hinted in the second chapter, silica is formed during the formation of the silicone elastomer, particularly near the air-surface interface as water ingress from the atmosphere occurs at this location first to allow hydrolysis and the condensation of TEOS to form silica. Silica particles are commonly formed within alcoholic-aqueous mixtures using sol-gel methodology. However, the formation of narrowly dispersed, micron sized, silica particles within a hydrophobic

matrix is highly unusual. Although no liquid water was required, the atmospheric water content was important for controlling both the process of particle formation and particle size. The key for particle stabilization during synthesis was the catalyst, which also acted as a surfactant to stabilize the particle charge. Even though silica particles form negatively charged silanolate groups on the surface, which would normally not be colloidally stable outside of a polar, protic medium, with the correct surfactant narrowly dispersed silica particles could be formed within a hydrophobic medium.

Chapter 4 discussed forming silica particles with varying morphologies within a hydrophobic silicone medium. Unlike the solid silica particles formed in chapter 3, the macroporous and hollow silica particles formed in chapter 4 required the hydrophilic PEG phase in order to form. The solubilities of the basic catalysts used (benzylamine and dodecylamine, respectively) in the PEG phase determined the morphology of the resulting silica particles. Benzylamine readily solubilized within the PEG phase, thus catalyzing silica formation directly within the PEG droplets. Due to spinodal decomposition, both the silica and PEG phase separate to yield a macroporous silica particle. Conversely, dodecylamine did not solubilize readily in either phase, and was localized at the PEG-silicone interface. As a result, catalysis of silica formation took place around the silica droplet leading to the formation hollow particles. When utilizing these particles for drug release, it was discovered that the particles were too porous to inhibit the release small molecules and proteins such as fluorescein and HSA. However larger drug surrogates such as metal nanoparticles could potentially be released in a controlled manner from these silica particles.

In chapter 5, the Piers-Rubinsztajn reaction was used to form hydrophobic siloxane films with varying morphologies from surfactant-free siloxane-in-water emulsions. The silicone-in-water emulsions were first introduced by Ganachaud et al.^{1,2} as a medium in which to form various polymers. It is believed that the emulsions are stabilized by negatively charged boron-water adducts that present at the siloxane-water interface. Without the boron catalyst, phase separation of the siloxanes and water occurs. Catalyst concentrations also affected emulsion stability. However, these emulsion behaved

differently compared to organic surfactant-stabilized emulsions, as a specific concentration of catalyst gave the most stable emulsions: higher or lower concentrations resulted in lower stability. The different film morphologies that could be formed from these structures included foamed, monolithic and even particulate films. Aging a given mixture over several days enabled these different morphologies to form. In addition, the catalyst concentration could affect the morphologies of the films produced. Higher catalyst concentrations resulted in films of annealed particles that rapidly formed. The particulate-based films were of greatest interest for applications in gas chromatography because of their high surface area. Preliminary experiments with glass capillary tubes demonstrated that these hydrophobic particulate films could be incorporated into capillary-based columns.

Finally, chapter 6 discusses ink-jet printing hydrophobic siloxane barriers onto paper for paper-based microfluidics and diagnostics. The state-of-the-art wax and alkyl ketene dimer (AKD) hydrophobic barriers, which are printed onto paper, are unable to contain most surfactant based solutions and there is a growing need to be able to pattern more robust barriers onto paper for more complex analytes.³ Thus, the use of rapidly curing hydrophobic siloxane barriers, via the PR reaction, appeared to be a potential method to form more robust barriers on paper. A low concentration of alcohol was added to a tetrafunctional hydrosilane and alkoxy silane mixture that also contained the boron catalyst, which was then loaded into the black ink cartridge of the ink-jet printer utilized. Hollowed circles were then printed on the paper using up to 4 passes of ink that was rapidly cured with a heat gun to drive off the inhibitory alcohols. Coupling of the hydrosilane and alkoxy silane then occurred to form a crosslinked hydrophobic siloxane resin around the cellulose fibers. Although the barriers produced were effective, this specific printing methodology led a great deal of clogging of the cartridge nozzles: the active alcoholic solutions would dry/cure and clog the ink cartridge. This problem could be avoided by separating the mixture into two different ink cartridges and printers. Using the approach, the chemistry occurred directly on the paper, eliminating the clogging of the cartridges. The robustness of the silicone barriers produced was compared to the wax

barriers by testing them against various aqueous surfactant solutions and solvents. All surfactant solutions and both DMSO and DMF solvents were contained by the hydrophobic silicone barriers, whereas wax barriers could not contain any of the surfactant solutions or the tested solvents. The surface tension values measured for the surfactant solutions were also lower than the reported surface tension limit of the AKD barriers. To demonstrate the utility of the barriers, a paper-based sensor for coliform detection was adapted from Zakir et al.⁴ and printed within both the wax barriers and the silicone barriers. A surfactant solution was required for the paper sensor and was only contained within the silicone barriers.

The importance of interfaces in controlling material morphology cannot be overstated. Nature demonstrates this concept best in organisms such as diatoms, sponges, and radiolarians, which produce extravagant silica structures.⁵ In this thesis, I have used a variety of control elements: catalyst type, reaction type, substrate type and reaction conditions; to control interfaces between polar substrates including water, silica, PEG and paper, and a variety of mobile, lightly crosslinked, or highly crosslinked silicones. The methods and materials are broadly applicable and it is anticipated that these technologies will be adopted in future to make devices.

7.1 References

- (1) Longuet, C.; Joly-Duhamel, C.; Ganachaud, F. *Macromol. Chem. Phys.*, **2007**, *208*, 1883.
- (2) Kostjuk, S. V.; Radchenko, A. V.; Ganachaud, F. *Macromolecules*, **2007**, *40*, 482.
- (3) Li, X.; Ballerini, D. R.; Shen, W. *Biomicrofluidics*, **2012**, *6*, 011301.
- (4) Hossain, S. M. Z.; Ozimok, C.; Sicard, C.; Aguirre, S.; Ali, M. M.; Li, Y.; Brennan, J. *Anal. Bioanal. Chem.*, **2012**, *403*, 1567.
- (5) Brook, M. A. *Silicon in Organic, Organometallic, and Polymer Chemistry*; Wiley-VCH Verlag, 2000.

Appendix

Papers Published in Peer-Reviewed Journals

1. Vinodh Rajendra, Clémence Sicard, Michael A. Brook, John D. Brennan, Inkjet Printing Silicone-Based Hydrophobic Barriers on Paper for Microfluidic Assays, to be submitted to Journal of Materials Chemistry B (before Feb. 28, 2014).
2. Vinodh Rajendra, Michael A. Brook, Stable Siloxane-in-Water Emulsions to Form Various Film Morphologies, submitted to ACS Interfaces.
3. V. Rajendra, M. A. Brook, Controlled Formation of Macroporous or Hollow Silica Particles in Non-aqueous Silicone Dispersions, *RSC Adv.*, **2013**, 3, 2222-22238.
4. V. Rajendra, F. Gonzaga, M. A. Brook, Nearly Monodisperse Silica Particles Form in Silicone (Pre)elastomer Mixtures, *Langmuir*, **2012**, 28, 1470–1477.
5. V. Rajendra, Y. Chen, M. A. Brook, Structured Hydrophilic Domains on Silicone Elastomers, *Polym. Chem.*, **2010**, 1, 312 – 320.

Filed Patents

1. M. A. Brook, V. Rajendra, C. Sicard, J. D. Brennan, Creating hydrophobic siloxane films of various porosities on porous and non-porous substrates, US Provisional Patent Application, McMaster University, filed April 10, 2013.

Conference Presentations

1. Vinodh Rajendra, Michael A. Brook, *An Alternative Route for the Formation of Siloxane Based Films via Hydro/Alkoxysilane Condensation*, 96th Canadian Chemistry Conference and Exhibition, Quebec City, Quebec, May 2013, Abs. 1875 (Oral Presentation)
2. Vinodh Rajendra, Clémence Sicard, Michael A. Brook, John D. Brennan, *Ink-Jet Printing of Siloxane Based Hydrophobic Barriers on Paper*, 1st FIBRE Network Conference, Cornwall, Ontario, May 2013, Poster no. 163 (Poster Presentation)
3. Vinodh Rajendra, Michael A. Brook, *Active alcoholic solutions and silane-in-water emulsions for the formation of siloxane based films from hydrosilane/alkoxysilane*

- condensation*, 245th ACS National Meeting, New Orleans, Louisiana, April 2013, Paper no. COLL 744 (Oral Presentation)
4. Vinodh Rajendra, Michael A. Brook, *Controlling the morphology of silica particles in non-aqueous silicone dispersions*, 244th ACS National Meeting, San Diego, California, March 2012, Paper no. COLL 70 (Oral Presentation)
 5. Vinodh Rajendra, Ferdinand Gonzaga, Michael A. Brook, *Formation of Silica Particles in Non-Aqueous Dispersions*, 20/20 NSERC Ophthalmic Materials Network Fall Meeting, April 2012 (Poster Presentation)
 6. Vinodh Rajendra, Ferdinand Gonzaga, Michael A. Brook, *Formation of Silica Particles in Hydrophobic Systems and their Morphology*, 20/20 NSERC Ophthalmic Materials Network Fall Meeting, October 2011 (Poster Presentation)
 7. Vinodh Rajendra, Ferdinand Gonzaga, Michael A. Brook, *Controlling the Morphology of Silica Particles formed in non-aqueous Silicone (pre)elastomer Dispersions*, 16th International Symposium on Silicon Chemistry, Ontario, Hamilton, August 2011, Abs. 96 (Oral Presentation)
 8. Vinodh Rajendra, Ferdinand Gonzaga, Michael A. Brook, *Controlling the Morphology of Silica Particles formed in non-aqueous Silicone (pre)elastomer Dispersions*, 85th ACS Colloid and Surface Science Symposium, Quebec, Montreal, June 2011, Abs. 565 (Oral Presentation)
 9. Vinodh Rajendra, Ferdinand Gonzaga, Michael A. Brook, *Formation of Silica Particles in Hydrophobic Systems and their Morphology*, 94th Canadian Chemistry Conference and Exhibition, Quebec, Montreal, June 2011, Abs. 437 (Oral Presentation)
 10. Michael A. Brook, John B. Grande, Johan Alauzun, Yang Chen, Tim Dargaville, Daniel Keddie, Helen Y. So, Amanda S. Fawcett, Yongxin Wang, Vinodh Rajendra, David B. Thompson, *Structured Silicone Elastomers for Improved Biocompatibility*, 32nd Australasian Polymer Symposium, Coffs Harbour, Australia, February 2011

11. Vinodh Rajendra, M. A. Brook, *Formation of Silica Microspheres in Non-Aqueous Dispersions*, 93rd Canadian Chemistry Conference and Exhibition, June 2010 (Poster Presentation)
12. Vinodh Rajendra, M. A. Brook, *Formation of Silica Microspheres in Non-Aqueous Dispersions*, 43rd Silicon Symposium, St. Louis, MO, May 2010, DMEWJ6.ABS (Oral Presentation)
13. Vinodh Rajendra, Yang Chen, Helen So, M. A. Brook, *Structuring Silicone Elastomers for Drug Delivery*, Association for Research in Vision and Ophthalmology Annual Meeting, Florida; Fort Lauderdale, May 2010 (Poster Presentation)
14. Michael A. Brook, Heather D. Sheardown, Alison Holloway, Renita D`Souza, Yunping Shao, Ken Ng, Vinodh Rajendra, Amanda Fawcett, Helen So, Johan Alauzun, *Strategies to Improve Silicone Elastomer Biocompatibility*, Keynote address, 11th Pacific Polymer Conference, Cairns, Australia, December 2009
15. Vinodh Rajendra, Yang Chen, M. A. Brook, *Controlled Morphology of Silicone Elastomers*, 42nd Silicon Symposium, Long Branch, NJ, June 2009 (Oral Presentation)
16. Vinodh Rajendra, Yang Chen, M. A. Brook, *Structured Hydrophilic Domains on Silicone Elastomers*, 92nd Canadian Chemistry Conference and Exhibition, Ontario, Hamilton, June 2009 (Oral Presentation)